

**EXPLORING COMPLEX INTERACTIONS WITHIN MICROGELS AND
MICROGEL ASSEMBLIES**

A Dissertation
Presented to
The Academic Faculty

by

Emily Sue Herman

In Partial Fulfillment
of the Requirements for the Degree
Doctor of Philosophy in the
School of Chemistry and Biochemistry

Georgia Institute of Technology
December 2014

COPYRIGHT 2014 BY E.S. HERMAN

**EXPLORING COMPLEX INTERACTIONS WITHIN MICROGELS AND
MICROGEL ASSEMBLIES**

Approved by:

Dr. L. Andrew Lyon, Advisor
School of Chemistry and Biochemistry
Georgia Institute of Technology

Dr. Rigoberto Hernandez
School of Chemistry and Biochemistry
Georgia Institute of Technology

Dr. Robert Dickson
School of Chemistry and Biochemistry
Georgia Institute of Technology

Dr. Alberto Fernandez-Nieves
School of Physics
Georgia Institute of Technology

Dr. Lawrence Bottomley
School of Chemistry and Biochemistry
Georgia Institute of Technology

Date Approved: August 4, 2014

For my parents, Dan and Shari, whose never ending love, support, and encouragement brought me to where I am today.

ACKNOWLEDGEMENTS

There are a number of people that deserve acknowledgement for helping me throughout my journey, but first I have to acknowledge my parents for which this thesis is dedicated. I can't remember a time in my life when my parents haven't been encouraging. They always told me to follow my dreams and find what I love. To them, there was nothing I couldn't do. I was more than capable and if I put my mind to it, I could do it. They were always proud of my accomplishments and were always there cheering me on. The reason I am where I am today is because of an incredible support system, and my parents are a large part of that. I am just incredibly lucky to have such amazing parents.

Next, I want to thank the rest of the family. First, I would like to thank all of the wonderful women in my life. That includes my grandmother, Francis Coleman, who is an amazing woman and has always been incredibly supportive and loving. I also have some amazing grandmothers, aunts, cousins, and sisters-in-law, all of whom are strong women who bring perspective and wisdom. They are the backbone of this close knit family that I truly appreciate, even if it is hectic at times. Of course I have to thank my brothers, Mike, Tim, Slade and Jeremy. Family time with them, my nieces and sisters-in-law is truly priceless, and they were always there for advice and encouragement. Even though our younger years were full of annoying each other, I appreciate each one of them and know they are always there if I need them.

I owe a huge amount of gratitude to my boyfriend, Dan. Dan and I started dating 3 years ago and he has been interested, encouraging, and supportive of my journey through graduate school since the day we met. From the intellectual conversations that

keep me thinking to the jokes that keep me laughing daily, I am incredibly thankful to have had him with me through my most imperative and busy graduate school years. He is my best friend and he is my biggest fan. Every time I had to work late, he was always understanding, loving, and supportive. When I felt discouraged, he was there telling me I could do it. I am so grateful for everything he has done for me over the years and all of the times he has been there when I needed a shoulder to lean on.

Of course, I have to thank Kim Clarke next. I was blessed to be able to work directly next to one of my closest friends every day. Like long lost sisters separated at birth, we became friends almost immediately after she joined the Lyon group. All of the great talks, kickball games, coffee breaks, understanding each other by just a look, and goofy inside jokes make graduate school, and life in general, more enjoyable. Not to mention she was there when I needed someone to slap some sense into me and tell me I could do it. The years we had as labmates will always be some of my favorite memories.

I have to thank the rest of the Lyon lab as well, which includes Dr. Toni South, Dr. Mike Smith, Dr. Jeff Gaulding, Dr. Grant Hendrickson, Mark Spears, Purva Kodlekere, Shalini Saxena, Caroline Hansen, and Haylee Bachman. They each brought their own perspective, sense of humor and all around good attitude that made working in lab a really amazing interactive experience. I have also worked with some absolutely amazing post-docs, namely Dr. Ashlee Brown, Dr. Nicole Welsch, Dr. Xiaobo (Bob) Hu, Dr. Ling Zhang, and Dr. Hiro Yoshida. Not to mention the great undergraduates we had working in the lab, which includes Angel Santiago-Lopez, Kabir Dhata and Akriti Singh, the latter of whom had a helping hand in the work presented in Appendix B.

I also had some amazing collaborations that have led to several publications and some of that work is presented within. A long standing collaboration with John Hyatt, Andrea Scotti, Urs Gasser (PSI), and Dr. Alberto Fernandez-Nieves has been incredibly informative and has helped me develop my synthesis skills over the years. I also want to thank Richard Bedell, who designed the conductivity meter described in Appendix A. Richard enjoys what he does and it is obvious in his willingness to talk with you about anything electronic and help fix/design any kind of electronics.

Last but certainly not least, I have to thank the bossman himself, Dr. L. Andrew Lyon. He has always believed in my knowledge and abilities as a scientist, even when I didn't. During the times I needed encouragement the most he was not only there with kind words, he was understanding and supportive. He struck a balance in his leadership wherein he allowed us to build projects and ideas individually while still maintaining a grasp on what everyone was doing and giving insight and forethought. His group was always a priority and even though his schedule was incredibly busy, he always found a way to respond and meet with his group. Sometimes this meant going over data while grabbing a bite to eat or grabbing coffee, but he was always there when we needed him. I couldn't have asked for a better mentor, someone with such a deep passion for science and helping other scientist grow to their full potential.

TABLE OF CONTENTS

	Page
ACKNOWLEDGEMENTS	iv
LIST OF TABLES	xii
LIST OF FIGURES	xiii
LIST OF SCHEMES	xvii
LIST OF SYMBOLS	xviii
LIST OF ABBREVIATIONS	xix
SUMMARY	xxii
<u>CHAPTER</u>	
1 Introduction	1
1.1. Polymer Thin Films	1
1.2. Hydrogels	3
1.3. Microgels	5
1.3.1. Microgel Synthesis	6
1.3.2. Characterization	8
1.3.2.1. Dynamic Light Scattering (DLS)	8
1.3.2.2. Atomic Force Microscopy (AFM)	10
1.3.2.3. Optical Microscopy Techniques	12
1.3.3. Microgels as Building Blocks for Multilayer Thin Films	15
1.4. Dynamic Behavior of Microgel Thin Films	17
1.5. References	19
2 Revealing Complex Network Structure Within Hollow Microgels	26

2.1. Introduction	26
2.2. Experimental Section	31
2.2.1. Materials	31
2.2.2. Microgel Core and Core/Shell Synthesis	31
2.2.3. Core Degradation	33
2.2.4. Characterization	33
2.3. Results and Discussion	34
2.4. Conclusions and Future Outlook	44
2.5. References	46
3 Probing Charge Distribution Within Microgels and Microgel Assemblies	49
3.1. Introduction	49
3.2. Experimental	52
3.2.1. Materials	52
3.2.2. Microgel Synthesis and Characterization	52
3.2.3. Microgel Sample Preparation	53
3.2.3.1. MG-20 and MG-10 Deposition	53
3.2.3.2. MG-26 Multilayer Thin Films	54
3.2.3.3. MG-26 Thin Film Damage and Healing	55
3.2.3. Characterization	55
3.3. Results and Discussion	56
3.4. Conclusions and Outlook	64
3.5 References	67
4 Direct Visualization of the Interactions of Microgel Thin Film Building Blocks	71

4.1. Introduction	71
4.2. Experimental	74
4.2.1. Materials	74
4.2.2. Microgel Synthesis and Characterization	74
4.2.3. PLL* Preparation and Characterization	74
4.2.4. Sample Preparation and Microscopy	76
4.2.5. Real-Time Microgel Tracking	78
4.3. Results and Discussion	79
4.3.1. Microgel Interactions with PLL-Labeled Microgel Surfaces	80
4.3.2. Microgel Interactions with PDADMAC-Labeled Microgel Surfaces	91
4.4. Conclusions and Outlook	94
4.5. References	98
5 Exploring Polyelectrolyte Behavior in Microgel Multilayer Thin Films	101
5.1. Introduction	101
5.2. Experimental	105
5.2.1. Materials	105
5.2.2. Microgel Synthesis and Characterization	105
5.2.3. Polyelectrolyte Preparation	105
5.2.4. Microgel Thin Film Assembly	106
5.2.5. Polyelectrolyte Diffusion and Exchange Characterization	106
5.2.6. Microgel Thin Film Thickness Measurements	107
5.2.7. Mechanical Deformation and Polyelectrolyte Exchange in Microgel Thin Films	108

5.3. Results and Discussion	108
5.3.1. Polyelectrolyte Diffusion and Exchange	109
5.3.2. Mechanical Film Deformation	115
5.3.3. Mechanical Perturbation of PLL-Microgel Films	117
5.4. Conclusions and Outlook	120
5.5. References	121
6 Conclusions and Future Directions	125
6.1. Hollow Microgels	125
6.2. Surface Charge of Microgels and Microgel Assemblies	126
6.3. Polyelectrolyte Behavior in Microgel Multilayer Films	127
6.3.1. Future Directions	129
6.3.2. Preliminary Results	130
6.3.2.1. Revealing Microgel Multilayer Film Growth Behavior	130
6.3.2.2. Altering the Incorporation of Polyelectrolyte	133
6.4. Concluding Remarks	134
6.5. References	134
Appendix A The Formation of Glass Nanopores for Use in Resistive Pulse Analysis (RPA)	136
A.1. Introduction	136
A.2. Experimental	137
A.2.1. Materials	137
A.2.2. Disk Electrode Formation	138
A.2.3. Glass Nanopore Formation	143

A.3. Conclusions and Future Outlook	145
A.4. References	146
Appendix B Design Parameters for the Synthesis of Large Scale and Deuterated Microgels	147
B.1. Introduction	147
B.2. Experimental	149
B.2.1. Materials	149
B.2.2. Synthesis of Microgels with Varied r_h	149
B.2.3. Synthesis of Deuterated Microgels	150
B.2.4. Characterization Techniques	152
B.3 Results	153
B.3.1. Neutral Microgels with Varied r_h	153
B.3.2. Deuterated NIPAm Synthesis	156
B.4. Conclusions	159
B.5. Acknowledgements	159
B.6. References	159
VITA	162

LIST OF TABLES

	Page
Table 2.1: Synthesis Parameters of DHEA Containing Core and Core/Shell Microgels	35
Table 2.2: Light Scattering Data of Various Stages of “Hollow” Microgel Construction	37
Table B.1: DLS r_h data of microgel solutions with varied total monomer concentration. *Value obtained by Akriti Singh.	154
Table B.2: DLS Cumulants data and SAXS data of microgel samples prepared with varied SDS concentration (sample number and measurements provided by Andrea Scotti).	155
Table B.3. DLS data for D-pNIPAm and H-pNIPAm microgels of similar size. *Values presented were taken from Reference 12 and were obtained by John Hyatt. Differences in r_h and polydispersity can be attributed to variation in solvent.	157
Table B.4. DLS data for D-pNIPAm microgels produced through varying the SDS concentration.	158

LIST OF FIGURES

	Page
Figure 1.1: Inverted microscope image. The microscope shown is a Zeiss Axio Observer inverted microscope similar in design to the Olympus IX-71 inverted microscope. From Reference 72.	13
Figure 2.1: Possible routes of self-cross-linking in NIPAm and NIPMAm: (a) the located on the tertiary C of the isopropyl group or (b) the hydrogen located on the tertiary C of the main chain backbone. Adapted from Reference 16.	28
Figure 2.2: Solutions of core/shell microgels before (b) and after (c) exposure to NaIO ₄ . For comparison, degraded core particles (a) are also shown.	38
Figure 2.3: Volume phase transition curves of non-degraded (black squares) and degraded Core 1/shell microgels (red circles) (a). Deswelling curves of non-degraded (black squares) and degraded (red circles) (b).	39
Figure 2.4: Volume phase transition of non-degraded Core 2/shell microgels (grey squares) and degraded core/shell microgels (red triangles) (a). Volume phase transitions of Core 2 (red circles) and Core 2/shell microgels (grey squares) (b).	41
Figure 2.5: AFM images of microgels containing Core 1 before (a) and after (b) degradation and microgels containing Core 2 before (c) and after (d) degradation with representative line traces.	43
Figure 3.1: AFM height images of MG-20 deposited in HIS PBS (a), LIS PBS (b) and H ₂ O (c) with their corresponding KPFM height maps (d, e, and f, respectively). All contain line traces of representative microgels. All images are 20 × 20 μm.	57
Figure 3.2: AFM height images of MG-20 before (a) and after PDADMAC exposure (c) with their respective potential maps (b,d, respectively). Representative line traces are also presented. All images are 20 × 20 μm.	60
Figure 3.3: AFM height and KPFM potential maps of mixed one layer films (a,b) and two layer films (c,d) with representative height traces. Both films contain MG-10 and MG-20. Images are 20 × 20 μm.	63
Figure 3.4: KPFM height and potential maps of 5 layer microgel films composed of MG-26 and PDADMAC before damage (a,d), during damage (b,e), and after healing (c,f). Scale bar = 1 μm.	66

- Figure 4.1: Beer's Law plot of absorbance (at 495 nm) versus PLL concentration (mg/mL). From this, the % conjugation of AlexaFluor to PLL was calculated ($4.2 \pm 0.5\%$). 76
- Figure 4.2: Images of passively (a) and actively (d) deposited microgels after exposure to PLL* are shown. After a second exposure to MG-20 by passive (b,d) and active (c,f) deposition films were imaged in brightfield and fluorescence, respectively. Areas lacking PLL* are shown in red squares and areas exhibiting PLL* diffusion are circled in blue. Passive deposition time = 1 hr, scale bar = 1 μm . 81
- Figure 4.3: Composite images of samples composed from two microgel deposition steps with passive deposition times of 1 hr (a), 5 hr (b), 15 hr (c), and centrifugal deposition (d). The % overlap (e) and particles per μm^2 (f) are shown for varied deposition times (in hrs) and centrifugation. $n = 5$, scale bar = 5 μm . 82
- Figure 4.4: Real-time tracking of microgels depositing onto a PLL-microgel surface. Microgels from solution deposited either directly onto the surface (a-d), "sampled" the microgel surface before deposition (e-h), directly landed on microgels and slid to the substrate surface (i-l), or landed and settled between previously deposited microgels (m-p). Red circles indicate areas of deposition. Scale bar = 1 μm . 86
- Figure 4.5: Real-time tracking of microgels depositing onto a centrifugally deposited microgel surface after exposure to PLL. The yellow square shows microgel deposition onto an underlying microgel (a) and slide-off onto the substrate (b). The red circle also shows deposition onto the microgel (c) and slide-off onto the substrate (d). The blue square shows deposition of a microgel between 3 PLL-labeled microgels. Fluorescence images show PLL redistribution after microgel deposition (f). Scale bar = 1 μm . 89
- Figure 4.6: AFM height images of microgel films after a single MG-20 exposure (a), after PDADMAC and subsequent MG-10 exposure (b) and upon an additional PDADMAC exposure and subsequent deposition of MG-20 (c). Images are $20 \times 20 \mu\text{m}$. 92
- Figure 4.7: Real-time tracking of microgels from solution interacting with a PDADMAC-microgel surface. Microgels from solution deposited directly onto a PDADMAC-microgel (a) and slid off (b-c), deposited directly to the silanized substrate (d), moved into PDADMAC-microgels after depositing onto the silanized substrate (e-g), or sampled the PDADMAC-microgel surface and deposited onto the silanized substrate (h-k). Microgel surface testing is marked with a black arrow (j). Interactions are shown in red circles. Scale bar = 1 μm . 93

- Figure 4.8: AFM images of an MG-20 microgel film assembly after microgel deposition 1 (a), deposition 2 (b), deposition 3 (c), and deposition 4 (d). PDADMAC was deposited between each microgel deposition step. Images are 20x20 μm . 97
- Figure 5.1: CLSM images of PLL-microgel films containing 11 microgel layers and 10 PLL layers. Each panel shows the addition of a labeled polyelectrolyte layer, PLL^{*}₁ (a,d) PLL^{*}₅ (b,e) and PLL^{*}₁₀ (c,f). Scale bar (a,b,c) = 10 μm and inset (red) = 2 μm . Scale bar (d,e,f) = 5 μm . Rhodamine-labeled polyanion beads are shown in microgel layers 1 and 11 (d) and in layer 5 (e,f) for film depth information. 110
- Figure 5.2: In-liquid AFM images of PLL₁₀-microgel₁₁ films with PLL^{*}₁ (a) PLL^{*}₅ (b) and PLL^{*}₁₀ (c). The heights of the films were calculated from height maps, and representative height maps for a, b, and c are shown in d (1.1 \pm 0.2 μm), e (0.9 \pm 0.2 μm) and f (1.3 \pm 0.2 μm), respectively. 111
- Figure 5.3: Normalized absorbance (at 495 nm) of PLL₁₀-microgel₁₁ films with PLL^{*}₁ (a) PLL^{*}₅ (b) and PLL^{*}₁₀ (c). Green arrows indicate the point of incorporation of PLL^{*}. n=44. 112
- Figure 5.4: Normalized absorbance (at 495 nm) of wash and microgel solutions. After the addition of PLL^{*}₅ (a) and PLL^{*}₁₀ (b), films were washed 3 times and an additional microgel layer was added. These solutions were collected and the absorbance was recorded at 495 nm. n=44. 113
- Figure 5.5: The plateau absorbance (at 495 nm) of films composed through the incorporation of PLL^{*} at varied PLL deposition step. PLL Deposition Step corresponds to the PLL deposition step at which the PLL^{*} was incorporated. n=44. 114
- Figure 5.6: AFM images of PLL-microgel films before (a), after damage (b), and after healing (c). Images are 20 \times 20 μm . 116
- Figure 5.7: CLSM images of the PLL^{*}_{all} film before (a), after stretching (b), after scratching (c) and after healing (d) with representative orthogonal views (z-dimension). Scale bar = 10 μm . 118
- Figure 5.8: CLSM images of films with fluorescently labeled PLL at PLL^{*}₁ (a-d), PLL^{*}₅ (e-h) and PLL^{*}₁₀ (i-l) before damage, during stretching and scratching, and after damage. Scale bar for main images = 10 μm , and inset image scale bar = 5 μm . 119
- Figure 6.1: Absorbance (at 495 nm) of microgel-PLL^{*} films after each deposition step as recorded by UV-VIS spectrometry. PLL^{*} was added at each polyelectrolyte deposition step. 131

Figure 6.2: Absorbance (at 495 nm) as a function of microgel deposition step, or layer number.	132
Figure A.1: Resistance versus disk radii. These results were obtained from simulations of the resistance of a glass-sealed Pt disk electrode during polishing. Taken from Reference 9.	141
Figure A.2: CV representing the voltammetric response of a Pt microelectrode in a ferrocene solution.	142
Figure A.3: A representative graph of the current as a function of applied potential for a glass nanopore.	144

LIST OF SCHEMES

	Page
Scheme 1.1: Scheme showing the production NIPam-AAc microgels containing the cross-linker BIS through free-radical precipitation polymerization.	7
Scheme 1.2: A generalized set-up of AFM optical lever detection in which a laser light is reflected from the cantilever and recorded by a position-sensitive detector. Image taken from Asylum Research	10
Scheme 1.3: Anionic microgels are centrifugally deposited onto a silanized substrate and introduced to a cationic polyelectrolyte; this process is repeated until a desired thickness is achieved	17
Scheme 2.1: Proposed structure of pNIPAm-DHEA and pNIPMAM-DHEA microgels. Adapted from Reference 15.	30
Scheme 2.2: Core particles containing the degradable cross-linker DHEA and pNIPAm or pNIPMAM are used as templates for the subsequent addition of a shell composed of pNIPAm-BIS. The core is then degraded by exposure to NaIO ₄ and removed by centrifugation leaving a “hollow” microgel.	36
Scheme 4.1: Conjugation of PLL to AlexaFluor 488 Carboxylic Acid, Succinimidyl Ester to create the conjugated PLL (PLL [*]).	75
Scheme 5.1: Schematic drawing of the mechanism of exponential polyelectrolyte film growth, starting with a negatively charged film (a). The film is put in contact with a polycation solution (b), which diffuses into the film concentrating at the top of the film and creating charge overcompensation. After rinsing (c), some interpenetrated polycation remains within the film. Exposure to an oppositely charged polyanion (d) creates diffusion of the excess polycation “out” of the film and polyanion will diffuse “in”. Concomitant charge overcompensation and charge reversal results (e).	103
Scheme A.1: Scheme showing the experimental setup for the chemical etching of Pt Wires to produce sharp Pt tips.	139
Scheme A.2: Pt wire etching with CaCl ₂ and subsequent removal to create a hollow glass nanopore.	143

LIST OF SYMBOLS

α	radius of Pt wire
D	diffusion coefficient
F	Faraday's constant
κ	conductivity (Appendix A)
κ	time constant (Chapter 1)
k	Boltzmann's constant
λ_{em}	emission wavelength
λ_{ex}	excitation wavelength
η	viscosity
q	wave vector
R	resistance
r_h	hydrodynamic radius
r_{rms}	root-mean-square radius
τ	delay time
T	temperature
θ	half-cone angle
ω	drive frequency
W	tungsten

LIST OF ABBREVIATIONS

AAc	acrylic acid
AC	alternating current
AFM	atomic force microscopy
Alg	sodium alginate
AM	amplitude modulation
APS	ammonium persulfate
APTMS	3-aminopropyl trimethoxysilane
BIS	<i>N,N'</i> -methylenebisacrylamide
CaCl ₂	calcium chloride
CCD	charge coupled device
CPD	contact potential difference
CLSM	confocal laser scanning microscope
CV	cyclic voltammogram
D-NIPAm	deuterated <i>N</i> -isopropyl acrylamide
DC	direct current
DHEA	(1,2-dihydroxyethylene) bisacrylamide
DLS	dynamic light scattering
EDC	ethyl-3-(3-dimethylaminopropyl) carbodiimide
GNM	glass nanopore membrane
HIS	high ionic strength
KCl	potassium chloride
KOH	potassium hydroxide

KPFM	kelvin probe force microscopy
KPS	potassium persulfate
LbL	layer-by-layer
LCST	lower critical solution temperature
LIS	low ionic strength
MPTMS	3-mercaptopropyl trimethoxysilane
M_w	molecular weight
NaCN	sodium cyanide
NaIO ₄	sodium periodate
PAH	polyallylamine hydrochloride
PDADMAC	poly (diallyldimethylammonium) chloride
PDMS	polydimethylsiloxane
PEG-DA	poly (ethylene glycol) diacrylate
PLL	poly-L-lysine
PNVF	poly (<i>N</i> -vinylformamide)
PSS	polystyrene sulfonate
RPA	resistive pulse analysis
SANS	small angle neutron scattering
scLbL	spin-coating layer-by-layer
SDS	sodium dodecyl sulfate
SEM	scanning electron microscopy
STM	scanning tunneling microscopy
TBAPF ₆	tetra-n-butylammonium hexafluorophosphate

TEM	tunneling electron microscopy
TRPS	tunable resistive pulse sensing
UCST	upper critical solution temperature
V_{CPD}	voltage of the contact potential difference
V_{AC}	voltage of the applied alternating current bias
V_{DC}	direct current voltage
VPTT	volume phase transition temperature

SUMMARY

Hydrogels are water-swelling cross-linked polymeric networks that are capable of incorporating a variety of functionalities and responsivities. The stable colloidal form of a hydrogel is known as a microgel and ranges in size from the nano- to the micrometer scale. Microgels can exhibit similar properties to hydrogels, but the colloidal size of the microgel creates differences in their responsive behavior, such as faster reaction kinetics, as compared to their macrogel counterpart. Microgels have been explored for a broad range of applications, either as individual entities or within large scale assemblies. Although these materials have shown a great deal of utility, microgels have also demonstrated a great deal of complexity due to the fact that they exhibit both polymeric and colloidal properties. This so-called polymer/colloid duality creates intricacies in characterizing the behavior of these materials, especially when coupled with an oppositely charged component within multilayered assemblies.

In this dissertation, work is focused primarily on building a greater fundamental understanding of microgels and their behavior within large scale assemblies. This is done through the development of new characterization techniques, or through a direct visualization of the interactions of microgels with their surrounding environment, which includes their interaction with an oppositely charged species. From a more developed fundamental understanding of these materials, a greater grasp of their utility can be realized. In **Chapter 1**, the background of hydrogels and microgels is given and current characterization techniques and applications are outlined. This fundamental understanding of microgel synthesis is used to create hollow microgels with varied

topology (**Chapter 2**) and uncharged or deuterated microgels in a controlled manner (**Appendix B**).

A method for characterizing individual microgels is presented in **Appendix A**, wherein the creation of glass nanopore membranes is described. The use of these pores in conjunction with resistive pulse analysis is presented as a potential method for unveiling the properties of individual microgels. An additional method for characterizing individual microgels is discussed in **Chapter 3**, in which the surface charge is probed in conjunction with the topography of individual microgels. From this, the effect of various solvent conditions on microgel deposition is proposed, and results suggest complex interactions between the microgel and a linear polyelectrolyte.

Chapter 4 uses optical techniques to explore this multifaceted interaction between the microgel and a linear polyelectrolyte revealing a close relationship between microgel packing during deposition and short-range redistribution of polyelectrolyte. The long-range behavior of a polyelectrolyte was then explored across the depth of a microgel multilayer film (**Chapter 5**), and the diffusivity and exchange behavior of the polyelectrolyte was analyzed. From this, an intricate interaction of the two components is suggested and discussed. In **Chapter 7** additional experiments are proposed to continue building on this fundamental understanding of the complex interactions within microgel assemblies, as well as suggest relevant directions for each of the prior chapters. As a whole, this work serves to show the complexity of microgels, whether individual or within an assembly, and the methods or tools available for developing a more robust understanding of these materials. Through a more robust understanding, a more

developed understanding of the applications or complex behavior of microgels and microgel assemblies can be understood.

CHAPTER 1

INTRODUCTION

Portions adapted from:

Spears, M. W.; Herman, E. S.; Gaulding, J. C.; Lyon, L. A., Dynamic Materials from Microgel Multilayers. *Langmuir*. **2014**, *30*, 6314–6323.

1.1. Polymer Thin Films

Coatings, or films, are an extremely broad class of materials that encompass a large area of study. The use of coatings dates back as far as human existence, with early examples of coatings prevailing within cave paintings which served as one of the first means of art and communication.^{1,2} Since these early examples of coatings, an industry surrounding coatings has been cultivated and continues to mature and expand. The interest in coatings lies in the wide range of applications, from the everyday (i.e. paints, paper, surface protection, insulation); to biological (i.e. drug delivery, tissue engineering, antimicrobial). As broad as the available applications of thin film coatings, the list of available materials for such films is increasing continually. Within this field, polymeric materials continue to grow in interest due to their numerous capabilities, such as adaptability to environments, conversion of biochemical and chemical signals, and incorporation of responsivity^{3,4} to name a few.

A prominent method for the formation of polymeric thin films is known broadly as self-assembly. The appeal of this technique lies in the ability to deposit a single molecular layer onto a substrate from which an ordered multilayer film can be created.⁵ The first notable method that employed self-assembly was developed in the 1930's and is

known as the Langmuir-Blodgett technique.^{6,7} Films produced through the Langmuir-Blodgett technique were first shown conceptually when a monomolecular oil film was deposited onto a substrate by dipping the substrate into a water solution containing the oil at the surface.⁶ Although this technique seemed ideal for the quick formation of thin films, it tended to produce films that were limited in terms of film quality, stability and versatility.⁵ Because of this, techniques that improved upon these limitations were desired.

One such technique is known as Layer-by-Layer (LbL) deposition. The LbL deposition technique allows for the alternating deposition of building blocks to form multilayer thin films.⁸ This can be done through a variety of driving forces, from hydrogen bonding⁹ to charge transfer interactions.¹⁰ However, the most predominant method for LbL deposition is Coulombically-driven assembly due to its ability to incorporate most charged species. This method was initially investigated by Iler et al. in 1964.¹¹ It was later expanded upon and popularized by the Decher group in 1992 when the ease of use and versatility of the technique were brought to light.¹² In this first example, a positively charged substrate was dipped into a solution of negatively charged species, thereby decorating the surface and resulting in charge reversal. Subsequent immersion into a solution of positively charged species resulted in the adsorption and concomitant charge reversal, returning the film surface to the original positive charge. This process can be repeated until the desired thickness or number of alternating layers is achieved.⁵ The technique offers a simple and versatile method for building thin films that can theoretically be composed of any oppositely charged pairs. The approach has been employed for films composed of more than 100 layers without compromising stability.¹³

An expansive body of work has focused on studying the use of polyelectrolytes and other charged species in Coulombically-driven assembly since the early work of Decher et al. From this, a deeper and more enriched understanding of thin film assembly and growth has been developed. Initially it was believed that multilayer films created through Coulombically-driven LbL assembly always grew linearly, with the same amount of polymer (or thickness) being added in each step. However, continued efforts with polyelectrolytes led to the production of multilayer films exhibiting exponential growth,^{14,15} revealing a previously unrealized complexity in polyelectrolyte multilayer film growth. In this case, non-linear growth behavior was attributed to the mobility of one or both polyelectrolytes involved in film formation, which allows for the diffusion of polyelectrolytes “in” and “out” of the film as each layer is added.^{15,16,17} Film composed with other charged components, such as proteins^{18,19} or hard spheres^{20,21}, have also shown complex growth behavior. However, in this case the non-linear growth behavior is attributed to changes in environmental conditions that alter the homogeneity of multilayer film assembly. An understanding of this homogenous growth behavior will not be discussed in this chapter, but the large body of work surrounding homogeneous film growth will be described in more detail within this thesis, particularly as it relates to the supramolecular assembly of charged microgels.

1.2. Hydrogels

Hydrogels are cross-linked networks of hydrophilic polymers capable of swelling and holding large quantities of solvent.^{22,23,24} These solvent swollen networks are attractive for a variety of applications due to their capacity to act as reservoirs for drug loading²² as well as their ability to incorporate biocompatibility²³ and responsivity.²⁵

Hydrogels have been of particular interest within the realm of biomedical applications,²³ such as drug delivery,^{23,26} cell encapsulation,²⁷ and tissue engineering,²⁸ with particular interest lying in the incorporation of responsivity for the production of “smart” hydrogels.^{29,30}

Responsive gel networks were first shown in 1949 by Katchalsky, who showed swelling or de-swelling of a gel network consisting of cross-linked polyelectrolytes in response to pH changes.³¹ However, the utility of water swollen hydrogel networks in biomedical applications wasn't realized until 1960. In this year, Wichterle, proposed the use of water swollen networks in place of plastics to solve the (then current) biocompatibility issue.³² He proposed that by using water swollen cross-linked networks, issues such as mechanical irritation and tumorous growth would be alleviated, and from this foundational work the soft contact lens was created. Although the work of Wichterle did not incorporate responsivity, his work became a foundation for the development of many of the responsive hydrogel systems available currently.³³ Wichterle et al. were able to outline the necessary features of hydrogel systems for biological application, such as permission of water, inertness to biological environment, and permeability of metabolites, which still hold true for the design of biologically friendly materials today. Research has expanded tremendously from this and now encompasses a large variety of biologically relevant responsive materials, which are capable of responding to stimuli such as temperature³⁴, electric signal,³⁵ biomolecules,³⁶ or light^{37,38} just to name a few.

The responsivity of hydrogels typically takes place in the form of a volume phase transition. For example, hydrogels with an incorporated thermo-responsive moiety exhibit a reversible volume phase transition upon heating.²² This phase transition is

related to a polymer phase separation as the network is raised above the lower critical solution temperature (LCST), or in some special cases cooled below the upper critical solution temperature (UCST) of the incorporated thermo-responsive polymer.^{23,39} The most widely studied thermo-responsive polymer is poly(*N*-isopropylacrylamide) (pNIPAm), which exhibits an LCST of 31 °C.⁴⁰ At lower temperatures hydrogen bonding between the solvent and the polymer dominate, but at the LCST hydrophobic interactions become strengthened, resulting in water expulsion and a coil to globule transition.²² When this transition takes place in a cross-linked network, this is commonly known as the volume phase transition temperature (VPTT).⁴¹

1.3. Microgels

Colloidally-stable hydrogels ranging from nano- to several micrometers in size are typically referred to as microgels.⁴² Microgels hold similar characteristics to macroscopic hydrogels, such as a VPTT near the LCST of the polymer,⁴³ and ability to incorporate various types of responsivity.^{43,44,45} These characteristics coupled with the size range of microgels makes them a particularly attractive class of materials. For example, the available colloidal size range of microgels makes them ideal for encapsulation and delivery of therapeutics,^{46,47} and their versatility allows for the design of advanced architectures for a variety of applications.⁴⁸ Responsive microgels can also be incorporated into macroscopic assemblies⁴⁹ which can hold the properties of the microscopic building blocks.⁵⁰ The remainder of this chapter will focus on the design and characterization of microgels, as well as their incorporation and utilization within larger scale assemblies.

1.3.1. Microgel Synthesis

There are a variety of methods that have been employed for the synthesis of microgels, such as emulsion polymerization,⁵¹ photolithographic and micromolding methods,⁵² microfluidic preparation,⁵³ and controlled living polymerization.⁵⁴ The method used throughout this work takes advantage of the thermo-responsive properties of pNIPAm or poly(*N*-isopropylmethacrylamide) (pNIPMAm), and is known as free radical precipitation polymerization. First reported in 1986 by Pelton,⁵⁵ this facile method allows for the creation of monodisperse thermo-responsive microgel particles. For this, the monomer (NIPAm or NIPMAm, for example), co-monomers (such as acrylic acid (AAc), if desired) and cross-linker (such as *N,N'*-methylenebisacrylamide (BIS)) are dissolved in distilled deionized water, heated to approximately 70 °C (above the LCST of the polymer) and purged with nitrogen to remove oxygen. A radical initiator is then added to the solution, commonly ammonium persulfate (APS) or potassium persulfate (KPS). The heightened temperature allows for the thermal decomposition of the initiator to sulfate radicals and polymer chain growth begins. Once the growth of the polymer chain reaches a critical length, it collapses into a precursor particle.⁴³ This precursor particle can then continue growth through collapse onto an existing particle, through monomer capture, or aggregation with other precursor particles.⁴³ Polymerization and growth will continue until the particle reaches a colloidally stable size, at which point the final microgel is formed.⁴³ The size and monodispersity of microgel particles formed through precipitation polymerization can be controlled by changing the concentrations of initiator and surfactant,⁵⁶ or ramping the temperature used during polymerization, which has been shown to create larger microgels.⁵⁷ The synthesis of microgels is shown

schematically in **Scheme 1.1**. Included in this schematic is the surfactant sodium dodecyl sulfate (SDS), a commonly used surfactant for particle stabilization during precipitation polymerization.



Scheme 1.1. Scheme showing the production of pNIPam-AAc microgels containing the cross-linker BIS through free-radical precipitation.

Precipitation polymerization not only allows (via co-polymerization) for the incorporation of various responsive moieties such as pH^{58,59} or degradability,^{60,61} but also allows for the formation of multi-compartment microgels, such as core/shell^{62,63} through a seeded precipitation polymerization method. This was first shown in 2000 by Jones et al. when core/shell microgels were synthesized with an incorporated pH responsive co-monomer, AAc, within the core.⁵⁸ For this method, core particles synthesized through precipitation polymerization as described above are used as templates for the production of a microgel shell. This is done by heating a solution of purified core particles and the shell monomer and cross-linkers above the LCST of the thermo-responsive component (typically 70 °C) while purging with nitrogen. Surfactant is also typically used to stabilize the polymerization. The initiator is then added and chain growth begins. Once oligomeric growth reaches a critical point, the shell precursor particle collapses onto the core particle. The shell will grow on the core template until the shell monomer and cross-linker is exhausted or until the solution is cooled. The resultant core/shell structure can contain a diverse array of responsivity and since the initial work of Jones et al.

advanced architectures have been created,⁶⁴ such as core/ double shell⁴⁸ or hollow microgels, wherein a degradable component is incorporated into the core.⁶³ **Chapter 2** will discuss the utilization of this seeded precipitation polymerization technique for the formation of more robust hollow microgels for potential efficacy as drug delivery vehicles.

1.3.2. Characterization

Several techniques will be used throughout this thesis to analyze and characterize microgels and microgel assemblies. In this section, a general overview of the techniques will be given in order to set the stage for subsequent chapters which will give detailed information about microgel and microgel assemblies as characterized by dynamic light scattering (DLS), atomic force microscopy (AFM) and optical microscopy techniques.

1.3.2.1. Dynamic Light Scattering (DLS)

In a dilute solution of particles, the movement of individual particles can be described as a 3D random walk (also known as Brownian motion), which is described by a diffusion coefficient.⁴¹ This diffusion coefficient, D , can be used to gain size information about particles in solution through the Stokes-Einstein equation:

$$r_h = \frac{kT}{6\pi\eta D} \quad \text{Equation 1.1.}$$

Where k , T , and η are Boltzmann's constant, temperature in kelvin, and viscosity of the solvent, respectively.

DLS is a technique used to determine the diffusion coefficient, and therefore size, of a particle in solution. First, a dilute solution of particles is hit with a monochromatic laser light. This light is then scattered from the particles in all directions, a phenomenon known as Rayleigh scattering. The light intensity fluctuations from the particles in

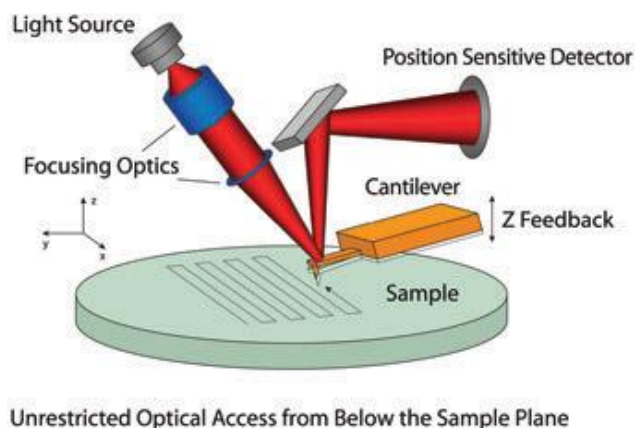
solution are recorded over time at a specific detector angle. For the work shown within this angle is 90° . An autocorrelation function is then used to plot the average change in light intensity over time as a function of delay time (τ). A cumulant fit, which assumes a single exponential decay, is then used to determine the time constant (κ) associated with the autocorrelation function, and this is then used to determine the diffusion coefficient (D):

$$\kappa = \frac{1}{2Dq^2} \quad \text{Equation 1.2.}$$

Here, q is the wave vector, which is dependent on the scattering angle. Once the diffusion coefficient is known, the Stokes-Einstein equation (**Equation 1.1.**) can be used to determine the hydrodynamic radius (r_h) of the particle. Taking these two equations together, we see that the time-dependent intensity fluctuations are directly correlated to the diffusion of the particle in solution (**Equation 1.2.**) and the r_h is inversely related to the diffusion coefficient (**Equation 1.1.**). Because of this, it can be concluded that the recorded intensity fluctuations are dependent on the size of the particle. Fundamentally, this means that as the size of the particle increases, the diffusion coefficient will decrease due to slower movement in solution and therefore the larger the particle, the smaller the intensity fluctuations. Qualitatively this is exhibited by late decay in the autocorrelation function. DLS measurements on microgels presented in **Chapter 2** were calculated at various temperatures. This was to determine the r_h of the microgels when swollen and deswollen or below and above their characteristic VPTT, respectively.

1.3.2.2. Atomic Force Microscopy (AFM)

AFM is a common method for gaining topographical information of surfaces. AFM was first designed as an improved method of imaging over scanning tunneling microscopy (STM). Although STM was a technique that grew in success in a very short time frame, and won the inventors a Nobel Prize in 1986, it was limited to samples that were conductive.⁶⁵ AFM was developed, and is used as a standard imaging technique today, in order to gain topographical information of surfaces on a small scale (down to 1 nm) without the limitations presented with STM. This means that samples can be soft or hard, and can be imaged in-liquid,⁶⁶ in-air and in some cases under vacuum.⁶⁷ This technique is also beneficial over other microscopy techniques, such as scanning electron microscopy (SEM) or tunneling electron microscopy (TEM), because AFM samples do not need to be conductive, coated, or stained in any way, minimizing the necessary sample preparation.



Scheme 1.2. A generalized set-up of AFM optical lever detection. A laser light is reflected from the cantilever and recorded by a position-sensitive detector. Image taken from Asylum Research.⁸⁹

The general set-up of AFM can be seen in **Scheme 1.2**. A sharp tip attached to a flexible cantilever is scanned across a sample surface. A laser is reflected from the back

of the cantilever and into a position-sensitive photodiode detector, which records small changes in the deflection of the cantilever as it is introduced to surface features. In response, small directional changes are achieved using piezo-electric material located in the AFM stage (x,y) and the AFM head (z-direction).

In the simplest form, AFM is used in contact mode. For this, the tip is rastered over the surface and the bending up and down of the tip in response to surface features is recorded as a topographical map in x,y. Due to the softness of microgels, it is necessary to use a mode of operation that is less invasive and minimizes the chance of damage to the surface. Typically, soft materials are imaged through an intermittent contact mode known as “tapping” mode, wherein a tip is oscillated near its resonant frequency. Instead of being in constant contact, the tip is tapped over the sample, intermittently coming into contact with the soft surface. For this mode, amplitude modulation (AM) is used with the z-piezo scanner to maintain a constant amplitude and this information is used to generate a topographical mapping of the surface.⁶⁷

The use of more advanced imaging techniques is also of interest for characterizing different microgel constructs. For example, in-liquid AFM has been shown to be a useful technique for monitoring the degradation of microgels in solution.⁶⁸ Another advanced technique that will be discussed in detail in **Chapter 3** is kelvin probe force microscopy (KPFM), which measures potential differences between a surface and the tip thereby mapping the surface potential of the sample.⁶⁹ This is done by using a conductive AFM tip, which upon exposure to an alternating current (AC) bias, will tap the surface of the sample. The big difference between AFM and KPFM is the way in which the tip is driven. There is no mechanically induced drive and the oscillation of the tip is

completely dictated by an electrical bias that is added to the system. Since the mode with which the tip is being oscillated differs, the feedback loop used to compensate for deflections of the tip will also differ. Whereas in AC tapping mode the amplitude is adjusted to compensate for surface interactions, in KPFM a direct current (DC) voltage is added to maintain the electrically-driven tip. The detailed potential information given from this feedback loop is recorded in conjunction with the topographical information through a two pass technique wherein the first pass is done in AC mode using a piezo-electrically driven tip in tapping mode to gain topological information, and on second pass the tip is raised above the surface (nap mode) and is driven electrically to record potential information. Although traditionally used to gain insight into conductive surfaces, this technique has shown promising results for non-conductive materials deposited onto a conductive substrate.^{70,71} More detailed information regarding the fundamentals of KPFM will be discussed in **Chapter 3** and its application for mapping charge distribution in microgels and microgel assemblies will be presented.

1.3.2.3. Optical Microscopy Techniques

Large portions of **Chapter 4** and **Chapter 5** will discuss the use of optical microscopy techniques, such as brightfield, epi-fluorescence and confocal fluorescence microscopy, for the analysis of polyelectrolyte and microgel behavior on surfaces as well as microgel/polyelectrolyte behavior within macroscopic structures. These microscopy techniques are useful for visualizing individual components or macroscopic structures, and as will be shown in subsequent chapters allowed for a more in-depth analysis of individual microgel particles and their assemblies.

Optical microscopy has been in use for many years as a way of directly visualizing small structures on a surface. In its simplest form, a light microscope is used to illuminate a sample under magnification and this magnified sample image is recorded for later analysis, such as particle size. Optical microscopes come in either upright or inverted, with the main difference being the location of the light source, the condenser and objective. The latter two are important lens components; the condenser focuses light on the sample and the objective collects and focuses light from the sample to produce an image. In an inverted microscope, The light source and condenser are located above the sample, with the objectives located below, which has been shown to be beneficial for imaging samples in solution.⁷² In **Chapter 4**, an IX-71 inverted Olympus microscope was used in conjunction with a charge coupled device (CCD) to image samples using a 40x or 100x objective. An example of an inverted microscope is shown in **Figure 1.1**.

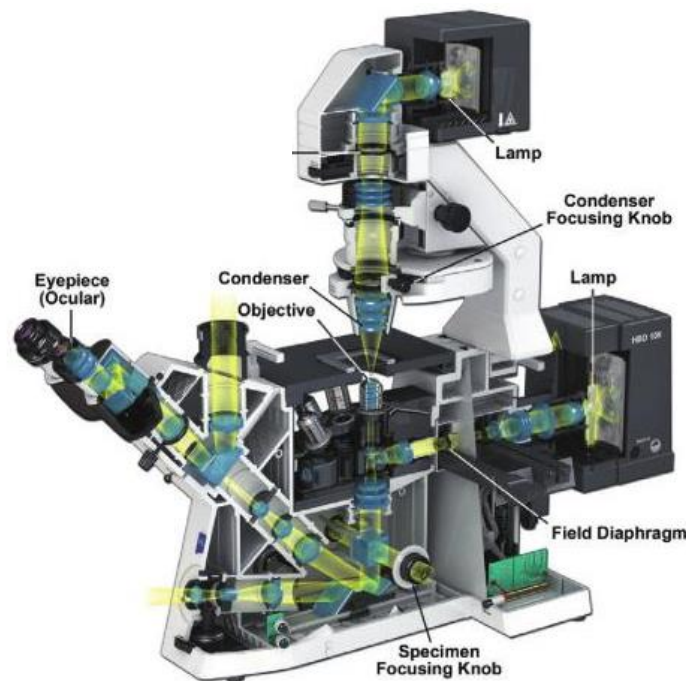


Figure 1.1. Inverted microscope image.⁷² The microscope shown is a Zeiss Axio Observer inverted microscope similar in design to the Olympus IX-71 inverted microscope.

Two sources of illumination are shown in **Figure 1.1**, and this is due to the fact that the optical microscope can house a light source for both brightfield and fluorescence. The light source located at the back of the microscope is filtered to illuminate the sample at a specific wavelength known as the excitation wavelength (λ_{ex}) and collect light at a wavelength known as the emission wavelength (λ_{em}).⁷³ These excitation and emission wavelengths are built into filters, which are usually located in a single block below the objective. These emission and excitation filters can be adjusted for specific fluorophores that are incorporated into the illuminated sample. The application of this will be shown for assemblies containing microgels and a fluorescent polyelectrolyte in **Chapter 4**.

Confocal microscopy is an advanced method of fluorescence microscopy that is commonly used. Whereas in epi-fluorescence microscopy a sample is imaged without the ability to obtain depth information, in confocal microscopy point illumination and a pinhole are used to gain optical resolution in the z-dimension by eliminating out of focus light. This means that a sample can be imaged at specific depths, known as optical sectioning, and these sections can be reconstructed to give a 3D profile of a sample.⁷⁴ First described in 1957 by Marvin Minsky, this technique has grown immensely over the years because it allows for increased resolution, reduced blurring, improved signal-to-noise, as well as the aforementioned increased optical resolution in the z-dimension.⁷⁵ For the studies shown in **Chapter 5**, a confocal laser scanning microscope (CLSM), specifically a Zeiss LSM 700, is used with a laser light excitation source. This is a commonly used type of confocal microscope, which holds all of the advantages listed

above making it ideal for probing components within the confines of an assembly. This will be shown for microgel-polyelectrolyte multilayer films in **Chapter 5**.

1.3.3. Microgels as Building Blocks for Multilayer Thin Films

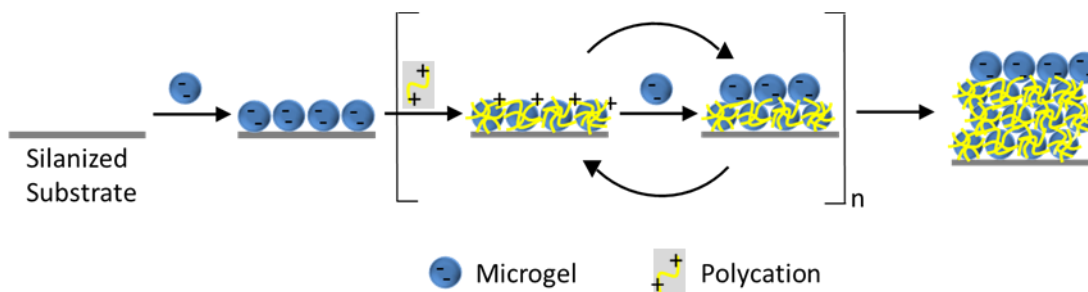
As stated above, hydrogels and hydrogel microparticles (or microgels) can be environmentally responsive. However, Tanaka et al. were able to show that the de-swelling of a gel is diffusion limited, and the swelling rate is inversely proportional to the square of the gel dimension.⁷⁶ Therefore, the swelling kinetics of hydrogel materials is closely related to the size of the material, and it was shown that reducing hydrogel size resulted in changes in de-swelling behavior in response to stimuli.^{77,78,79} Because of this size dependence, it is of great interest to create larger assemblies by incorporating microgels into a bulk assembly. These assemblies could contain responsivity, however by reducing the size of the responsive hydrogel component, the swelling constraints of bulk hydrogel systems could be alleviated. This could possibly improve the utilization of such materials in applications such as drug delivery or biointerfaces, two common applications of hydrogels.⁸⁰

In addition, microgel assemblies could be beneficial because response can be more controllable or the system could possibly respond to multiple stimuli. An example of this can be seen in the “plum pudding” gel created by Dawson et al., which is constituted of a gel matrix with embedded responsive microgels. This system showed the controlled release of two solutes with differing physicochemical properties from two different microgel types within the same gel matrix.⁸¹ More recently, a microgel assembly was constructed with microgels containing varying degrees of responsive components. The swelling behavior of these assemblies suggested that independent

microgel particles can act autonomously to one another.⁵⁰ This study showed the potential of controlled bulk hydrogel systems composed through the incorporation of smaller microgel components and continued efforts within this area are ongoing.

In the Lyon group, we have developed a modified LbL assembly technique for the incorporation of microgels into larger bulk systems. Because ionizable monomer units are incorporated during synthesis, microgels are trivially used for the formation of thin films via Coulombic LbL. As described above, LbL is a versatile technique, which allows for the formation of multilayered systems from charged species. The formation of LbL films using environmentally responsive microgels as the polyanion was first shown in 2003⁸² using passive deposition. Although the use of nanoparticles in the formation of LbL films was not in itself a novel idea, the use of soft, porous colloidal particles as opposed to hard spheres was unique, as was the incorporation of environmental responsivity within such films. These initial studies of microgel films built using the LbL technique, although promising, were lacking because the microgels did not deposit in a homogeneous way and therefore created a “patchy” surface. This was not ideal for the formation of well-defined films, and an improved deposition technique was desired. The first approach involved the use of the spin-coating layer-by-layer technique (scLbL)⁸³ in which a specific microgel volume was deposited and rinsed with water and a polyelectrolyte was deposited in the same fashion, all while the substrate was spinning at a specific speed. This technique allowed for quicker assembly of more densely packed films, but the high concentrations and large solution volumes necessary proved to be materially inefficient. Following this, an “active” deposition technique^{84,85} known as centrifugal deposition was developed to maintain efficiency and reproducibility but also

to allow for a more economical and efficient use of materials. This technique uses centrifugation to assemble microgel particles into a monolayer onto substrates in a much more well-defined, close-packed fashion. The change in packing of the particles on the surface can be attributed to the added force applied by centrifugal deposition, which appeared to overcome some particle–particle interactions and decrease the particle footprint as compared to passive deposition. Tight packing continues as each successive layer is added, causing a decrease in particle size and what appears to be particle rearrangement.⁸⁴ This technique is still employed today for the formation of well-packed microgel multi-layer films and is diagrammed in **Scheme 1.3**.



Scheme 1.3. Anionic microgels are centrifugally deposited onto a silanized substrate and introduced to a cationic polyelectrolyte; this process is repeated until a desired thickness is achieved.

1.4. Dynamic Behavior of Microgel Thin Films

Continued work in more recent years with microgel multilayer thin films has unveiled dynamic behavior. This was first shown for microgel multilayer films upon damage events. For this, films were built using the centrifugation based LbL technique as shown above on the elastic substrate polydimethylsiloxane (PDMS). Upon mechanical deformation of the film from poking, bending, or stretching, the films

exhibited a noticeable optical change from clear to opaque. These films were then immersed in deionized water, and upon drying under nitrogen they no longer exhibited any defect.^{84,85} This self-healing was validated by light microscopy and AFM. It has also been shown that microgel multilayer films are able to alter cell adhesion.^{86,87}

Efforts to determine the source of the dynamic behavior of microgel thin films have focused on probing the behavior of multilayer microgel films during and after mechanical deformation. The resultant data suggested the healing behavior of microgel thin films is influenced by the swellability of microgels within the structure.⁸⁸ Disruption of the self-healing behavior has also been explored through the incorporation of cross-linking agents, such as glutaraldehyde or 1-ethyl-3-(3-dimethylaminopropyl) carbodiimide (EDC) coupling.⁸⁶ This showed that by cross-linking the components within microgel films, the film becomes much stiffer and self-healing behavior is interrupted creating irreparable fractures to the surface. This suggests an inability of individual components within microgel thin films to rearrange into a more favorable composition, or to a healed arrangement.

Although these more recent efforts have shown how microgel films as a whole could be easily manipulated and dynamic behavior could be modulated, a true fundamental understanding of microgels and their cationic counterpart, the polyelectrolyte, has yet to be revealed within the larger bulk structure of microgel multilayer thin films. An understanding of the behavior of these individual components within larger bulk films will create a more robust picture of film assembly and dynamic behavior. In **Chapters 4** and **Chapter 5** following, the interaction of microgels and

polyelectrolyte will be probed and analyzed, and the implications of these interactions will be discussed.

1.5. References

- [1] Australia, S. C. A.; Association, O. C. C., *Surface Coatings: Volume 1 Raw Materials and Their Usage*. Springer Netherlands: 1993.
- [2] Marrion, A.; Chemistry, R. S. o., *The Chemistry and Physics of Coatings*. Royal Society of Chemistry: 2004.
- [3] Stuart, M. A. C.; Huck, W. T. S.; Genzer, J.; Muller, M.; Ober, C.; Stamm, M.; Sukhorukov, G. B.; Szleifer, I.; Tsukruk, V. V.; Urban, M.; Winnik, F.; Zauscher, S.; Luzinov, I.; Minko, S., Emerging Applications of Stimuli-Responsive Polymer Materials. *Nat. Mater.* **2010**, *9*, 101-113.
- [4] Hammond, P. T., Form and Function in Multilayer Assembly: New Applications at the Nanoscale. *Adv. Mater.* **2004**, *16*, 1271-1293.
- [5] Decher, G., Fuzzy Nanoassemblies: Toward Layered Polymeric Multicomposites. *Science* **1997**, *277*, 1232-1237.
- [6] Blodgett, K. B., Monomolecular Films of Fatty Acids on Glass. *J. Am. Chem. Soc.* **1934**, *56*, 495-495.
- [7] Blodgett, K. B.; Langmuir, I., Built-up Films of Barium Stearate and Their Optical Properties. *Physical Review* **1937**, *51*, 964-982.
- [8] Zhang, X.; Chen, H.; Zhang, H., Layer-by-Layer Assembly: From Conventional to Unconventional Methods. *Chem. Commun.* **2007**, 1395-1405.
- [9] Stockton, W. B.; Rubner, M. F., Molecular-Level Processing of Conjugated Polymers. 4. Layer-by-Layer Manipulation of Polyaniline Via Hydrogen-Bonding Interactions. *Macromolecules* **1997**, *30*, 2717-2725.
- [10] Shimazaki, Y.; Mitsuishi, M.; Ito, S.; Yamamoto, M., Preparation of the Layer-by-Layer Deposited Ultrathin Film Based on the Charge-Transfer Interaction. *Langmuir* **1997**, *13*, 1385-1387.
- [11] Iler, R. K., Multilayers of Colloidal Particles. *J. Colloid Interface Sci.* **1966**, *21*, 569-594.

- [12] Decher, G.; Hong, J. D.; Schmitt, J., Buildup of Ultrathin Multilayer Films by Self-Assembly Process .3. Consecutively Alternating Adsorption of Anionic and Cationic Polyelectrolytes on Charged Surfaces. *Thin Solid Films* **1992**, *210*, 831-835.
- [13] Knoll, W., Self-Assembled Microstructures at Interfaces. *Curr. Opin. Colloid Interface Sci.* **1996**, *1*, 137-143.
- [14] Lavallo, P.; Voegel, J. C.; Vautier, D.; Senger, B.; Schaaf, P.; Ball, V., Dynamic Aspects of Films Prepared by a Sequential Deposition of Species: Perspectives for Smart and Responsive Materials. *Adv. Mater.* **2011**, *23*, 1191-1221.
- [15] Porcel, C.; Lavallo, P.; Ball, V.; Decher, G.; Senger, B.; Voegel, J. C.; Schaaf, P., From Exponential to Linear Growth in Polyelectrolyte Multilayers. *Langmuir* **2006**, *22*, 4376-4383.
- [16] Lavallo, P.; Picart, C.; Mutterer, J.; Gergely, C.; Reiss, H.; Voegel, J. C.; Senger, B.; Schaaf, P., Modeling the Buildup of Polyelectrolyte Multilayer Films Having Exponential Growth. *J. Phys. Chem. B* **2004**, *108*, 635-648.
- [17] Picart, C., Polyelectrolyte Multilayer Films: From Physico-Chemical Properties to the Control of Cellular Processes. *Curr. Med. Chem.* **2008**, *15*, 685-697.
- [18] Lvov, Y.; Ariga, K.; Ichinose, I.; Kunitake, T., Assembly of Multicomponent Protein Films by Means of Electrostatic Layer-by-Layer Adsorption. *J. Am. Chem. Soc.* **1995**, *117*, 6117-6123.
- [19] Hodak, J.; Etchenique, R.; Calvo, E. J.; Singhal, K.; Bartlett, P. N., Layer-by-Layer Self-Assembly of Glucose Oxidase with a Poly(Allylamine)Ferrocene Redox Mediator. *Langmuir* **1997**, *13*, 2708-2716.
- [20] Kotov, N. A.; Dekany, I.; Fendler, J. H., Layer-by-Layer Self-Assembly of Polyelectrolyte-Semiconductor Nanoparticle Composite Films. *J. Phys. Chem.* **1995**, *99*, 13065-13069.
- [21] Hicks, J. F.; Seok-Shon, Y.; Murray, R. W., Layer-by-Layer Growth of Polymer/Nanoparticle Films Containing Monolayer-Protected Gold Clusters. *Langmuir* **2002**, *18*, 2288-2294.
- [22] Qiu, Y.; Park, K., Environment-Sensitive Hydrogels for Drug Delivery. *Adv. Drug Delivery Rev.* **2001**, *53*, 321-339.
- [23] Peppas, N. A.; Hilt, J. Z.; Khademhosseini, A.; Langer, R., Hydrogels in Biology and Medicine: From Molecular Principles to Bionanotechnology. *Adv. Mater.* **2006**, *18*, 1345-1360.

- [24] Hoffman, A. S., Hydrogels for Biomedical Applications. *Adv. Drug Delivery Rev.* **2002**, *54*, 3-12.
- [25] Gehrke, S., Synthesis, Equilibrium Swelling, Kinetics, Permeability and Applications of Environmentally Responsive Gels. In *Responsive Gels: Volume Transitions II*, Dušek, K., Ed. Springer Berlin Heidelberg: 1993; Vol. 110, pp 81-144.
- [26] Dinarvand, R.; Demanuele, A., The Use of Thermoresponsive Hydrogels for on-Off Release of Molecules. *J. Controlled Release* **1995**, *36*, 221-227.
- [27] Halstenberg, S.; Panitch, A.; Rizzi, S.; Hall, H.; Hubbell, J. A., Biologically Engineered Protein-Graft-Poly(Ethylene Glycol) Hydrogels: A Cell Adhesive and Plasm in-Degradable Biosynthetic Material for Tissue Repair. *Biomacromolecules* **2002**, *3*, 710-723.
- [28] Bhattarai, N.; Ramay, H. R.; Gunn, J.; Matsen, F. A.; Zhang, M., Peg-Grafted Chitosan as an Injectable Thermosensitive Hydrogel for Sustained Protein Release. *J. Controlled Release* **2005**, *103*, 609-624.
- [29] Bajpai, A. K.; Shukla, S. K.; Bhanu, S.; Kankane, S., Responsive Polymers in Controlled Drug Delivery. *Prog. Polym. Sci.* **2008**, *33*, 1088-1118.
- [30] Miyata, T.; Asami, N.; Uragami, T., A Reversibly Antigen-Responsive Hydrogel. *Nature* **1999**, *399*, 766-769.
- [31] Katchalsky, A., Rapid Swelling and Deswelling of Reversible Gels of Polymeric Acids by Ionization. *Experientia* **1949**, *5*, 319-320.
- [32] Wichterle, O.; Lim, D., Hydrophilic Gels for Biological Use. *Nature* **1960**, *185*, 117-118.
- [33] Gupta, P.; Vermani, K.; Garg, S., Hydrogels: From Controlled Release to Ph-Responsive Drug Delivery. *Drug Discov. Today* **2002**, *7*, 569-579.
- [34] Bromberg, L. E.; Ron, E. S., Temperature-Responsive Gels and Thermogelling Polymer Matrices for Protein and Peptide Delivery. *Adv. Drug Delivery Rev.* **1998**, *31*, 197-221.
- [35] Tanaka, T.; Nishio, I.; Sun, S. T.; Uenonishio, S., Collapse of Gels in an Electric-Field. *Science* **1982**, *218*, 467-469.
- [36] Miyata, T.; Uragami, T.; Nakamae, K., Biomolecule-Sensitive Hydrogels. *Adv. Drug Delivery Rev.* **2002**, *54*, 79-98.

- [37] Mamada, A.; Tanaka, T.; Kungwatchakun, D.; Irie, M., Photoinduced Phase-Transition of Gels. *Macromolecules* **1990**, *23*, 1517-1519.
- [38] Suzuki, A.; Tanaka, T., Phase-Transition in Polymer Gels Induced by Visible-Light. *Nature* **1990**, *346*, 345-347.
- [39] Seuring, J.; Agarwal, S., Polymers with Upper Critical Solution Temperature in Aqueous Solution. *Macromol. Rapid Commun.* **2012**, *33*, 1898-1920.
- [40] Schild, H. G., Poly(N-Isopropylacrylamide): Experiment, Theory and Application. *Prog. Polym. Sci.* **1992**, *17*, 163-249.
- [41] Shibayama, M.; Tanaka, T., Volume Phase-Transition and Related Phenomena of Polymer Gels. *Adv. Polym. Sci.* **1993**, *109*, 1-62.
- [42] Baker, W. O., Microgel, a New Macromolecule. *Industrial & Engineering Chemistry* **1949**, *41*, 511-520.
- [43] Pelton, R., Temperature-Sensitive Aqueous Microgels. *Adv. Colloid Interface Sci.* **2000**, *85*, 1-33.
- [44] Nayak, S.; Lyon, L. A., Soft Nanotechnology with Soft Nanoparticles. *Angew. Chem., Int. Ed.* **2005**, *44*, 7686-7708.
- [45] Gaulding, J. C.; Smith, M. H.; Hyatt, J. S.; Fernandez-Nieves, A.; Lyon, L. A., Reversible Inter- and Intra-Microgel Cross-Linking Using Disulfides. *Macromolecules* **2012**, *45*, 39-45.
- [46] Smith, M. H.; Lyon, L. A., Multifunctional Nanogels for Sirna Delivery. *Acc. Chem. Res.* **2012**, *45*, 985-993.
- [47] Hellweg, T.; Dewhurst, C. D.; Brückner, E.; Kratz, K.; Eimer, W., Colloidal Crystals Made of Poly(N-Isopropylacrylamide) Microgel Particles. *Colloid Polym. Sci.* **2000**, *278*, 972-978.
- [48] Hu, X. B.; Tong, Z.; Lyon, L. A., Multicompartment Core/Shell Microgels. *J. Am. Chem. Soc.* **2010**, *132*, 11470-11472.
- [49] Debord, J. D.; Lyon, L. A., Thermoresponsive Photonic Crystals. *J. Phys. Chem. B* **2000**, *104*, 6327-6331.
- [50] Clarke, K. C.; Lyon, L. A., Modulation of the Deswelling Temperature of Thermoresponsive Microgel Films. *Langmuir* **2013**, *29*, 12852-12857.
- [51] Saunders, B. R.; Vincent, B., Microgel Particles as Model Colloids: Theory, Properties and Applications. *Adv. Colloid Interface Sci.* **1999**, *80*, 1-25.

- [52] Oh, J. K.; Drumright, R.; Siegwart, D. J.; Matyjaszewski, K., The Development of Microgels/Nanogels for Drug Delivery Applications. *Prog. Polym. Sci.* **2008**, *33*, 448-477.
- [53] Zhang, H.; Tumarkin, E.; Sullan, R. M. A.; Walker, G. C.; Kumacheva, E., Exploring Microfluidic Routes to Microgels of Biological Polymers. *Macromol. Rapid Commun.* **2007**, *28*, 527-538.
- [54] Oh, J. K.; Perineau, F.; Matyjaszewski, K., Preparation of Nanoparticles of Well-Controlled Water-Soluble Homopolymers and Block Copolymers Using an Inverse Miniemulsion Atrp. *Macromolecules* **2006**, *39*, 8003-8010.
- [55] Pelton, R. H.; Chibante, P., Preparation of Aqueous Latices with N-Isopropylacrylamide. *Colloids Surf.* **1986**, *20*, 247-256.
- [56] Blackburn, W. H.; Lyon, L. A., Size-Controlled Synthesis of Monodisperse Core/Shell Nanogels. *Colloid Polym. Sci.* **2008**, *286*, 563-569.
- [57] Meng, Z.; Smith, M.; Lyon, L. A., Temperature-Programmed Synthesis of Micron-Sized Multi-Responsive Microgels. *Colloid Polym. Sci.* **2009**, *287*, 277-285.
- [58] Jones, C. D.; Lyon, L. A., Synthesis and Characterization of Multiresponsive Core-Shell Microgels. *Macromolecules* **2000**, *33*, 8301-8306.
- [59] Hoare, T.; Pelton, R., Functional Group Distributions in Carboxylic Acid Containing Poly(N-Isopropylacrylamide) Microgels. *Langmuir* **2004**, *20*, 2123-2133.
- [60] Smith, M. H.; South, A. B.; Gauding, J. C.; Lyon, L. A., Monitoring the Erosion of Hydrolytically-Degradable Nanogels Via Multiangle Light Scattering Coupled to Asymmetrical Flow Field-Flow Fractionation. *Anal. Chem.* **2009**, *82*, 523-530.
- [61] Smith, M. H.; Herman, E. S.; Lyon, L. A., Network Deconstruction Reveals Network Structure in Responsive Microgels. *The Journal of Physical Chemistry B* **2011**, *115*, 3761-3764.
- [62] Jones, C. D.; Lyon, L. A., Shell-Restricted Swelling and Core Compression in Poly(N-Isopropylacrylamide) Core-Shell Microgels. *Macromolecules* **2003**, *36*, 1988-1993.
- [63] Nayak, S.; Gan, D. J.; Serpe, M. J.; Lyon, L. A., Hollow Thermoresponsive Microgels. *Small* **2005**, *1*, 416-421.
- [64] Ballauff, M.; Lu, Y., "Smart" Nanoparticles: Preparation, Characterization and Applications. *Polymer* **2007**, *48*, 1815-1823.

- [65] Giessibl, F. J., Advances in Atomic Force Microscopy. *Rev. Mod. Phys.* **2003**, *75*, 949-983.
- [66] Hansma, P. K.; Cleveland, J. P.; Radmacher, M.; Walters, D. A.; Hillner, P. E.; Bezanilla, M.; Fritz, M.; Vie, D.; Hansma, H. G.; Prater, C. B.; Massie, J.; Fukunaga, L.; Gurley, J.; Elings, V., Tapping Mode Atomic-Force Microscopy in Liquids. *Appl. Phys. Lett.* **1994**, *64*, 1738-1740.
- [67] Haugstad, G., Overview of Afm. In *Atomic Force Microscopy*, John Wiley & Sons, Inc.: 2012; pp 1-32.
- [68] South, A. B.; Lyon, L. A., Direct Observation of Microgel Erosion Via in-Liquid Atomic Force Microscopy. *Chem. Mater.* **2010**, *22*, 3300-3306.
- [69] Melitz, W.; Shen, J.; Kummel, A. C.; Lee, S., Kelvin Probe Force Microscopy and Its Application. *Surf. Sci. Rep.* **2011**, *66*, 1-27.
- [70] Leung, C.; Kinns, H.; Hoogenboom, B. W.; Howorka, S.; Mesquida, P., Imaging Surface Charges of Individual Biomolecules. *Nano Lett.* **2009**, *9*, 2769-2773.
- [71] Sinensky, A. K.; Belcher, A. M., Label-Free and High-Resolution Protein/DNA Nanoarray Analysis Using Kelvin Probe Force Microscopy. *Nat. Nanotechnol.* **2007**, *2*, 653-659.
- [72] Murphy, D. B.; Davidson, M. W., Fundamentals of Light Microscopy. In *Fundamentals of Light Microscopy and Electronic Imaging*, John Wiley & Sons, Inc.: 2012; pp 1-19.
- [73] Quercioli, F., Fundamentals of Optical Microscopy. In *Optical Fluorescence Microscopy*, Diaspro, A., Ed. Springer Berlin Heidelberg: 2011; pp 1-36.
- [74] Carlsson, K.; Danielsson, P. E.; Lenz, R.; Liljeborg, A.; Majlof, L.; Aslund, N., 3-Dimensional Microscopy Using a Confocal Laser Scanning Microscope. *Opt. Lett.* **1985**, *10*, 53-55.
- [75] Inoué, S., Foundations of Confocal Scanned Imaging in Light Microscopy. In *Handbook of Biological Confocal Microscopy*, Pawley, J. B., Ed. Springer US: 2006; pp 1-19.
- [76] Tanaka, T.; Fillmore, D. J., Kinetics of Swelling of Gels. *J. Chem. Phys.* **1979**, *70*, 1214-1218.
- [77] Kuckling, D.; Harmon, M. E.; Frank, C. W., Photo-Cross-Linkable Pnippam Copolymers. 1. Synthesis and Characterization of Constrained Temperature-Responsive Hydrogel Layers. *Macromolecules* **2002**, *35*, 6377-6383.

- [78] Serizawa, T.; Nanameki, K.; Yamamoto, K.; Akashi, M., Thermoresponsive Ultrathin Hydrogels Prepared by Sequential Chemical Reactions. *Macromolecules* **2002**, *35*, 2184-2189.
- [79] Harmon, M. E.; Kuckling, D.; Frank, C. W., Photo-Cross-Linkable Pnippam Copolymers. 2. Effects of Constraint on Temperature and Ph-Responsive Hydrogel Layers. *Macromolecules* **2003**, *36*, 162-172.
- [80] Wiedemair, J.; Serpe, M. J.; Kim, J.; Masson, J.-F.; Lyon, L. A.; Mizaikoff, B.; Kranz, C., In-Situ Afm Studies of the Phase-Transition Behavior of Single Thermoresponsive Hydrogel Particles†. *Langmuir* **2006**, *23*, 130-137.
- [81] Lynch, I.; de Gregorio, P.; Dawson, K. A., Simultaneous Release of Hydrophobic and Cationic Solutes from Thin-Film "Plum-Pudding" Gels: A Multifunctional Platform for Surface Drug Delivery? *J. Phys. Chem. B* **2005**, *109*, 6257-6261.
- [82] Serpe, M. J.; Jones, C. D.; Lyon, L. A., Layer-by-Layer Deposition of Thermoresponsive Microgel Thin Films. *Langmuir* **2003**, *19*, 8759-8764.
- [83] Serpe, M. J.; Lyon, L. A., Optical and Acoustic Studies of Ph-Dependent Swelling in Microgel Thin Films. *Chem. Mater.* **2004**, *16*, 4373-4380.
- [84] South, A. B.; Whitmire, R. E.; Garcia, A. J.; Lyon, L. A., Centrifugal Deposition of Microgels for the Rapid Assembly of Nonfouling Thin Films. *ACS Appl. Mater. Interfaces* **2009**, *1*, 2747-2754.
- [85] South, A. B.; Lyon, L. A., Autonomic Self-Healing of Hydrogel Thin Films. *Angew. Chem., Int. Ed.* **2010**, *49*, 767-771.
- [86] Saxena, S.; Spears Jr, M. W.; Yoshida, H.; Gaulding, J. C.; Garcia, A. J.; Lyon, L. A., Microgel Film Dynamics Modulate Cell Adhesion Behavior. *Soft Matter* **2014**, *10*, 1356-1364.
- [87] Nolan, C. M.; Reyes, C. D.; Debord, J. D.; Garcia, A. J.; Lyon, L. A., Phase Transition Behavior, Protein Adsorption, and Cell Adhesion Resistance of Poly(Ethylene Glycol) Cross-Linked Microgel Particles. *Biomacromolecules* **2005**, *6*, 2032-2039.
- [88] Gaulding, J. C.; Spears, M. W.; Lyon, L. A., Plastic Deformation, Wrinkling, and Recovery in Microgel Multilayers. *Polymer Chemistry* **2013**, *4*, 4890-4896.
- [89] <http://www.asylumresearch.com/Applications/CombinedAFMOptical/CombinedAFMOptical.shtml>

CHAPTER 2

REVEALING COMPLEX NETWORK STRUCTURE IN HOLLOW MICROGELS

Portions adapted from:

Smith, M.H., Herman, E.S., Lyon L.A. Network Deconstruction Reveals Network Structure in Responsive Microgels. *J. Phys. Chem. B*, **2011**, *115*, 3761-3764.

2.1. Introduction

Advanced delivery options for therapeutics has been of interest for a number of years.¹ One particular focus within this area is the development of a drug delivery vehicle that is targetable, increases drug loading, increases drug efficacy, and reduces systemic side effects.² Microgels are a class of responsive materials that have shown potential in this area due to their size, inherent versatility and tunability.³⁻⁷ These features have allowed for the incorporation of responsivity to external stimuli, such as pH⁸ or temperature,⁹ or degradability through the incorporation of a degradable cross-linker.⁶ This last feature has been utilized in the construction of several types of degradable microgel constructs,^{6,10,11} including hollow microgels in which a degradable component is incorporated into the core of a core/shell microgel. After exposure to a degradation agent, a hollow reservoir is left within a polymer mesh, or shell. Other methods have been explored for the construction of hollow capsules,¹²⁻¹⁴ but have suffered from various issues (i.e. payload leakage, hydrophobicity, and poor biocompatibility).² Hollow microgels, however, may alleviate some of these issues by exhibiting the characteristic increased

drug loading of hollow constructs in conjunction with an incorporated responsivity, which would allow for a modulation of the delivery rate of an encapsulated therapeutic.

The incorporation of the degradable cross-linker (1,2-dihydroxyethylene)-bisacrylamide (DHEA) into the core of core/shell microgels is a simple and effective way to create hollow microgel constructs as has been shown previously.⁶ DHEA contains a vicinal diol that is degraded in the presence of the degradation agent, sodium periodate (NaIO_4). In a previous investigation, core/shell pNIPAm microgels containing the degradable cross-linker, DHEA, and a fluorescent component within the core were synthesized and the degradation of the core in the presence of NaIO_4 was analyzed by UV-vis spectroscopy.⁶ While this study showed a decrease in fluorescence upon degradation, suggesting degradation of the core, additional work looking at the degradation pathway of pNIPAm-DHEA microgels showed that these constructs may suffer from poor incorporation of DHEA and self-cross-linking of NIPAm.¹⁵ This work also showed that the use of another monomer, *N*-isopropylmethacrylamide (NIPMAm), may minimize this monomer self-cross-linking by eliminating the sites available for self-cross-linking.¹⁶ These results strongly suggest that cores composed of poly pNIPMAm-DHEA are more capable of complete degradation upon exposure to NaIO_4 , and these results may indicate that core/shell microgels constructed with pNIPMAm-DHEA may create a more truly hollow construct as compared to pNIPAm-DHEA.

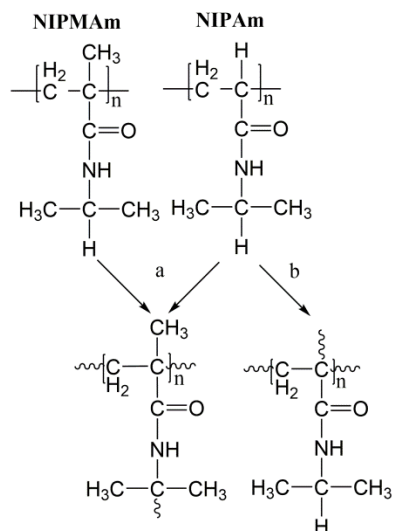


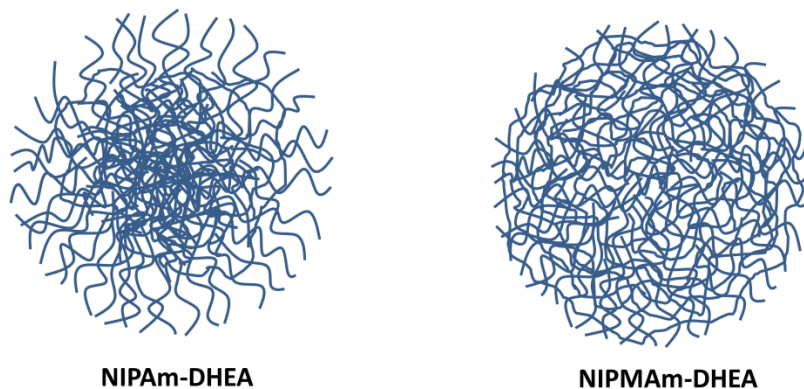
Figure 2.1. Possible routes of self-cross-linking in NIPAm and NIPMAm: (a) the located on the tertiary C of the isopropyl group or (b) the hydrogen located on the tertiary C of the main chain backbone.¹⁶

The two sites available for self-cross-linking are shown in **Figure 2.1**. For this, a hydrogen atom from a tertiary C is donated to a free radical and chain growth is initiated resulting in self-cross-linked networks. Route (a) shows chain growth from the tert-C located on the isopropyl group of both NIPAm and NIPMAm. Route (b) shows chain growth from the tertiary hydrogen located on the main backbone and is only available for the monomer NIPAm. It has been suggested that growth from Route (a) is a more likely route of self-cross-linking because it is less spatially hindered.¹⁶ The hydrolysis of a similar monomer, poly (*N*-vinylformamide) (PNVF), has been tested and results presented a lack of self-crosslinking after base hydrolysis but continued self-cross-linking after acid hydrolysis, which strongly suggested a preference of the monomer to self-cross-link at the amide group.¹⁷ This may suggest an inability of monomer units to significantly self-cross-link along the monomer backbone, however additional testing is needed to determine whether the behavior observed for PNVF hydrolysis can be

transferred to other monomer systems. However, taken in conjunction with the lower spatial hindrance and more electron-rich environment of Route (a) as compared to Route (b), it may be hypothesized that Route (a) is the predominant route of self-cross-linking.

If Route (a) is considered the main source of self-cross-linking, both NIPAm and NIPMAM are theoretically capable of self-cross-linking. However, it has been suggested previously that mismatched reaction rates between monomer could affect the self-cross-linking as well as the degree of heterogeneity of microgels composed through precipitation polymerization.^{15, 18} It has been shown that NIPAm has a faster reaction rate than NIPMAM¹⁹ and this difference in reaction rate has been suggested as a cause of heterogeneity in microgels containing the degradable crosslinker, DHEA.¹⁵ In a light scattering study, deconstruction of pNIPAm and pNIPMAM microgels containing DHEA revealed the network structure of both microgel types. In this study, the topography of both particle types were inferred from a ratio of the hydrodynamic radius (r_h) and the root-mean-square radius (r_{rms}) and results indicated a homogenous distribution of polymer in pNIPMAM-DHEA microgels and an inhomogenous, radial distribution of polymer within pNIPAm-DHEA microgels. Erosion kinetics of these two microgel types also showed stark differences, wherein pNIPMAM-DHEA microgels followed an exponential decrease in molecular weight (M_w) over time, as is characteristic for bulk eroding polymers, and in contrast pNIPAm-DHEA microgels exhibited an initially high erosion velocity followed by a deceleration and plateau in velocity. After extended time, pNIPMAM-DHEA microgels were able to completely degrade whereas pNIPAm-DHEA microgels never fully degraded, even after extended time and increased NaIO_4 concentration.

The differences in topology and erosion were attributed to a higher preference for homopropagation of NIPAm, which caused limited incorporation of DHEA within the interior of the microgel and poor incorporation in the periphery of the microgel. This would explain the radial distribution of polymer and the inability of pNIPAm-DHEA microgels to completely degrade. This was not seen with pNIPMAm-DHEA microgels, which contained a higher polymer density and smoother sphere topology. This is likely the result of even incorporation of reactants during synthesis, as NIPMAm reacts more slowly allowing for a more statistically random incorporation of the DHEA cross-linker.¹⁵ Also, the ability of the pNIPMAm-DHEA microgels to completely degrade may indicate a lack of or minimal self-cross-linking. **Scheme 2.1** shows the structure of the two core types based on the discussion above.



Scheme 2.1. Proposed structure of pNIPAm-DHEA and pNIPMAm-DHEA microgels. Adapted from Reference 15.

This chapter will compare the use of NIPAm and NIPMAm within degradable cores for the construction of thermo-responsive hollow microgels. These two hollow constructs are produced by first creating a core/shell microgel using free radical precipitation polymerization followed by a seeded precipitation polymerization technique

in which the core particles are used as a template for the production of a microgel shell. The shell for both core/shell constructs contains NIPAm and a non-degradable cross-linker, BIS. After core/shell production the core was degraded through exposure to NaIO₄. Using AFM and DLS the degradation of the cores and the swelling behavior of these constructs was analyzed. From these studies, the viability of pNIPAm versus pNIPMAm with the degradable cross-linker, DHEA, as templates for the production of hollow microgels with potential utility as vehicles for drug delivery was assessed.

2.2 Experimental Section

2.2.1. Materials

All reagents were purchased from Sigma-Aldrich (St Louis, MO) and used as received, unless otherwise noted. The monomers *N*-isopropylacrylamide (NIPAm) and *N*-isopropylmethacrylamide (NIPMAm) were recrystallized from hexanes (VWR international, West Chester, PA) and dried in vacuo prior to use. The reagents *N,N'*-methylenebisacrylamide (BIS), sodium dodecyl sulfate (SDS), ammonium persulfate (APS), NaIO₄, and DHEA were all used as received. Water used in all reactions and particle purifications was purified to a resistance of 18 MΩ (Barnstead E-Pure system), and filtered through a 0.2 μm filter to remove particulate matter.

2.2.2. Microgel Core and Core/Shell Synthesis

The syntheses of pNIPAm-DHEA and pNIPMAm-DHEA particles were performed via free radical precipitation polymerization as previously described⁶ with a molar composition of 90 % monomer (NIPAm or NIPMAm) and 10 % DHEA and a total monomer concentration of 70 mM (for pNIPAm) and 140 mM (for pNIPMAm). The

total synthesis volume for both syntheses was 100.0 mL. The reactions were performed by separately dissolving NIPAm or NIPMAm monomer (0.713 g or 1.426 g) in 99.0 mL of distilled, deionized water. A mass of 0.140 g DHEA was dissolved in the NIPAm solution, whereas 0.280 g DHEA was dissolved in the NIPMAm solution. A mass of 0.044 g SDS was added to both solutions for a concentration of 1.5 mM. Each solution was filtered through a 0.2 μm Acrodisc syringe filter and added to separate 100 mL three-neck round-bottom flasks. The reactions were heated to 70 $^{\circ}\text{C}$ and purged with N_2 for an hour while stirring (400 RPM). The polymerizations were then initiated by delivering a 1.0 mL aliquot of a 2 mM APS solution by pipette. All reactions were allowed to proceed for 24 hours under an N_2 blanket while continuously stirring. Once cooled, both solutions were filtered through 0.8 μm Acrodisc syringe filters and purified via repeated ultracentrifugation and resuspension in distilled, deionized water.

The core-shell constructs were produced by a two-stage seeded polymerization technique.⁶ For this, the DHEA cross-linked particles are used as seed particles for the polymerization of a shell containing the monomer NIPAm and cross-linker BIS. To begin, a solution of DHEA cross-linked particles (10 mL) are mixed with SDS (4 mg) in 5 mL distilled, deionized water. This core solution is heated to 70 $^{\circ}\text{C}$ while purging with nitrogen. Separately, NIPAm (98 %) and BIS (2%) were dissolved in distilled deionized water to create a total molar concentration of 50 mM. After the core solution equilibrated for 1 hour, the shell solution was added. Finally, APS (5 mg) was added to initiate the reaction. The reaction was allowed to proceed for 4 hours at 70 $^{\circ}\text{C}$ after which it was removed from heat. Once cooled, the solution was purified via repeated ultracentrifugation and resuspension in distilled, deionized water.

2.2.3. Core Degradation

To degrade DHEA within core and core/shell constructs, the degradation agent sodium periodate (NaIO_4) was used. The amount of NaIO_4 added was based on the degree to which degradation was desired. The amount of DHEA to be degraded was calculated from the amount of DHEA in solution prior to initiation. In general, an equivalent number of moles of NaIO_4 is added to a 1.0 mL solution of particles and deionized water is added to create a final volume of 1.5 mL and the reaction continued overnight. The resultant “hollow” microgels were purified by ultracentrifugation and resuspension in distilled deionized water.

2.2.4. Characterization

The hydrodynamic radii of the core and core/shell microgels before and after degradation were measured by Dynamic Light Scattering (DLS) using a Dynapro DLS (Wyatt Technology, Santa Barbara, CA) equipped with a temperature-controlled sample chamber. Microgel solutions were diluted in distilled deionized water and light scattering data was collected at 20 °C. Particle morphology was assessed using an MFP-3D AFM (Asylum Research, Santa Barbara, CA) in tapping mode using silicon Pointprobe cantilevers (Neuchatel, Switzerland) with a force constant of 42 N/m.

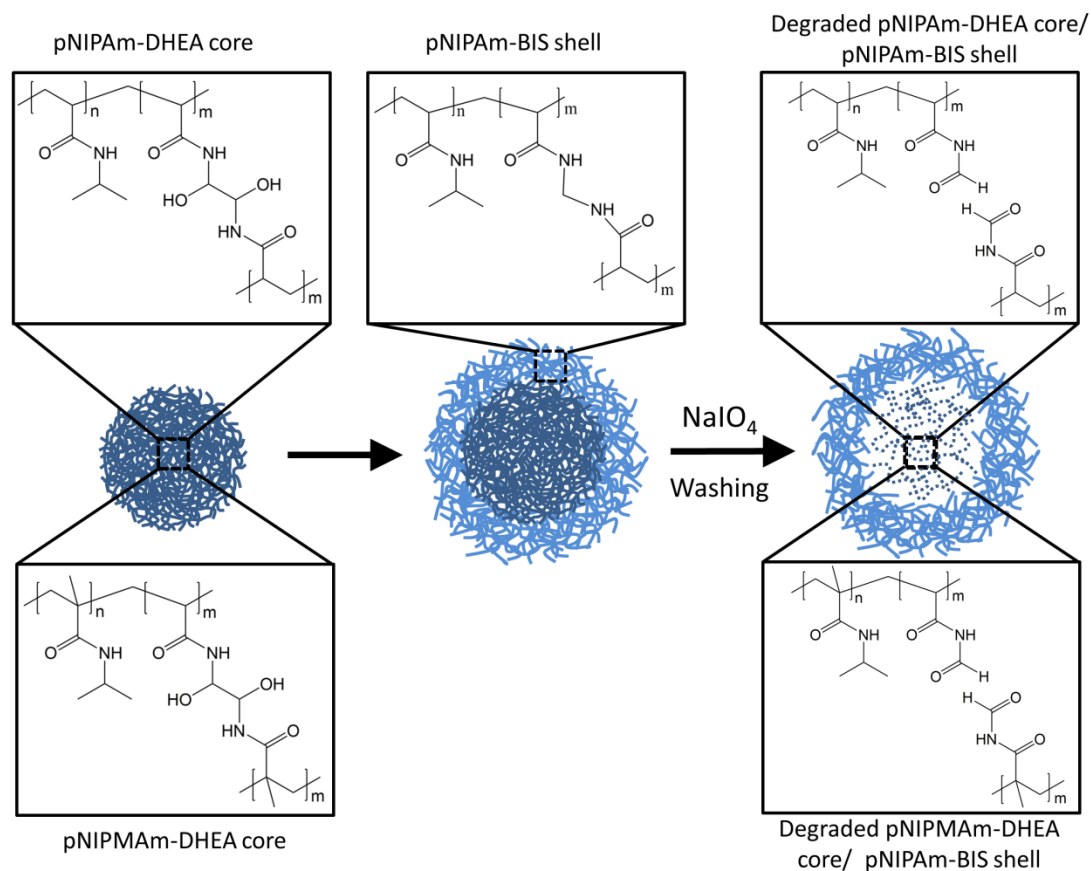
2.3. Results and Discussion

To analyze the viability of both pNIPAm-DHEA and pNIPMAm-DHEA cores as templates for the production of hollow constructs, core/shell microgels were first constructed. The core/shell microgels described herein were synthesized using techniques described previously by the Lyon group.^{6,8} The synthesis conditions used for

the construction of these core/shell microgels are shown in **Table 2.1**. Two cores were synthesized; pNIPAm-DHEA and pNIPMAm-DHEA, herein referred to as Core 1 and Core 2, respectively. These cores were then used (separately) as templates for the synthesis of a pNIPAm-BIS shell. The same shell composition was used for both shell additions (98% NIPAm, 2% BIS) in order to limit compositional variability between the two microgel types. The final core/shell composition and degradation process is shown in **Scheme 2.2**. Again, the critical feature of these two constructs is the use of the degradable cross-linker, DHEA. This cross-linker contains a vicinal diol group, which can be cleaved in the presence of the degradation agent, NaIO_4 , leaving a hollow vesicle-like structure (**Scheme 2.2**) after purification.

Table 2.1. Synthesis Parameters of DHEA Containing Core and Core/Shell Microgels

Sample	Core Volume (mL)	Total Volume (mL)	Total Monomer conc. (mM)	Monomer Mass (g), mol%	Cross-linker mass (g), mol%	SDS (g), Conc. (mM)	APS (g), Conc. (mM)
NIPAm/ DHEA Core (Core 1)	--	100	70	NIPAm: 0.713, 90%	DHEA: 0.140, 10%	0.044, 1.5	0.034, 1.5
NIPMAm/ DHEA Core (Core 2)	--	100	140	NIPMAm: 1.426, 90%	DHEA: 0.280, 10%	0.044, 1.5	0.034, 1.5
NIPAm/ BIS Shell	10	35	20	NIPAm: 0.055, 98%	BIS: 0.002, 2%	0.004, 1	0.005, 2



Scheme 2.2. Core particles containing the degradable cross-linker DHEA and pNIPAm or pNIPMAm are used as templates for the subsequent addition of a shell composed of pNIPAm-BIS. The core is then degraded by exposure to NaIO_4 and removed by centrifugation leaving a “hollow” microgel.

The r_h of these microgels at various stages of hollow microgel production (core, core/shell, degraded) were measured by DLS and these results are shown in **Table 2.2**.

The addition of the shell to the Core 1 and Core 2 microgels resulted in small or statistically insignificant changes in particle size at 20 °C. Although one may believe addition of a microgel shell onto a core would result in a significant increase in r_h due to polymer addition, interactions present at the core/shell interface can result in relatively small changes in microgel size after shell addition.¹¹ This is due to the elevated temperature (70 °C) of shell addition, which is well above the LCST of NIPAm (32 °C).

During shell addition at this elevated temperature, the core is in its deswollen state as it acts as a template for the growth of a polymer shell. After completion of shell addition the solution is cooled but the core will remain compressed. This can cause moderate to no significant changes in the overall size (r_h).²⁰ However, the r_h of core 1/shell microgels (~95 nm) and core 2/shell microgels (~136 nm) above the lower critical solution temperature (LCST) of NIPAm (~32 °C)²¹ and/or NIPMAm (~43 °C) are slightly larger than core microgels alone, indicating a more dense structure and validating the addition of a pNIPAm-BIS shell (**Table 2.2**). After degradation by NaIO₄, a significant increase in r_h is observed. This increase acts as validation of an alleviation of tight cross-linking between the compressed core and the outer shell layer,¹¹ suggesting degradation of the internal core. This also validates the formation of a core/shell structure because complete degradation would result in an immeasurable r_h .

Table 2.2. Light Scattering Data of Various Stages of “Hollow” Microgel Construction

	r_h , (20 °C)	r_h , (45 °C)	r_h , (65 °C)
pNIPAm-DHEA Core (Core 1)	182±30 nm	82±15 nm	--
Core 1/pNIPAm-BIS Shell	182±33 nm	95±19 nm	--
Degraded Core 1/pNIPAm-BIS Shell	210±32 nm	88±20 nm	--
pNIPMAm-DHEA Core (Core 2)	227±16 nm	--	131±25 nm
Core 2/pNIPAm-BIS Shell	229±17 nm	--	136±23 nm
Degraded Core 2/pNIPAm-BIS Shell	312±95 nm	--	--

The degradation of the DHEA-containing cores upon introduction of NaIO₄ can be observed by eye due to changes in the turbidity of core and core/shell solutions.

Shown in **Figure 2.1** are solutions of Core 1 microgels (a) and Core 1/shell microgels

before (b) and after (c) degradation. This is also seen with Core 2 (not shown), and is a visual demonstration of the ability of microgels containing an incorporated degradable component to react to a degradation agent. The important thing to note here is the completely clear solution of degraded cores, whereas the degraded core/shell exhibits a more opaque color. This implies differences in the degradation behavior of the core and core/shell microgels, which indicates that the core/shell microgels contain a non-degradable component, and are therefore being degraded locally, specifically within the DHEA core.

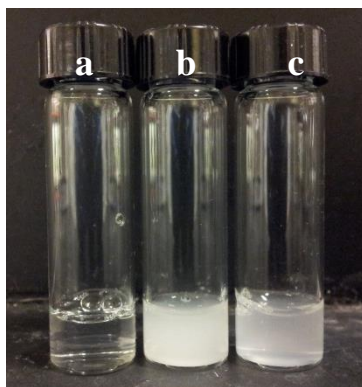


Figure 2.2. Solutions of Core 1/pNIPAm-BIS shell microgels before (b) and after (c) exposure to NaIO_4 . For comparison, Core 1 after degradation (a) is also shown.

To reaffirm that the color change observed in **Figure 2.2c** can be attributed to changes in microgel core structure, the r_h of the core/shell microgels as a function of temperature was measured across the LCST of pNIPAm for Core 1 (**Figure 2.3a**) before and after degradation. These temperature curves show the point at which the microgel overcomes the polymer-solvent interactions present within the microgel and water is expelled.²² At this point an entropically-driven polymer phase separation takes place and a decrease in overall particle size is observed.²⁰ In cross-linked networks, this transition is commonly called the volume phase transition temperature (VPTT)^{9,23} and is related

thermodynamically to the LCST of the analogous linear polymer chain. For Core 1 microgels, the volume phase transition observed before and after degradation (**Figure 2.3a**) exhibited similar transition temperatures at ~ 34 °C. This is to be expected since the core and shell contain the same thermo-responsive polymer (pNIPAm), and therefore the volume transition upon heating should be similar before and after degradation.⁸ The larger magnitude transition observed in the non-degraded Core 1/shell structure can be attributed to a release of cross-linked networks after degradation, and similar behavior as has been seen previously.⁸

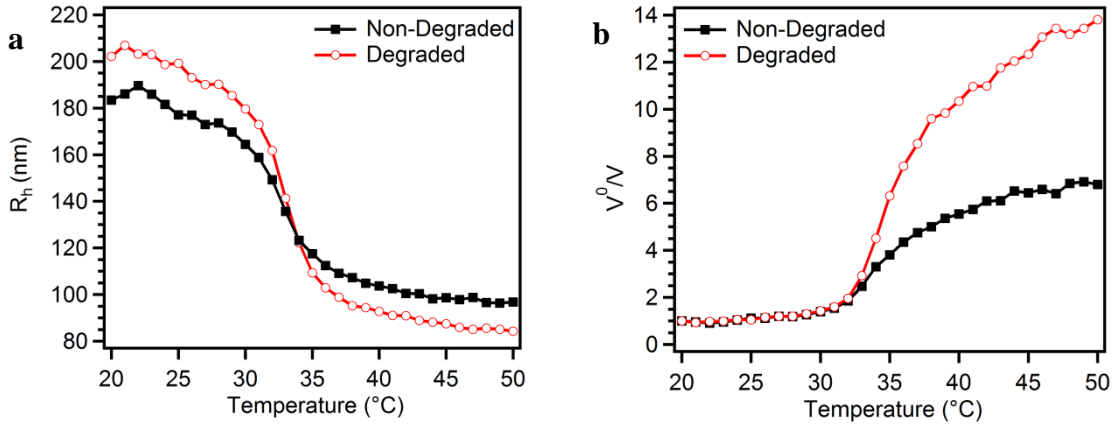


Figure 2.3. Volume phase transition curves of non-degraded (black squares) and degraded Core 1/shell microgels (red circles) (a). Deswelling curves of non-degraded (black squares) and degraded (red circles) (b).

The deswelling behavior of Core 1/shell microgels before and after degradation can be analyzed by the swelling ratio. The deswelling ratio is defined as⁶:

$$\frac{V^0}{V} = \left(\frac{R_h^0}{R_h} \right)^3 \quad \text{Equation 2.1.}$$

where V^0 and R_h^0 are the volume and hydrodynamic radius before deswelling, respectively, and V and R_h are the volume and hydrodynamic radius at a specific temperature, respectively. The deswelling ratio as a function of temperature for Core

1/shell microgels before and after degradation is shown graphically in **Figure 2.3b**. The degraded Core 1/shell microgels showed an increase in the deswelling volume ratio compared to non-degraded Core 1/shell microgels. It can be inferred from this information that the NaIO₄ was in fact oxidizing the DHEA present in the core and therefore breaking apart the core construct, creating an increase in the overall size of the particle as observed the volume transition curve and affirmed by the increase in the swelling ratio of degraded Core 1/shell microgels.

In **Figure 2.4a**, the volume phase transition of Core 2/shell microgels before and after degradation is shown. The phase transition after degradation of Core 2/shell microgels was unreliable above 48 °C due to aggregation and high polydispersity, and therefore a comparison of the deswelling ratio across the full volume transition for Core 2/shell microgels before and after degradation could not be obtained. However, the volume phase transitions of Core 2 microgels and Core 2/shell microgels (**Figure 2.4b**) gave insight into Core 2/shell microgel composition. In **Figure 2.4b**, Core 2 microgels exhibit a volume phase transition at higher temperature (~47 °C) due to the presence of the thermo-responsive polymer pNIPAm within the core. Upon addition of a shell, this transition takes place over a markedly wider temperature range. This change in the transition is due to the presence of more than one thermo-responsive monomer, as has been observed previously.^{11,24} and can be used as a validation of the addition of a shell containing the monomer NIPAm. Worth noting is the lack of individual transitions for each component, which could possibly be due to the thinness of the pNIPAm/BIS shell or a high cross-linking density within the core, which would limit compression of the overall structure upon reaching the LCST of pNIPAm (32 °C). At this point the core

would remain hydrated, and if incapable of compression a distinct transition would not be visible. In this way, interplay between the core and shell can cause indiscernible individual transitions as has been observed previously.^{24,25}

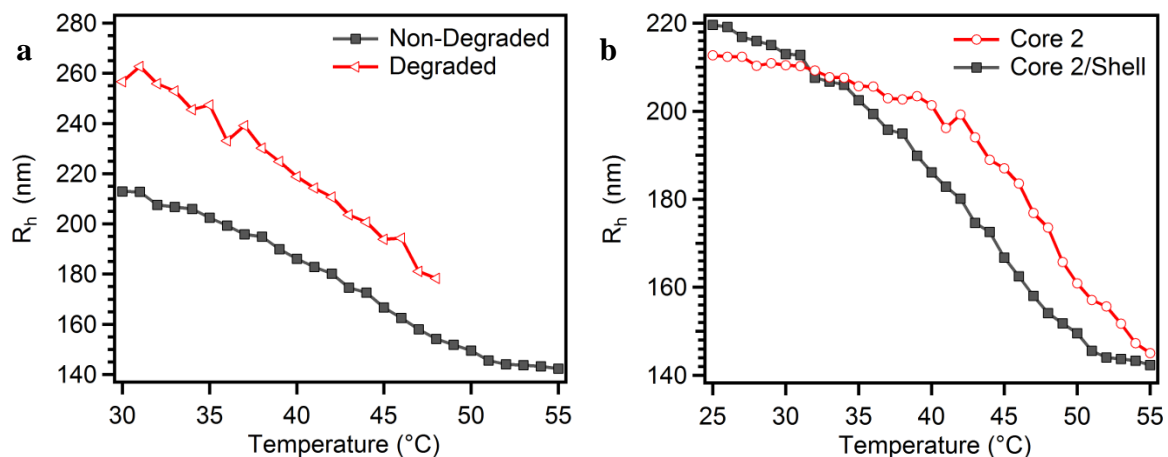


Figure 2.4. Volume phase transition of non-degraded Core 2/shell microgels (grey squares) and degraded core/shell microgels (red triangles) (a). Volume phase transitions of Core 2 (red circles) and Core 2/shell microgels (grey squares) (b).

As an alternative method for characterizing the Core 2/shell microgel before and after degradation, AFM was utilized. This technique that has been employed for gaining topographical information of soft surfaces for a number of years.^{26,27} For this, microgels are placed on a glass substrate and analyzed in air. When microgels deposit on the surface, they spread due to their high porosity and high mechanical flexibility. Changes in this porosity, or mechanical flexibility, can be visualized by AFM, and the topographical information can be analyzed by height mapping to give insight into changes in microgel density.^{11,28} Thus, morphological changes in the core/shell microgels before and after degradation can be analyzed by this method.

Core/shell microgels composed of Core 1 and Core 2 before (**Figure 2.5a,c**) and after (**Figure 2.5b,d**) degradation are shown. Representative line traces accompany each

image and act as a visual representation of the measured height and spreading of individual microgels. The height of Core 1/shell microgels before degradation is ~11 nm (**Figure 2.5a**) and after degradation the microgel height is approximately half (~6 nm) (**Figure 2.5b**), showing a decrease in the overall density of the core/shell microgel, indicative of mass loss. An even more drastic change can be seen for Core 2/shell microgels before (**Figure 2.5c**) and after degradation (**Figure 2.5d**). For this, the height of the Core 2/shell microgel before degradation is ~40 nm (**Figure 2.5c**) and the height after degradation is ~7 nm (**Figure 2.5d**), a height >4 times smaller than the original Core/shell structure. Core 2/shell microgels after degradation also exhibit a greater degree of microgel spreading (~1 μm) as compared to before degradation (~500 nm). Taking the height and spreading information together for these core/shell and hollow microgels, it can be inferred that there was in fact mass loss after degradation, resulting in a more mechanically flexible “hollow” microgel.

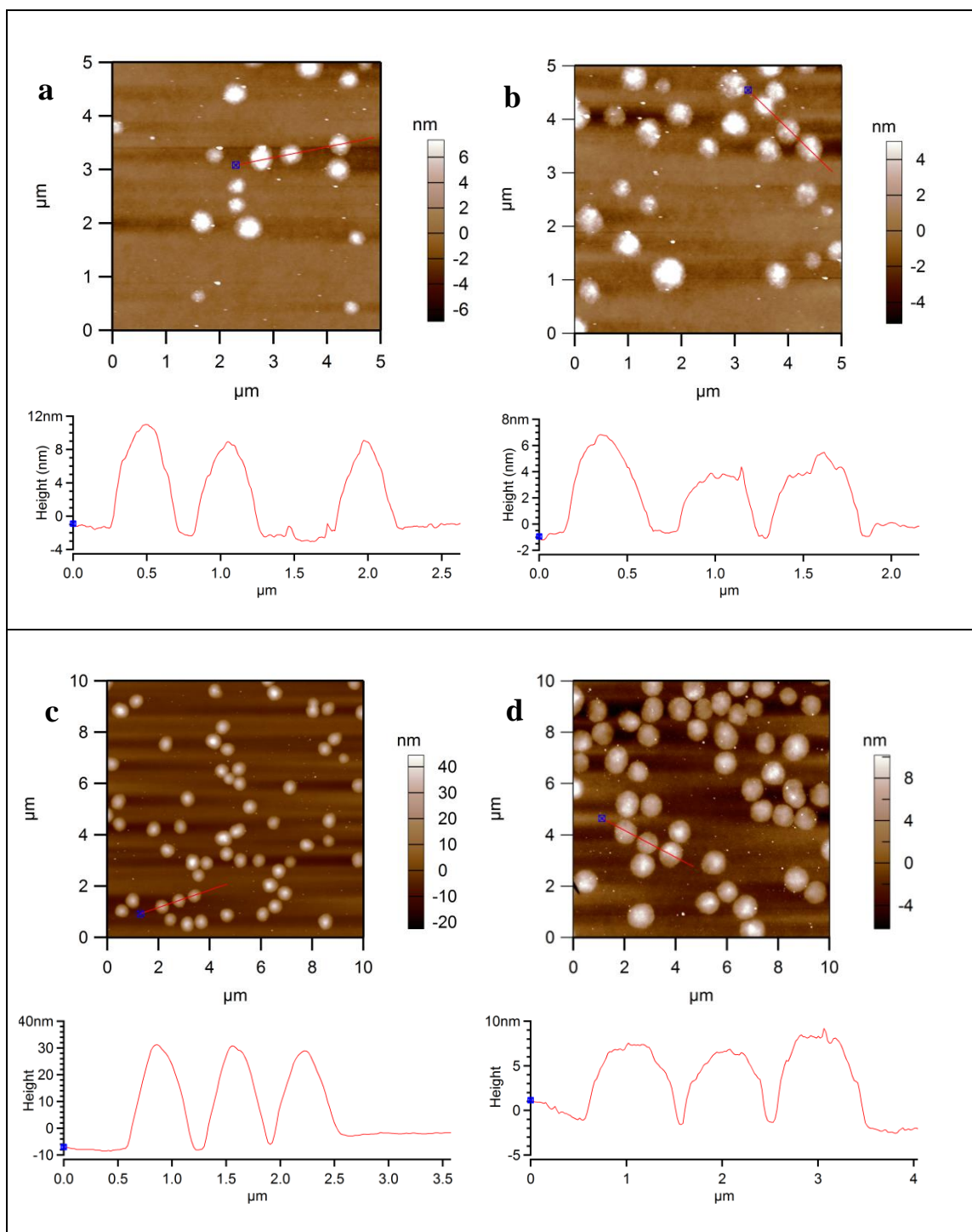


Figure 2.5. AFM images of microgels containing Core 1 before (a) and after (b) degradation and microgels containing Core 2 before (c) and after (d) degradation with representative line traces.

2.4. Conclusions and Future Outlook

The formation of core/shell microgels containing a sacrificial core composed of pNIPAm-DHEA (Core 1) or pNIPMAm-DHEA (Core 2) were both explored and the results presented above show the behavior of these constructs before and after exposure to NaIO₄, a degradation agent used to cleave the vicinyl diol bond found in DHEA. The monomer units, NIPAm and NIPMAm, differ by a single methyl group, but the final “hollow” macromolecular structures from which they are composed differ in notable ways.

The first notable difference between Core 1 and Core 2 was discussed previously based on light scattering studies of the degradation of these constructs as a function of time.¹⁵ It is important when considering the results presented herein to remember this initial study, which created a picture of the network structure of Core 1 and Core 2 as presented in **Scheme 2.1**. A more robust understanding of results presented herein regarding the use of Core 1 and Core 2 as templates for the production of “hollow” microgels can be attained by keeping in mind this foundational research.

To understand the swelling of the core/shell microgels before and after degradation, the volume phase transition curves (**Figure 2.2a** and **Figure 2.3b**) were first analyzed. For Core 1/shell microgels, a less broad transition is observed for degraded Core 1/shell microgels as compared to non-degraded Core 1/shell microgels. This broader transition of degraded Core 1/shell microgels also results in a higher deswelling volume (**Figure 2.2b**), suggesting that polymer networks within the core had been degraded, resulting in a less rigid structure and thus a greater swellability. For Core 2/shell microgels, the swellability of the microgel proved difficult to understand by DLS alone

due to aggregation of the microgels in solution at higher temperature, but volume phase transitions showed a shift in the VPTT before the addition of a NIPAm-containing shell (Core 2 microgels) and after (Core2/shell microgels), which results from the addition of pNIPAm, which has a characteristically different LCST, and thus validating the addition of a microgel shell.

In order to understand the resultant “hollow” microgel obtained after degradation, AFM images were obtained and analyzed of microgels before and after degradation of Core 1 (**Figure 2.5a,b**) and Core 2 (**Figure 2.5c,d**). By AFM, it was observed that Core 2/shell microgels exhibited greater spreading (2-fold) and a greater decrease in height (4-fold). The increased spreading and decreased height of the microgel indicates a lower particle rigidity, which allows for greater microgel spreading and is indicative of mass loss from the core of the structure. In this case, these results suggest a greater mass loss from Core 2 containing core/shell microgels after degradation as compared to Core 1. Also worth noting is the smaller height for Core 1/shell microgels (**Figure 2.5a**, ~10 nm) as compared to Core 2/shell microgels (**Figure 2.5c**, ~40 nm). Since the r_h (see **Table 2.2**) of the two particle types does not differ greatly and the spreading on the surface is approximately the same, this difference can be attributed to a greater microgel rigidity of Core 2/shell microgels. Taken in conjunction with previously published data (see **Section 2.1** and **Scheme 2.1**), this can be attributed to a greater density of Core 2 and thus a greater density of Core2/shell microgels. It can also be inferred that more mass is lost in Core 2/shell microgels after degradation, and therefore the inner cavity of these “hollow” microgels may be of a greater volume.

Considering all of this data together, it could be suggested that hollow microgels polymerized with a sacrificial core containing pNIPMAm-DHEA pose a greater utility as a hollow vesicle as compared to hollow constructs constructed from pNIPMAm-DHEA templates. This is due to the greater density within pNIPMAm-DHEA core/shell microgels, as well as the greater mass lost after pNIPMAm-DHEA core degradation, as suggested by the topographical information obtained by AFM. Additional testing, such as light scattering studies of the degradation pathway of the core/shell microgels, should be conducted in order to understand the release of the sacrificial core and thus the “hollow” characteristics of both constructs, but these studies show promising results suggesting the development of a hollow microgel vehicle that may contain a greater degree of “hollowness” and therefore potential to increase payload capacity over previously studied hollow microgel constructs.

2.4. References

- [1] De Geest, B. G.; Dejurnat, C.; Sukhorukov, G. B.; Braeckmans, K.; De Smedt, S. C.; Demeester, J., Self-rupturing microcapsules. *Adv. Mater.* **2005**, *17* (19), 2357-2361.
- [2] Nayak, S.; Lyon, L. A., Soft Nanotechnology with Soft Nanoparticles. *Angew. Chem., Int. Ed.* **2005**, *44* (47), 7686-7708.
- [3] Dickerson, E.; Blackburn, W.; Smith, M.; Kapa, L.; Lyon, L. A.; McDonald, J., Chemosensitization of cancer cells by siRNA using targeted nanogel delivery. *BMC Cancer* **2010**, *10* (1), 10.
- [4] Oh, J. K.; Drumright, R.; Siegwart, D. J.; Matyjaszewski, K., The development of microgels/nanogels for drug delivery applications. *Prog. Polym. Sci.* **2008**, *33* (4), 448-477.
- [5] Murthy, N.; Xu, M.; Schuck, S.; Kunisawa, J.; Shastri, N.; Fréchet, J. M. J., A macromolecular delivery vehicle for protein-based vaccines: Acid-degradable protein-loaded microgels. *Proceedings of the National Academy of Sciences* **2003**, *100* (9), 4995-5000.

- [6] Nayak, S.; Gan, D. J.; Serpe, M. J.; Lyon, L. A., Hollow thermoresponsive microgels. *Small* **2005**, *1* (4), 416-421.
- [7] Raemdonck, K.; Demeester, J.; De Smedt, S., Advanced nanogel engineering for drug delivery. *Soft Matter* **2009**, *5* (4), 707-715.
- [8] Jones, C. D.; Lyon, L. A., Synthesis and Characterization of Multiresponsive Core–Shell Microgels. *Macromolecules* **2000**, *33* (22), 8301-8306.
- [9] Pelton, R., Temperature-sensitive aqueous microgels. *Adv. Colloid Interface Sci.* **2000**, *85* (1), 1-33.
- [10] Smith, M. H.; South, A. B.; Gaulding, J. C.; Lyon, L. A., Monitoring the Erosion of Hydrolytically-Degradable Nanogels via Multiangle Light Scattering Coupled to Asymmetrical Flow Field-Flow Fractionation. *Anal. Chem.* **2009**, *82* (2), 523-530.
- [11] Gaulding, J. C.; South, A. B.; Lyon, L. A., Hydrolytically degradable shells on thermoresponsive microgels. *Colloid Polym. Sci.* **2013**, *291* (1), 99-107.
- [12] Zha, L. S.; Zhang, Y.; Yang, W. L.; Fu, S. K., Monodisperse temperature-sensitive microcontainers. *Adv. Mater.* **2002**, *14* (15), 1090-1092.
- [13] Huang, H. Y.; Remsen, E. E.; Kowalewski, T.; Wooley, K. L., Nanocages derived from shell cross-linked micelle templates. *J. Am. Chem. Soc.* **1999**, *121* (15), 3805-3806.
- [14] Hotz, J.; Meier, W., Vesicle-Templated Polymer Hollow Spheres. *Langmuir* **1998**, *14* (5), 1031-1036.
- [15] Smith, M. H.; Herman, E. S.; Lyon, L. A., Network Deconstruction Reveals Network Structure in Responsive Microgels. *The Journal of Physical Chemistry B* **2011**, *115* (14), 3761-3764.
- [16] Gao, J.; Frisken, B. J., Cross-linker-free N-isopropylacrylamide gel nanospheres. *Langmuir* **2003**, *19* (13), 5212-5216.
- [17] Gu, L.; Zhu, S.; Hrymak, A. N.; Pelton, R. H., The Nature of Crosslinking in N-Vinylformamide Free-Radical Polymerization. *Macromolecular Rapid Communications* **2001**, *22* (3), 212-214.
- [18] Baselga, J.; Llorente, M. A.; Nieto, J. L.; Hernández-Fuentes, I.; Piérola, I. F., Polyacrylamide networks. sequence distribution of crosslinker. *Eur. Polym. J.* **1988**, *24* (2), 161-165.

- [19] Duracher, D.; Elaïssari, A.; Pichot, C., Preparation of poly(N-isopropylmethacrylamide) latexes kinetic studies and characterization. *Journal of Polymer Science Part A: Polymer Chemistry* **1999**, *37* (12), 1823-1837.
- [20] Blackburn, W. H.; Lyon, L. A., Size-controlled synthesis of monodisperse core/shell nanogels. *Colloid Polym. Sci.* **2008**, *286* (5), 563-569.
- [21] Pelton, R. H.; Chibante, P., Preparation of aqueous latices with N-isopropylacrylamide. *Colloids Surf.* **1986**, *20* (3), 247-256.
- [22] Hendrickson, G. R.; Smith, M. H.; South, A. B.; Lyon, L. A., Design of Multiresponsive Hydrogel Particles and Assemblies. *Adv. Funct. Mater.* **2010**, 1697-1712.
- [23] Dušek, K.; Patterson, D., Transition in swollen polymer networks induced by intramolecular condensation. *Journal of Polymer Science Part A-2: Polymer Physics* **1968**, *6* (7), 1209-1216.
- [24] Zeiser, M.; Freudensprung, I.; Hellweg, T., Linearly thermoresponsive core-shell microgels: Towards a new class of nanoactuators. *Polymer* **2012**, *53* (26), 6096-6101.
- [25] Jones, C. D.; Lyon, L. A., Shell-restricted swelling and core compression in poly(N-isopropylacrylamide) core-shell microgels. *Macromolecules* **2003**, *36* (6), 1988-1993.
- [26] Zhong, Q.; Inniss, D.; Kjoller, K.; Elings, V. B., Fractured polymer/silica fiber surface studied by tapping mode atomic force microscopy. *Surface Science Letters* **1993**, *290* (1-2), L688-L692.
- [27] Magonov, S. N.; Elings, V.; Whangbo, M. H., Phase imaging and stiffness in tapping-mode atomic force microscopy. *Surf. Sci.* **1997**, *375* (2-3), L385-L391.
- [28] South, A. B.; Lyon, L. A., Direct Observation of Microgel Erosion via in-Liquid Atomic Force Microscopy. *Chem. Mater.* **2010**, *22* (10), 3300-3306.

CHAPTER 3

PROBING CHARGE DISTRIBUTION WITHIN MICROGELS AND MICROGEL ASSEMBLIES

3.1. Introduction

As noted in previous chapters, microgels are a class of mechanically flexible colloidal materials that have shown promise in a wide range of applications. The first synthesis of poly(*N*-isopropyl acrylamide) (pNIPAm) microgels was published in 1986,¹ and since that year the number of publications encompassing complex microgel structures, including core/shell^{2,3} or hollow⁴, and their applications, such as drug delivery vehicles⁵ or the construction of microgel assemblies with non-fouling characteristics⁶, has expanded tremendously. As the complexity of these constructs increased, there was an interest in finding additional and more robust ways of characterizing microgels and their assemblies. One method commonly used for visualizing and characterizing microgels and microgel assemblies, is atomic force microscopy (AFM). AFM is a promising technique for characterization because it allows for a visualization of individual microgels⁷ or microgel thin film assembly and morphology⁸ from which height or morphological information can be obtained. AFM also can be used for more advanced techniques, such as in-liquid imaging, which has been used to probe microgel degradation over time,⁹ or force mapping, in which the stiffness of microgel thin films was shown to affect cell adhesion,¹⁰ just to name a few of the characterization possibilities for flexible colloidal materials using AFM as a platform.

One AFM technique that has yet to be utilized in the characterization of microgels, or porous colloidal materials in general, is kelvin probe force microscopy (KPFM). KPFM is an AFM-based technique that allows for the characterization of the surface potential of a variety of materials.¹¹ Initially introduced in 1991 as a method for determining the work function of conductive surfaces,¹² KPFM has since grown to encompass the characterization of the electrical properties of organic^{13,14} and biological materials.^{15,16,17,18} In one particularly interesting case, the surface charge of single-stranded DNA and proteins before and after complexation was mapped.¹⁶ This study served as one of the first reports showing the ability of KPFM to be used to gain topographical information in conjunction with electrical information of non-metal/non-semiconductor materials.

To understand KPFM from a fundamental standpoint, it is important to first understand the kelvin probe as it was originally designed by Lord Kelvin in 1898.¹⁹ The microscopy technique known as KPFM was first shown in 1991, but the kelvin probe was originally designed as a separate entity to determine the contact potential difference (CPD) of two surfaces.²⁰ In this system, a vibrating parallel plate capacitor was created in which both plates had a characteristically different work function. Because of the differing work functions of the two plates, a current forms between the two plates. For this original model, a voltage was applied to maintain a zero current between the two plates, and that voltage was defined as the CPD.^{20,21}

Modern day KPFM utilizes a modified version of the original kelvin probe with a standard AFM. The sample and the AFM tip can be modeled as a parallel plate capacitor,

wherein an electrostatic force is developed between the surface and the tip and this force is proportional to the square of the applied voltage and C is the capacitance:

$$F = -\frac{1}{2} \frac{\partial C}{\partial z} V^2 \quad \text{Equation 3.1}$$

The tip is operated in alternating current (AC) mode and a direct current voltage (V_{DC}) is applied to minimize the electrostatic forces between the sample and the tip. The total voltage associated with the system is equal to:

$$V = V_{CPD} + V_{DC} + V_{AC} \sin \omega t \quad \text{Equation 3.2}$$

Where V_{CPD} is the contact potential difference between the surface and the tip, V_{AC} is the applied AC bias, and ω is the AC voltage drive frequency. Through substitution and rearrangement, the equation for electrostatic interactions becomes:

$$F = \frac{1}{2} \frac{\partial C}{\partial z} \left(\left[(V_{DC} - V_{CPD})^2 + \frac{1}{2} V_{AC}^2 \right] + 2[(V_{DC} - V_{CPD})V_{AC} \sin(\omega t)] - \left[\frac{1}{2} V_{AC}^2 \cos(2\omega t) \right] \right) \quad \text{Equation 3.3}$$

The first term of this equation has no frequency dependence and is considered static force and can therefore be ignored. The last term of the equation depends on 2 times the drive frequency. The most important part of this equation is the middle term ($2[(V_{DC} - V_{CPD})V_{AC} \sin(\omega t)]$) because it occurs at the voltage drive frequency ($V\omega$) and depends on the voltage difference between the tip and the sample, multiplied by the applied AC voltage. Operationally, a feedback loop between the tip and the sample is created to make $V_{DC} = V_{CPD}$. This is the point at which ω is null and electrostatic forces are minimized. What this means is that a voltage can be applied (V_{DC}) to null the oscillations at the drive frequency (ω), and this will give us the voltage of the contact potential difference (V_{CPD}) between the tip and the surface. This information is then used to map the surface potential of the sample.

As noted above, KPFM can be used to characterize the electrical properties of a variety of materials. Because microgels commonly incorporate a charged component, KPFM could be beneficial in giving additional insight into microgels and their assemblies when used in conjunction with other AFM characterization techniques. In this chapter, AFM will be utilized in conjunction with KPFM to visualize potential distribution on microgel-containing surfaces in an effort to understand and develop a technique to characterize the degree of charge localization and charge heterogeneity in microgel thin films.

3.2. Experimental

3.2.1. Materials

All materials were purchased and used as described in **Chapter 2**. Additionally, acrylic acid (AAc), 3-aminopropyl trimethoxysilane (APTMS), 3-mercaptopropyl trimethoxysilane (MPTMS), and 2-mercaptoethylamine (MEA), poly (diallyldimethylammonium) chloride (PDADMAC), and poly (ethylene glycol) diacrylate (PEG-DA) were all used as received.

3.2.2. Microgel Synthesis and Characterization

Microgels were synthesized through a previously described aqueous free radical precipitation polymerization method.^{22,23} Microgel particles were composed of NIPAm (70%), AAc (26%), and PEG-DA (4%), herein referred to as MG-26, with a total monomer concentration of 120 mM; SDS and APS were used during synthesis as surfactant and initiator, respectively. NIPAm, BIS and SDS were dissolved in distilled deionized water, filtered through a 0.2 μm filter into a 3-neck round-bottom flask and heated to 70 $^{\circ}\text{C}$ while purging under N_2 for 1 h. Ten min prior to initiation, AAc was

added and allowed to equilibrate with the heated monomer solution. After initiation through the addition of APS, the reaction proceeded for 17 h and was quenched upon cooling to room temperature. Microgels were purified through centrifugation and resuspension in distilled deionized water and were lyophilized to increase storage time.

Microgels composed of NIPAm (88%), AAc (20%) and BIS (2%), designated herein as MG-20, and microgels composed of NIPAm (75%), AAc (10%) and BIS (5%), designated MG-10, were also synthesized by precipitation polymerization with total monomer concentrations of 150 mM and 120 mM, respectively. These syntheses were carried out in the same manner as the microgels described above, and were also cleaned by centrifugation and lyophilized to increase storage time.

The hydrodynamic radii of the microgels were measured by Dynamic Light Scattering (DLS) using the instrument described in **Chapter 2**. All microgel types were diluted in pH 7.4 PBS buffer with an ionic strength of 100 mM (high ionic strength (HIS) PBS), and the r_h was measured at 20 °C.

3.2.3. Microgel Sample Preparation

3.2.3.1. MG-20 and MG-10 Deposition

To monitor the size, morphology, and electrical properties of individual microgels, MG-10 and MG-20 were deposited in a manner that allowed for both densely and poorly packed microgels on gold coated glass coverslips. First, a previously described method was used to functionalize glass coverslips using a mercapto- containing silane to create a thiol-rich surface.²⁴ For this, clean glass coverslips were placed in an MPTMS (2.5% V/V) solution in EtOH while shaking for 2 hr and thermally cured at 80 °C overnight. After curing, the glass coverslips were gold coated using a Hummer 6

Gold Sputterer under vacuum with a plasma discharge current of approximately 20 mA for 3 min. Gold coated glass slides were then functionalized with 1.0 mM MEA in absolute EtOH for 24 h to create an amine-modified, positively charged surface.

To deposit microgels in a poorly packed fashion, microgels were deposited onto gold coated coverslips by passive deposition. For MG-20, this was done by exposing a gold surface to a 0.1 wt% solution of the microgels for 30 min, rinsing the films with distilled deionized water and drying under N₂. To analyze MG-20 and MG-10 simultaneously, mixing of the two particle types was done in two ways. First, a clean and functionalized glass coverslip was exposed to a 1:1 ratio of MG-10 and MG-20 with a total microgel concentration of 0.1 wt% in HIS PBS for 30 min and washed with distilled deionized water to remove non-adhered microgels and dried under a stream of N₂. Second, samples with a mixture of MG-20 and MG-10 were created by first depositing a 0.1 wt% of MG-20 onto clean and functionalized glass for 30 min, then subsequently exposing samples to a 0.1 monomolar PDADMAC solution for 30 min, followed by exposure to a 0.1% solution of MG-10 for 30 min with washing between each deposition step. Samples were then washed and dried under N₂.

3.2.3.2. MG-26 Multilayer Thin Films

Multilayer films were prepared as previously described, using a modified LbL technique.^{6,25} In short, a 0.1% solution of microgels composed of MG-26 was centrifuged onto an elastomeric substrate (PDMS) at 3700 x g for 10 min using an Eppendorf 5804 R centrifuge with a plate rotor. The substrate was then washed with distilled deionized water and placed in a PDADMAC solution for 30 min while shaking.

The substrate was then removed, washed and the microgel deposition step was repeated. This was done until a total of 5 microgel deposition steps had been achieved.

3.2.3.3. MG-26 Thin Film Damage and Healing

Multilayer films containing MG-26 and PDADMAC on PDMS were damaged by gently scraping the surface. For this, the sample was secured and a pipette tip was used to scrape vertically along the sample. This scraping caused the sample to turn opaque in the areas of damage, as had been seen previously.^{25,26} This opacity is caused by changes in the film morphology, or a wrinkling of the microgel thin film. Films were healed by washing the sample with water and drying gently under N₂.

3.2.3. Characterization

The height information of microgels was obtained in conjunction with surface potential mapping using an Asylum Research (Santa Barbara, CA) MFP-3D AFM equipped with an Olympus Electric-lever Cantilever (Force Constant = 70 kHz), which is a silicon probe with a platinum coated tip. For this, a two pass technique is used. During the first pass a topographical image is obtained and during the second pass a map of the surface potential is obtained. The first pass imaging is done in a regular AFM imaging mode as previously described (see **Chapter 1** and **Chapter 2**) and the second pass image uses a technique called nap mode in which the tip is raised some distance (typically 40 nm) above the sample surface. Samples were grounded to the bottom of the AFM instrument using metal wire attached to the sample surface in order to avoid charge buildup at the surface.

3.3. Results and Discussion

Microgels and microgel-containing thin films have been characterized by a variety of techniques,²⁷ but additional characterization tools could be useful to give a deeper level understanding of charge distribution in these materials. Using KPFM the surface potential can be measured in conjunction with the topography of microgels and microgel assemblies and from this we hypothesized that a more robust understanding of charge distribution within could be determined. Once the utility of this technique is determined, measured changes in charge distribution as the film is composed can give insight into the interaction of individual components within microgel assemblies and an understanding of the source of dynamic behavior within microgel thin films could be developed.²⁵

To begin exploring the utility of KPFM as a characterization technique, MG-20 microgels were deposited onto glass substrates. For this, microgels were deposited in HIS PBS, low ionic strength (LIS) PBS, and distilled deionized H₂O. By altering the ionic strength of the solution in which the microgels are deposited, the effect of salt concentration on the microgel morphology can be explored. The results for this can be seen in **Figure 3.1** below.

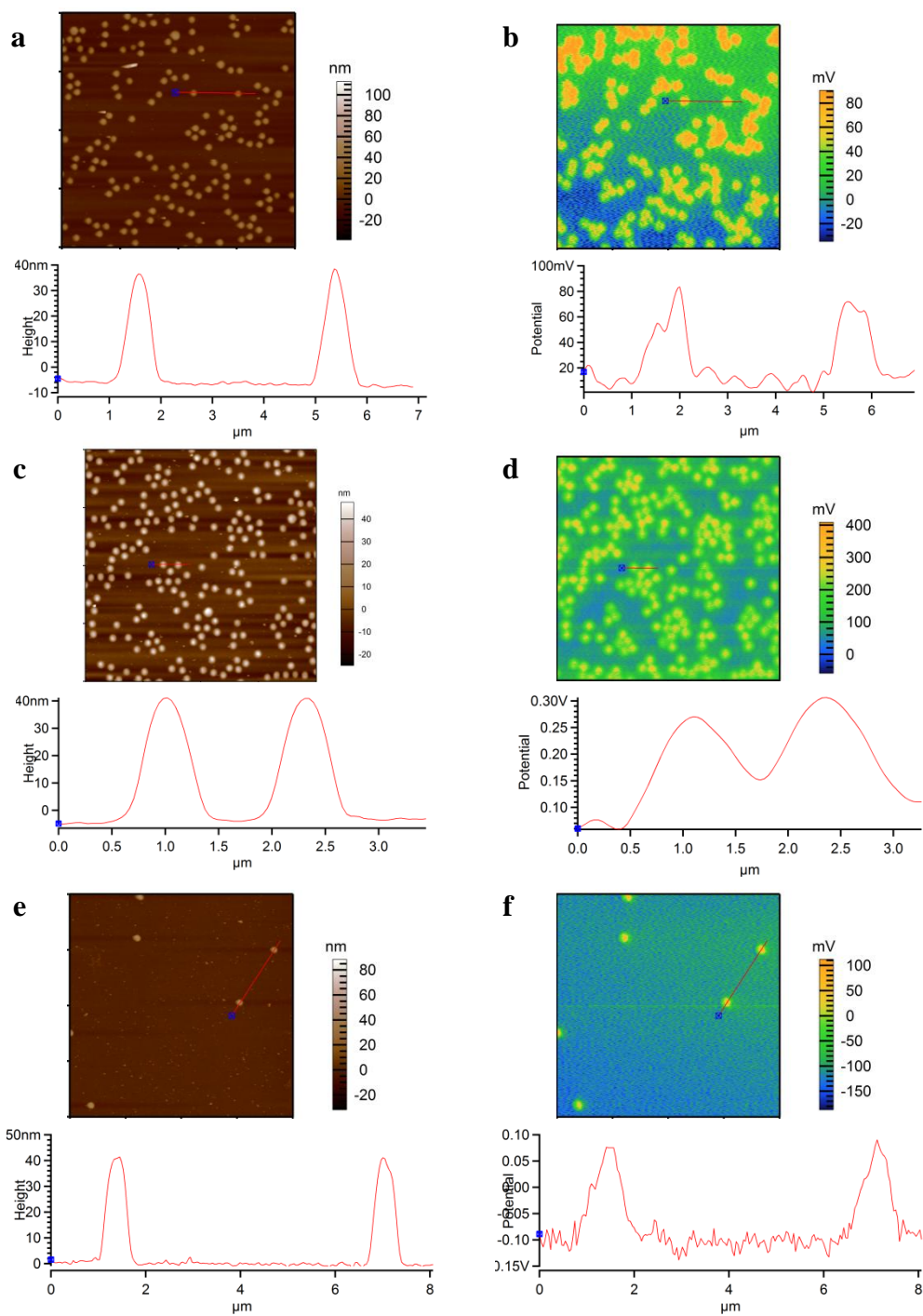


Figure 3.1. AFM height images of MG-20 deposited in HIS PBS (a), LIS PBS (b) and H₂O (c) with their corresponding KPFM height maps (d, e, and f, respectively). All contain line traces of representative microgels. All images are 20 \times 20 μm .

Images in **Figure 3.1** show the height and surface potential images for the 3 solvent conditions. To determine the surface charge of each microgel, line traces across the microgels were used to determine the surface potential difference between the microgel and the gold surface. This normalization gave a true value for the individual microgel, and allowed for an exclusion of the inherent surface charge of the conductive gold surface. Based on these line traces, the potential for microgels deposited in HIS PBS, LIS PBS, and H₂O are 75 mV, 175 mV and 200 mV, respectively, while the height of the particles in all 3 cases is ~45 nm. This suggests an increase in the ionic strength will result in a decrease in the surface potential of the microgel while the height of the particle changes negligibly.

The increase in potential with decreasing ionic strength shown in **Figure 3.1** may be caused by a shielding of the surface charge due to an increase in salt concentration. Typically a higher ionic strength is used for particle deposition because it allows for an increase in microgel packing on a surface. This is due to the fact that the microgels employed here are negatively charged, and in order to get tightly packed films some amount of charge compensation is necessary to reduce microgel-microgel repulsion. After drying samples, this charge compensation is not completely lost and the trend observed in **Figure 3.1** agrees with this. This would also explain why there are very few microgels on the surface in which microgels are deposited in distilled deionized water, in which case microgel-microgel repulsion is not compensated by any salt in solution, limiting the number of microgels capable of depositing on the surface. Additionally, these results show the possible utility of KPFM in monitoring small changes in surface charge due to solvent effects.

Building upon the results presented above, it would be of interest to see the response of the surface charge of a negatively-charged microgel upon exposure to a positively-charged species. This is of interest from the viewpoint of microgel thin film assembly because films are assembled by exposing microgels on a surface to an oppositely charged species. During exposure to this oppositely charged species, surface charge is overcompensated and the resultant film is positively charged.²⁸ Being able to monitor the surface charge of the film during film assembly would allow for a characterization of charge distribution, or possible redistribution of charged species. To test the ability of KPFM to monitor changes in microgel surface charge after exposure to a positive species, MG-20 were diluted in LIS PBS (0.1 wt%) and passively deposited onto glass surfaces to create sparsely packed monolayers. These microgels were then exposed to PDADMAC, a commonly used polyelectrolyte for the formation of multilayer microgel films.⁶ The results for this are shown in **Figure 3.2**.

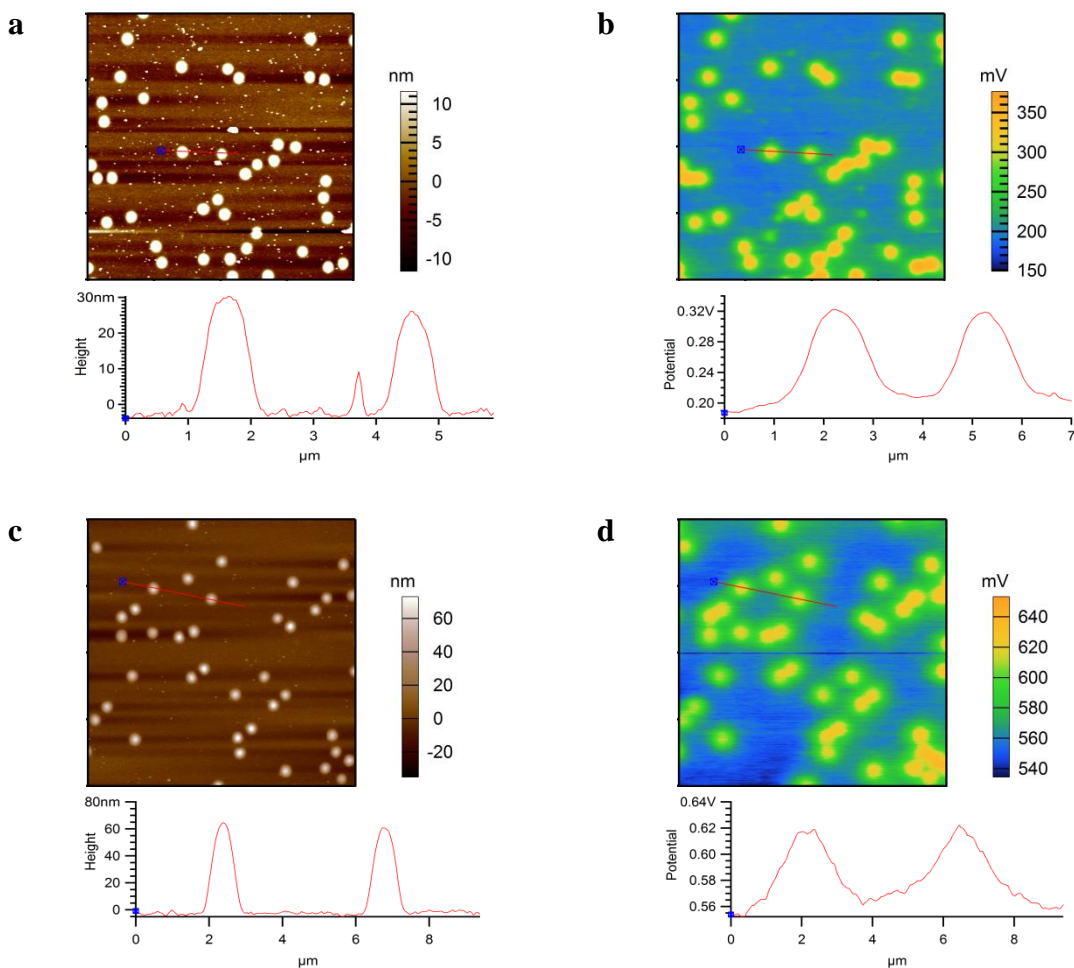


Figure 3.2. AFM height images of MG-20 before (a) and after PDADMAC exposure (c) with their respective potential maps (b,d, respectively). Representative line traces are also presented. All images are $20 \times 20 \mu\text{m}$.

The height (**Figure 3.2a,c**) and potential mapping (**Figure 3.2b,d**) show interesting results for microgels before and after PDADMAC exposure. The height of the microgel prior to exposure to the polyelectrolyte is ~ 30 nm, and after the addition of PDADMAC the height increases to ~ 60 nm. This increase in height may seem logical because additional mass is being added to the microgel, but previous studies have shown that the microgels contract upon exposure to polyelectrolyte in solution.^{29,30} Based on this increase in height shown in **Figure 3.2c**, the compression previously shown by Richtering et al. upon exposure to negatively charged polyelectrolyte does not translate to

the dried microgel. This may be an indication of size inclusion of the polyelectrolyte, but it may also be indicative of a complex interaction of the polyelectrolyte with the microgel, wherein a dense polyelectrolyte shell is created upon the microgel that creates compression and densification of the microgel. An increase in density would be apparent upon drying, wherein the bare microgel could spread on the surface to a greater degree than the denser microgel-polyelectrolyte complex. Although these results do not show which of these scenarios is true, it does show that there is a complexity within the microgel-polyelectrolyte interaction, especially when considered in the context of previously published literature.^{29,30}

When analyzing the surface potential of these microgels before and after PDADMAC exposure, the opposite trend is observed. Before exposure to PDADMAC the surface charge is ~120 mV (**Figure 3.2b**), and after exposure the surface potential is ~60 mV (**Figure 3.2d**). As noted above, when microgels were exposed to a buffer containing a lower ionic strength, there was less charge shielding or charge compensation and therefore a higher surface potential. These results suggest a similar behavior, wherein the PDADMAC is compensating for the negative charge of the microgel, which would create an overall lower surface charge. Surprisingly, the overall mapped potential was not reversed, as one would expect to be the case since the overall surface charge of the particle is being overcompensated and is therefore now positive. This should not be taken as an indication of a lack of charge overcompensation, as that aspect of film formation through LbL has become well-studied and characterized.^{6,31,32} Instead, these observations are more than likely due to environmental interactions, such as surface water or atmospheric ions from the ambient air within the AFM set-up. This has been

shown to affect the surface charge with KPFM previously^{33,34} and would also explain why the surface of the negatively charged microgels do not have a surface potential that is negative. Because of this, KPFM is better used as a qualitative method, to obtain an understanding of charge distribution and changes in charge distribution as opposed to gaining quantitative information from the given potential mapping. Therefore, the data presented in **Figure 3.2b,d** (and throughout) can be treated qualitatively, and it can be said that the decrease in the potential after exposure to PDADMAC may be explained as charge overcompensation and this conclusion can be validated by considering previous studies, wherein it has been shown that charge overcompensation takes place upon microgel exposure to an oppositely charged species.³⁵

Keeping in mind that the surface potential seems to be affected by charge compensation or lack thereof, the surface potential of microgels containing varying acid content were analyzed to determine discernibility on a surface by potential mapping. Although at this point it has been determined that KPFM is a qualitative method, it may still be useful from the standpoint of determining charge distribution in films assembled with varying acid content, which is of interest for the formation of multi-responsive or complex multilayer films. For this, two types of samples were prepared. First, a mixed microgel sample was created by depositing a mixed solution of MG-10 and MG-20 in equal parts. Second, a sparsely packed layer of MG-20 was exposed to PDADMAC, and then sequentially exposed to a solution of MG-10 using a passive layer-by-layer method. In this case, the MG-20 are exposed to the PDADMAC, but because MG-10 is deposited after PDADMAC exposure, it should not contain the polyelectrolyte. These results are

shown in **Figure 3.3**. For these images, the wider microgels are the MG-20 microgels, ($r_h = 495$ nm) and the more narrow particles are the MG-10 microgels ($r_h = 343$ nm).

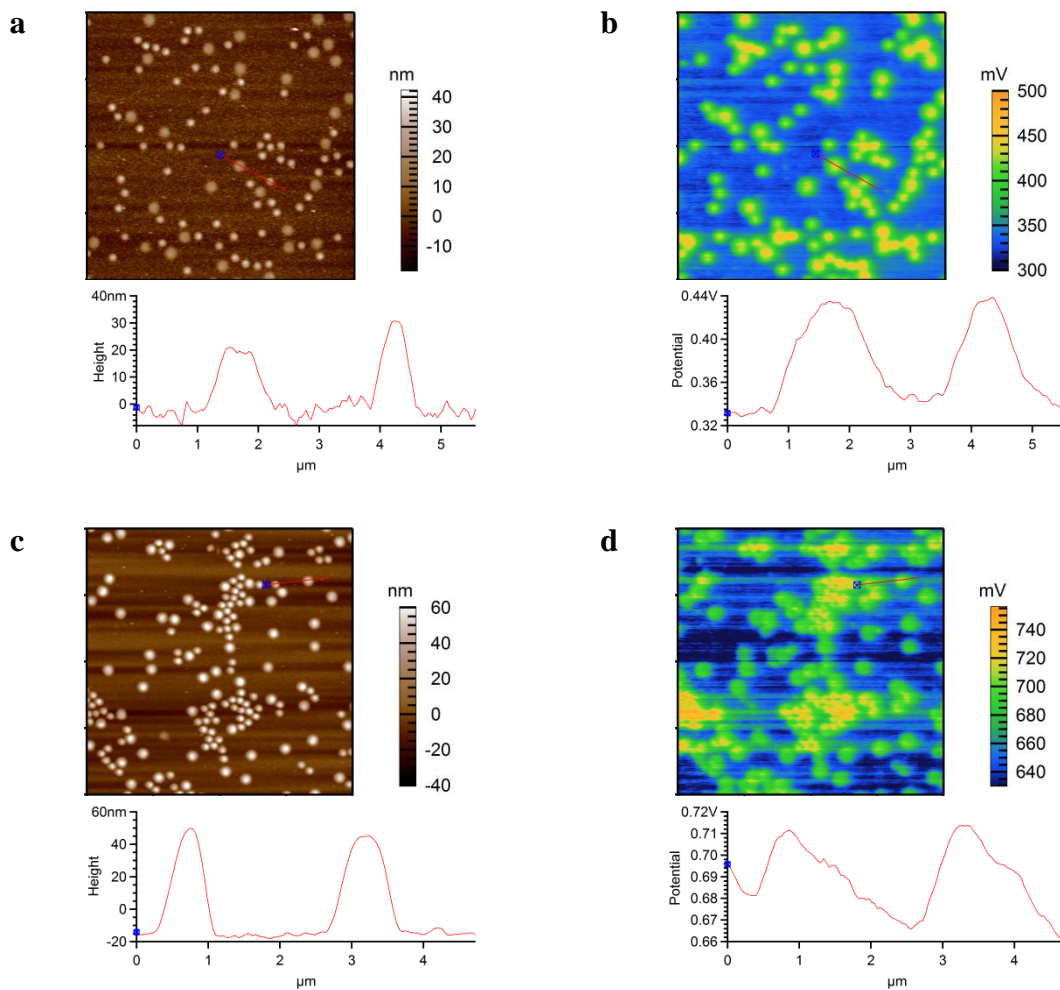


Figure 3.3. AFM height and KPFM potential maps of mixed one layer films (a,b) and two layer films (c,d) with representative height traces. Both films contain MG-10 and MG-20. All images are $20 \times 20 \mu\text{m}$.

Again, first it is worth noting the height changes between the two films. The mixed film that has not been exposed to polyelectrolyte (**Figure 3.3a**) contains microgels with heights of ~ 20 nm and ~ 35 nm for MG-20 and MG-10, respectively. This indicates that MG-10 microgels are denser due to an increased cross-linker concentration, which agrees with previous studies.³⁶⁻³⁸ However, in the mixed microgel sample wherein MG-

20 was deposited first and MG-10 was deposited after deposition of PDADMAC, the height of the microgels is ~60 nm for both particle types. If we consider the height MG-20 before exposure to PDADMAC (~20 nm), the height of MG-20 after exposure to PDADMAC has increased 3 fold. The increase of particle height is expected based on the results presented above (see **Figure 3.2a,c**). Additionally, there also appears to be a height increase (from ~35 nm to ~60 nm) of the second particle type, which was not expected because it was not exposed to PDADMAC. The potential maps of the two sample types (**Figure 3.3b,d**) do not seem to show distinguishable differences in potential between MG-20 and MG-10 in either sample, however the sample containing a mixed (MG-20 and MG-10) microgel deposition (**Figure 3.3a**) shows a potential of ~100 mV, whereas when MG-20 and MG-10 are deposited sequentially with a PDADMAC deposition step between, both microgel types show a potential of ~50 mV. This trend, wherein a decrease in microgel potential is observed after exposure to PDADMAC, agrees with the results seen in **Figure 3.2**. Taking all of this information together, these results could imply charge redistribution after MG-10 deposition. This would indicate a movement of polyelectrolyte and an overall microgel potential decrease, regardless of whether the microgel was deposited before or after PDADMAC. These results of course are suggestive, and possible charge redistribution within microgel films will be explored in more detail in **Chapters 4** and **5**.

3.4. Conclusions and Outlook

The work described in this chapter sought to better define KPFM as a characterization technique for microgels and microgel assemblies. Through the characterization of various surfaces using KPFM to monitor the topographical and

potential information, it was shown that KPFM may be a useful qualitative tool for monitoring changes in surface charge. Limitations in the method may be due to environmental conditions, such as environmental water within ambient air, and the method may benefit from improved control over atmospheric conditions. For example, it may be of use to flood the AFM chamber with N₂ before imaging to remove artifacts from ambient air. Although quantitative data was not obtained, these first pass results show the prospective use of KPFM as a characterization tool due to its sensitivity and ability to characterize microgels and their assemblies in new and interesting ways.

An interesting future application of KPFM would be the characterization of microgel multilayer films. It has been shown previously in the group that microgel multilayer films are capable of self-healing upon exposure to water.²⁵ It would be beneficial in characterizing this phenomenon to be able to monitor the charge distribution within such films before, during damage and after healing. This may give insight into charge redistribution during healing, which may be relevant to the pathway of healing. A first pass effort in understanding charge distribution during damage and healing is shown in **Figure 3.4**. For this, 5 layer films composed of MG-26 and PDADMAC were built on PDMS and damaged by stretching by 10% with healing of the film taking place after exposure to distilled deionized water.

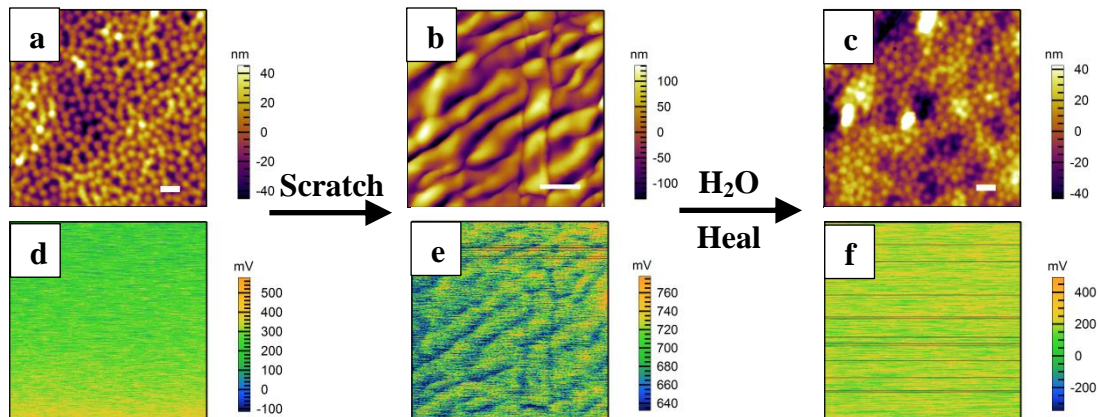


Figure 3.4. KPFM height and potential maps of 5 layer microgel films composed of MG-26 and PDADMAC before damage (a,d), during damage (b,e), and after healing (c,f). Scale bar = 1 μm .

The height images of the 5 layer microgel film at the different stages of damage and healing match nicely with the previously published results,^{25,26} with damage (**Figure 3.4b**) resulting in a wrinkling effect of the microgel film. The corresponding surface potential images show that the film before damage and after healing do not contain significant potential variation, whereas during damage there are noticeable differences in the potential that seem to coincide with the damaged regions of the film. These results are interesting from the standpoint of understanding microgel thin film damage and healing, as they suggest that damage creates uneven charge distribution, and upon healing there is a redistribution of this charge to a more energetically favorable state. However, as was true for the results shown in previous sections these results remain completely qualitative and also appear to suffer from imaging artifacts, as can be seen in the dark lines across the potential images in **Figure 3.4e,f**. These could be an indication of imperfect imaging parameters, such as scan speed. Alternatively, it could be a factor of the substrate chosen for damage and healing, which is an insulating substrate (PDMS), as opposed to a conductive substrate as was shown in the previous sections. The effect of

the chosen substrate on determining the potential of the surface is not known, although studies on both types of substrates have been done with very different materials.^{20,34} These damage and healing studies were another indication that quantitative information is currently not understood for these surfaces, however this shows once again that qualitative information about charge distribution can be obtained for microgel containing surfaces.

To summarize, the charge distribution of microgels before and after exposure was explored by mapping the topographical information and potential information of surfaces using a two pass technique. These results showed promise as a method for monitoring changes in surface potential due to environmental conditions, such as solvent conditions (**Figure 3.1**) or exposure to an oppositely charged species (**Figure 3.2**). There proved to be limitations in the method due to a lack of ability to gain quantitative information. Future experiments should focus on developing a richer understanding of the qualitative data obtainable during potential mapping. The development of a more quantitative analysis of such films may give insight into the potential variations shown during damage and healing, which would be helpful in gaining additional information about the damaging and healing process of microgel thin films. In the interim, this technique shows promise as a mode of detecting subtle changes in microgel charge density upon environmental changes, which may be useful during microgel thin film development.

3.5. References

- [1] Pelton, R. H.; Chibante, P., Preparation of Aqueous Latices with N-Isopropylacrylamide. *Colloids Surf.* **1986**, *20*, 247-256.
- [2] Blackburn, W. H.; Lyon, L. A., Size-Controlled Synthesis of Monodisperse Core/Shell Nanogels. *Colloid Polym. Sci.* **2008**, *286*, 563-569.

- [3] Hu, X. B.; Tong, Z.; Lyon, L. A., Multicompartment Core/Shell Microgels. *J. Am. Chem. Soc.* **2010**, *132*, 11470-11472.
- [4] Nayak, S.; Gan, D. J.; Serpe, M. J.; Lyon, L. A., Hollow Thermoresponsive Microgels. *Small* **2005**, *1*, 416-421.
- [5] Smith, M. H.; Lyon, L. A., Multifunctional Nanogels for Sirna Delivery. *Acc. Chem. Res.* **2012**, *45*, 985-993.
- [6] South, A. B.; Whitmire, R. E.; Garcia, A. J.; Lyon, L. A., Centrifugal Deposition of Microgels for the Rapid Assembly of Nonfouling Thin Films. *ACS Appl. Mater. Interfaces* **2009**, *1*, 2747-2754.
- [7] Wiedemair, J.; Serpe, M. J.; Kim, J.; Masson, J. F.; Lyon, L. A.; Mizaikoff, B.; Kranz, C., In-Situ Afm Studies of the Phase-Transition Behavior of Single Thermoresponsive Hydrogel Particles. *Langmuir* **2007**, *23*, 130-137.
- [8] Sorrell, C. D.; Lyon, L. A., Bimodal Swelling Responses in Microgel Thin Films. *J. Phys. Chem. B* **2007**, *111*, 4060-4066.
- [9] South, A. B.; Lyon, L. A., Direct Observation of Microgel Erosion Via in-Liquid Atomic Force Microscopy. *Chem. Mater.* **2010**, *22*, 3300-3306.
- [10] Saxena, S.; Spears Jr, M. W.; Yoshida, H.; Gaulding, J. C.; Garcia, A. J.; Lyon, L. A., Microgel Film Dynamics Modulate Cell Adhesion Behavior. *Soft Matter* **2014**, *10*, 1356-1364.
- [11] Melitz, W.; Shen, J.; Kummel, A. C.; Lee, S., Kelvin Probe Force Microscopy and Its Application. *Surf. Sci. Rep.* **2011**, *66*, 1-27.
- [12] Nonnenmacher, M.; Oboyle, M. P.; Wickramasinghe, H. K., Kelvin Probe Force Microscopy. *Appl. Phys. Lett.* **1991**, *58*, 2921-2923.
- [13] Hallam, T.; Duffy, C. M.; Minakata, T.; Aando, M.; Siringhaus, H., A Scanning Kelvin Probe Study of Charge Trapping in Zone-Cast Pentacene Thin Film Transistors. *Nanotechnology* **2009**, *20*, 1-8.
- [14] Liu, L.; Li, G., Electrical Characterization of Single-Walled Carbon Nanotubes in Organic Solar Cells by Kelvin Probe Force Microscopy. *Appl. Phys. Lett.* **2010**, *96*, 083302(1)-083302(3).
- [15] Thompson, M.; Cheran, L. E.; Zhang, M. Q.; Chacko, M.; Huo, H.; Sadeghi, S., Label-Free Detection of Nucleic Acid and Protein Microarrays by Scanning Kelvin Nanoprobe. *Biosens. Bioelectron.* **2005**, *20*, 1471-1481.

- [16] Sinensky, A. K.; Belcher, A. M., Label-Free and High-Resolution Protein/DNA Nanoarray Analysis Using Kelvin Probe Force Microscopy. *Nat. Nanotechnol.* **2007**, *2*, 653-659.
- [17] Finot, E.; Leonenko, Y.; Moores, B.; Eng, L.; Amrein, M.; Leonenko, Z., Effect of Cholesterol on Electrostatics in Lipid-Protein Films of a Pulmonary Surfactant. *Langmuir* **2010**, *26*, 1929-1935.
- [18] Clack, N. G.; Salaita, K.; Groves, J. T., Electrostatic Readout of DNA Microarrays with Charged Microspheres. *Nat. Biotechnol.* **2008**, *26*, 825-830.
- [19] Kelvin, L., Contract-Electricity of Metals. *Philos. Mag. & J. Sci.* **1898**, *46*, 82-120.
- [20] Sadewasser, S.; Glatzel, T., In *Kelvin Probe Force Microscopy: Measuring and Compensating Electrostatic Forces*. Springer: 2011.
- [21] Korokin, A.; Gusev, E.; Labanowski, J. K.; Luryi, S., In *Nanotechnology for Electronic Materials and Devices*. Springer: 2010.
- [22] Jones, C. D.; Lyon, L. A., Synthesis and Characterization of Multiresponsive Core-Shell Microgels. *Macromolecules* **2000**, *33*, 8301-8306.
- [23] Debord, J. D.; Lyon, L. A., Thermoresponsive Photonic Crystals. *J. Phys. Chem. B* **2000**, *104*, 6327-6331.
- [24] Halliwell, C. M.; Cass, A. E. G., A Factorial Analysis of Silanization Conditions for the Immobilization of Oligonucleotides on Glass Surfaces. *Anal. Chem.* **2001**, *73*, 2476-2483.
- [25] South, A. B.; Lyon, L. A., Autonomic Self-Healing of Hydrogel Thin Films. *Angew. Chem., Int. Ed.* **2010**, *49*, 767-771.
- [26] Gaulding, J. C.; Spears, M. W.; Lyon, L. A., Plastic Deformation, Wrinkling, and Recovery in Microgel Multilayers. *Polymer Chemistry* **2013**, *4*, 4890-4896.
- [27] Hendrickson, G. R.; Smith, M. H.; South, A. B.; Lyon, L. A., Design of Multiresponsive Hydrogel Particles and Assemblies. *Adv. Funct. Mater.* **2010**, *20*, 1697-1712.
- [28] Decher, G.; Hong, J. D.; Schmitt, J., Buildup of Ultrathin Multilayer Films by Self-Assembly Process .3. Consecutively Alternating Adsorption of Anionic and Cationic Polyelectrolytes on Charged Surfaces. *Thin Solid Films* **1992**, *210*, 831-835.

- [29] Greinert, N.; Richtering, W., Influence of Polyelectrolyte Multilayer Adsorption on the Temperature Sensitivity of Poly(N-Isopropylacrylamide) (PNiPAM) Microgels. *Colloid Polym. Sci.* **2004**, *282*, 1146-1149.
- [30] Wong, J. E.; Diez-Pascual, A. M.; Richtering, W., Layer-by-Layer Assembly of Polyelectrolyte Multilayers on Thermoresponsive P(NiPAM-Co-MAA) Microgel: Effect of Ionic Strength and Molecular Weight. *Macromolecules* **2009**, *42*, 1229-1238.
- [31] Decher, G., Fuzzy Nanoassemblies: Toward Layered Polymeric Multicomposites. *Science* **1997**, *277*, 1232-1237.
- [32] Serpe, M. J.; Jones, C. D.; Lyon, L. A., Layer-by-Layer Deposition of Thermoresponsive Microgel Thin Films. *Langmuir* **2003**, *19*, 8759-8764.
- [33] Sugimura, H.; Ishida, Y.; Hayashi, K.; Takai, O.; Nakagiri, N., Potential Shielding by the Surface Water Layer in Kelvin Probe Force Microscopy. *Appl. Phys. Lett.* **2002**, *80*, 1459-1461.
- [34] Rezende, C. A.; Gouveia, R. F.; da Silva, M. A.; Galembeck, F., Detection of Charge Distributions in Insulator Surfaces. *J. Phys.-Condes. Matter* **2009**, *21*.
- [35] Wong, J. E.; Muller, C. B.; Laschewsky, A.; Richtering, W., Direct Evidence of Layer-by-Layer Assembly of Polyelectrolyte Multilayers on Soft and Porous Temperature-Sensitive PNiPAM Microgel Using Fluorescence Correlation Spectroscopy. *J. Phys. Chem. B* **2007**, *111*, 8527-8531.
- [36] Nayak, S.; Lyon, L. A., Soft Nanotechnology with Soft Nanoparticles. *Angew. Chem., Int. Ed.* **2005**, *44*, 7686-7708.
- [37] Senff, H.; Richtering, W., Influence of Cross-Link Density on Rheological Properties of Temperature-Sensitive Microgel Suspensions. *Colloid Polym. Sci.* **2000**, *278*, 830-840.
- [38] Stieger, M.; Richtering, W.; Pedersen, J. S.; Lindner, P., Small-Angle Neutron Scattering Study of Structural Changes in Temperature Sensitive Microgel Colloids. *The Journal of Chemical Physics* **2004**, *120*, 6197-6206.

CHAPTER 4

DIRECT VISUALIZATION OF THE INTERACTIONS OF MICROGEL THIN FILM BUILDING BLOCKS

Portions adapted from:

Herman, E.S.; Lyon, L.A. Direct Visualization of the Interactions of Microgel Thin Film Building Blocks. *Colloid Polym. Sci.* **In Preparation.**

4.1. Introduction

As discussed in previous chapters, microgels are an incredibly appealing class of materials due to their inherent versatility. However, while it has been shown that the inherent properties and versatility of microgels (i.e. deformability, swellability, responsivity) are particularly appealing, the characterization of these materials has been shown to be a difficult task. This is due to the complexity contained within the microgel structure. This complexity stems from what is known as a polymer/colloid duality.¹ In short, the microgel contains both polymeric and colloidal properties. This makes microgels an incredibly versatile material, but also very complicated to define. Because of this duality, the behavior of a microgel cannot be equated to that of a linear polymer chain or a hard colloidal sphere. Instead, the properties and behavior of the microgel are unique, and must be treated as such.

This characteristic properties of microgels have been probed in a wide variety of studies, from the fundamental^{2,3} to application.⁴ For example, one particular group of studies conducted in the Lyon lab has aimed to define the mechanical flexibility of the microgel by analyzing their passage through glass nanopore membranes (GNM).^{2,5,6} The studies showed the translocation of microgel particles across GNM's with a much smaller

diameter than the microgel itself, and information regarding the mechanics and polymer physics of individual microgels^{2,6} could be divulged. The development of this method led to a better understanding of the capabilities of these flexible colloidal materials as drug delivery vehicles.²

The mechanical flexibility and deformability of microgels has also become integral in the formation of large scale microgel assemblies. One example of this can be seen in the formation of microgel multilayer thin films, wherein microgels are deposited using an active deposition technique. For this, negatively charged microgels are placed onto an oppositely charged substrate by using centrifugal force.⁷ This active deposition technique creates monodisperse monolayers with greater packing and lower particle footprints as compared to passive deposition, in which microgels are deposited by dip-coating.⁸ This close packing and decreased footprint can be attributed to the inherent deformability and “softness” of the microgels. These well-packed monolayers are then used as a template for the formation of multilayer microgel films using an oppositely charged polyelectrolyte in conjunction with a modified layer-by-layer (LbL) technique.⁷ These multilayer assemblies have shown promise for applications, such as non-fouling,⁷ self-healing⁹ or responsive interfaces.¹⁰

The compressibility and deformability microgels in colloidal crystals has also been shown,¹¹⁻¹³ and in one example a sample of smaller particles ($\sim 0.7 \mu\text{m}$ in diameter) was doped with larger microgels ($\sim 1.75 \mu\text{m}$ in diameter) and it was observed that the final microgel colloidal crystal was defect free. This study beautifully showed the ability of microgels to deform and create well-packed defect-forgiving monodisperse colloidal crystals.¹³

Although the use of microgels within assemblies has shown great utility¹⁴⁻¹⁶ and has been reviewed extensively,^{1,17-19} a complete picture of the complexity of microgels, particularly within large scale structures, is still not completely understood. This again can be attributed to the so called polymer/colloid duality of microgels,¹ which states that the colloidal behavior as well as polymeric behavior of microgels must be considered when characterizing this material. Because of this, the behavior of microgels within any dispersion or assembly contains far more intricacies than hard spheres or linear polyelectrolytes alone, and when characterizing these materials this must be considered.

This chapter is dedicated to understanding the behavior and interaction of microgel thin film building blocks within early stages of microgel thin film assembly. This behavior is assessed while keeping in mind the fundamental understanding of microgel deformability and swellability as presented above and the complexity contained within microgels. This work also seeks to divulge the fundamental differences between the original film model (**Scheme 1.3**), which depicts each deposition step resulting in an increase in film thickness, as well as irreversible incorporation of thin film building blocks, and begin developing a true model of microgel thin film assembly. The process of assembling a complex species such as the microgel with a linear polyelectrolyte, which also can exhibit complex behavior,²⁰⁻²² is multifaceted and therefore are not as easily defined as purely linear polyelectrolyte films.^{20,21} Although the true nature of the behavior of these two components within film assembly is a difficult question to divulge, an understanding of the early stages of film assembly and the interactions contained therein would aid in the creation of a more complete and robust picture of multilayer film assembly, which ultimately would enrich the current understanding of the dynamic

behavior of microgel multilayer films. This chapter will focus on creating a more full-bodied understanding of the significant interactions at play during the early stages of film assembly. By using varying microgel deposition parameters and monitoring the distribution of polyelectrolyte with the first two microgel deposition steps, behavior and interactions of the building materials of microgel thin films is visualized.

4.2. Experimental

4.2.1. Materials

All chemicals used herein and not listed below were purchased and used as described in **Chapter 2** and **Chapter 3**. Additionally, poly-L-Lysine (M.W. \geq 300,000) was purchased from Sigma Aldrich and used as received. Alexa Fluor[®] 488 Carboxylic Acid, Succinimidyl Ester was purchased from Life Technologies and used as received.

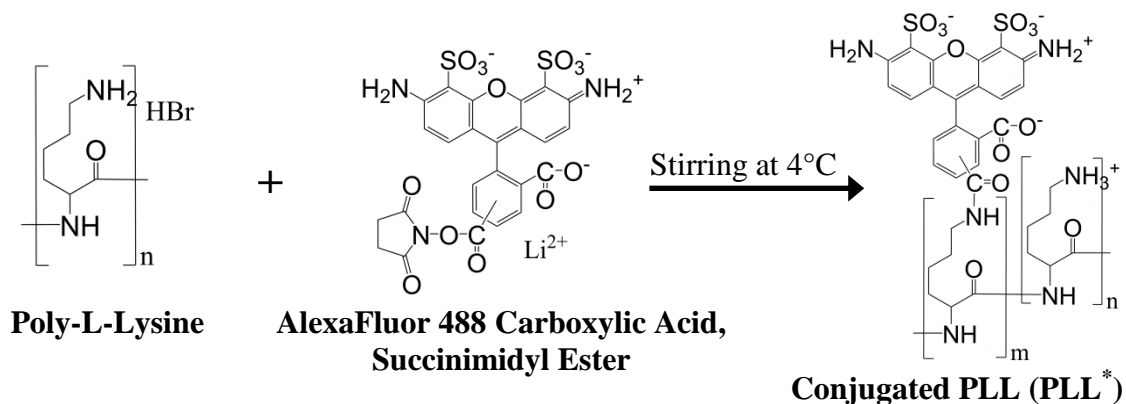
4.2.2. Microgel Synthesis and Characterization

Microgels composed of 88% NIPAm, 20% AAc and 2% BIS (MG-20) and 75% NIPAm, 10 % AAc, and 5 % BIS (MG-10) were used herein. The synthesis and characterization by DLS of MG-20 and MG-10 microgels can be found in **Chapter 2**. The lyophilized microgels were re-dispersed in a HIS PBS at a concentration of 1 mg/mL.

4.2.3. PLL* Preparation and Characterization

Poly-L-Lysine (PLL) was fluorescently labeled with the AlexaFluor 488 Carboxylic Acid, Succinimidyl Ester by first re-suspending the AlexaFluor 488 dye at a concentration of 10 mg/mL in tetrahydrofuran (THF). PLL with a MW \geq 300,000 was re-suspended in 20 mM HIS PBS at a concentration of 5 mg/mL. While stirring,

AlexaFluor 488 Carboxylic Acid, Succinimidyl Ester was added dropwise and allowed to stir for 1 h at 4 °C. The conjugated PLL was purified by dialysis with distilled deionized water using dialysis tubing with a molecular weight cutoff of 12-14,000 (VWR Scientific). The mechanism for the conjugation is shown in **Scheme 4.1** below.



Scheme 4.1. Conjugation of PLL to AlexaFluor 488 Carboxylic Acid, Succinimidyl Ester to create the conjugated PLL (PLL^{*}).

The % conjugation of the AlexaFluor dye to PLL was determined by UV-VIS. For this, the fluorescent PLL (PLL^{*}) was diluted to varying degrees and the absorbance at 495 nm was measured. A Beer's Law plot of the absorbance of the PLL^{*} versus the PLL concentration was constructed and the % conjugation was calculated. **Figure 4.1** shows the plot from which the % conjugation was calculated. The % conjugation was determined to be $4.2 \pm 0.5\%$.

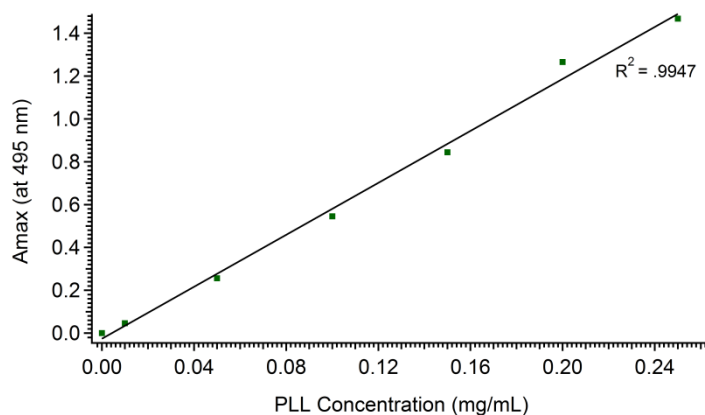


Figure 4.1. Beer's Law plot of absorbance (at 495 nm) versus PLL concentration (mg/mL). From this, the % conjugation of AlexaFluor to PLL was calculated ($4.2 \pm 0.5\%$).

4.2.4. Sample Preparation and Microscopy

To monitor the beginning stages of microgel film assembly, both passively and actively deposited monolayers composed of MG-20 were built on a silanized substrate.

For this, an amine rich glass substrate was first prepared by placing 12 mm round coverslips in a (3-aminopropyl) trimethoxysilane (APTMS) solution (1% v/v) for 2 hours while shaking. The functionalized glass coverslips were then removed from solution and rinsed with 70% ethanol and distilled deionized water and dried under N_2 . Glass coverslips were then placed in individual wells within a 24-well plate and allowed to equilibrate in HIS PBS. The PBS solution was then removed and replaced with a 0.1 mg/mL solution of microgels re-suspended in HIS PBS. Negatively charged microgels were deposited onto the positively charged surface by passive deposition using varied deposition times (10 min, 30 min, 1 hr, 2 hr, 3 hr, 4 hr, 5 hr, 10 hr, and 15 hr) or by centrifugal deposition ($2250 \times g$, 10 min). These samples were then rinsed with distilled deionized water and placed in a 1 mg/mL PLL* solution for 2 hr while shaking.

Samples were then removed from the PLL* solution, rinsed, and dried under N_2 . Next,

microgels were deposited onto the PLL rich surface by maintaining the same deposition time or technique as was used for the previous microgel deposition step (varied passive deposition time or centrifugal deposition).

Films were imaged before and after the deposition of the second microgel layer using an inverted IX-71 Olympus microscope equipped with an oil-immersion 100x objective and a Photometrics Coolsnap MYO charge-coupled device (CCD) camera (Tucson, AZ). The location of PLL* was imaged during fluorescence excitation using an LED light source equipped with an excitation band pass filter of 460-500 nm and emission band pass filter of 510-560 nm. The location of microgels in brightfield and in fluorescence was recorded using a cell counting plug-in available for the program ImageJ as a means of determining the percentage of microgels containing PLL* before after after the addition of the second microgel layer.

Samples containing the polyelectrolyte PDADMAC were also assembled to check for consistency of behavior across varied polyelectrolyte species. For this, a centrifugally ($2250 \times g$ for 10 min) deposited monolayer of MG-20 was first created on the clean, silanized glass substrate. After rinsing, the monolayer was exposed to a 0.1 mg/mL solution of positively charged PDADMAC (M.W. = 400-500 kDa) for 30 min while shaking. Films were removed from PDADMAC, rinsed, and placed in a 0.1 mg/mL solution of 10% AAc containing microgels (MG-10) for 10 min. This film was again rinsed and exposed to PDADMAC for 30 min while shaking, rinsed, and placed in a 0.1 mg/mL solution of MG-20 for 10 minutes. The deposition of each layer was monitored by AFM (see **Section 2.2.4** for AFM details).

Microgel film morphology after each microgel deposition step during the LbL assembly of microgel films by active deposition was also monitored. For this, MG-20 microgels were deposited by centrifugation (2250 x g, 10 min), rinsed, and the sample was placed in the polyelectrolyte, PDADMAC (0.1 monM) for 30 minutes while shaking. The sample was rinsed and additional 3 additional microgel and 2 additional polyelectrolyte deposition steps took place. The morphology of the film after the deposition of each microgel deposition step was monitored by AFM.

4.2.5. Real-Time Microgel Tracking

To monitor the interaction of microgels in solution with microgels on a surface in real-time, passively and actively deposited microgel monolayers exposed to PLL* as described above were placed on an IX-70 inverted microscope and a drop of HIS PBS buffer was added to the sample to allow for a rehydration of the film. After the sample had equilibrated, the buffer was removed and a drop of a 1 mg/mL solution of microgels was placed on the sample. The interaction of the microgels in solution with the microgels on the glass coverslips was observed using an Andor Luca electron multiplying charge coupled device (EMCCD) camera (Belfast, UK) with a frame rate of 220 ms for a total of 1000 frames. Tracking was also done for microgels exposed to the polyelectrolyte, PDADMAC, as a comparison of the observed interactions across different polyelectrolyte species. The frame rate used for PDADMAC containing samples was 500 ms for a total of 700 frames.

4.3. Results and Discussion

In **Chapter 3** it was observed that the charge distribution and morphology of microgels could be affected by the local environment (i.e. solvent or polyelectrolyte exposure). In this case, an increase in potential was shown for microgels exposed to a lower ionic strength, and a decrease in potential was observed for microgels after exposure to PDADMAC and subsequent addition of microgels. In the latter example, the change in potential was surprising because morphological changes were not limited to microgels that were exposed to polyelectrolyte, but seemed to span to newly deposited microgels. This result suggested a more complex interaction between microgel and polyelectrolyte than originally thought. Within the realm of multilayer microgel films, the deposition of the microgel and the polyelectrolyte has always been (perhaps naively) considered a one-to-one process, wherein each deposition step results in irreversible (on the timescale of deposition) incorporation. These early results from **Chapter 3** suggested this may not hold true and showed that there may be interactions at play not only between the microgel and the polyelectrolyte, but also with subsequently deposited microgels.

As noted above, microgels are an intricate species due to their polymer/colloid duality and their interactions with charged species are not instinctive. The results from **Chapter 3** emphasizes that microgel behavior with charged species cannot be compared or modeled based on previously understood systems, such as purely polyelectrolyte films²⁰ or nanoparticle-polyelectrolyte²³ films. A true understanding of microgel film formation must be developed by monitoring the interactions and behavior of these microgel thin film building blocks.

4.3.1. Microgel Interactions with PLL-Labeled Microgel Surfaces

To divulge the interaction of microgel thin film building blocks, first the polyelectrolyte was monitored by fluorescently tagging a well-studied polyelectrolyte, PLL (herein called PLL*),²⁴⁻²⁶ and directly visualizing the location of polyelectrolyte during two microgel deposition steps. For this, passive and centrifugal deposition were used to deposit MG-20 microgels onto a surface, and the microgels were then exposed to PLL* resulting in charge overcompensation and thus a positively charged surface. A second MG-20 deposition step followed, keeping constant the deposition time and technique used for microgel deposition. A first look at this behavior can be seen in **Figure 4.2**, which shows a comparison of samples created by either utilizing a 1 hr passive microgel deposition (**Figure 4.2a-c**) or active microgel deposition (**Figure 4.2d-f**).

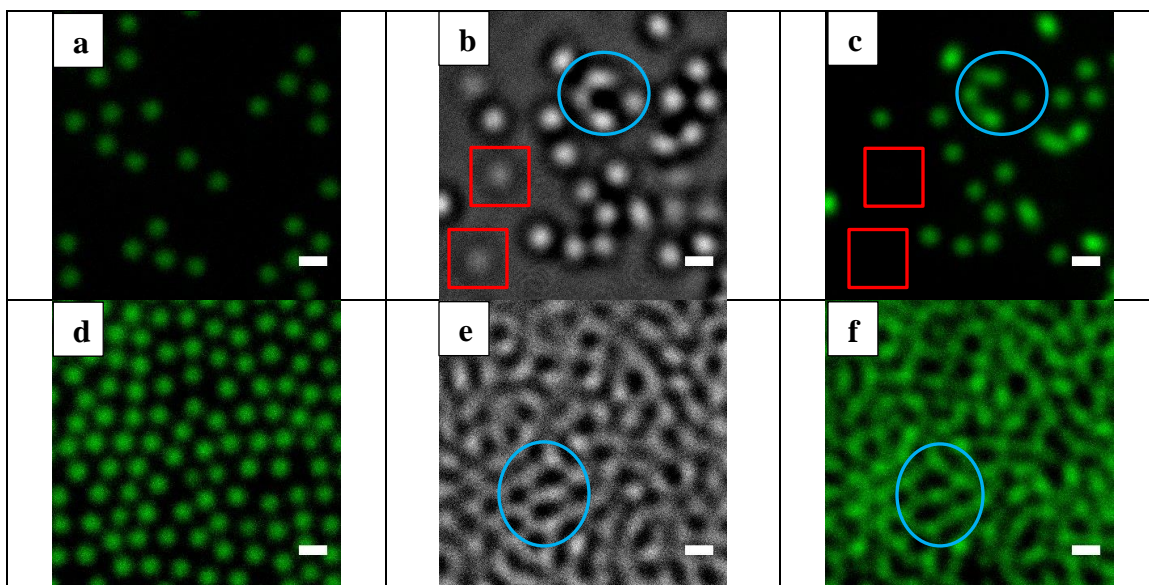


Figure 4.2. Images of passively (a) and actively (d) deposited microgels after exposure to PLL* are shown. After a second exposure to MG-20 by passive (b,d) and active (c,f) deposition films were imaged in brightfield and fluorescence, respectively. Areas lacking PLL* are shown in red squares and areas exhibiting PLL* diffusion are circled in blue. Passive deposition time = 1 hr, scale bar = 1

Both deposition techniques shown in **Figure 4.2** appear to show redistribution of the PLL* to microgels deposited during the second microgel deposition step. This is more obvious for the centrifugal deposition case (**Figure 4.2d-f**) as it appears that all of the microgels deposited by centrifugal deposition are fluorescently labeled, regardless of the deposition step in which they were deposited. The passive deposition case seems to exhibit less uniform distribution of the polyelectrolyte and several microgels after the second microgel deposition step (**Figure 4.2c**, red boxes) can be seen on the surface that are not fluorescently labeled. This implies that the redistribution of polyelectrolyte is dependent on the packing of microgels after the initial deposition step.

To understand the effect of packing on the redistribution of polyelectrolyte, a varied passive deposition times were explored and samples were analyzed by brightfield and fluorescence microscopy and compared to centrifugal deposition. To determine the extent of PLL exchange, a % overlap was calculated after the second microgel deposition step. For this, a brightfield image and a fluorescence image were taken of a representative area of the sample and individual microgels were counted on each image. A percentage of labeled microgels was determined by taking a ratio of these two values and deemed the % overlap between the two images. Representative composite brightfield and fluorescence images are shown in **Figure 4.3a-d** along with the % overlap (**Figure 4.3e**) and microgels per μm^2 (**Figure 4.3f**) in samples prepared with varying deposition times.

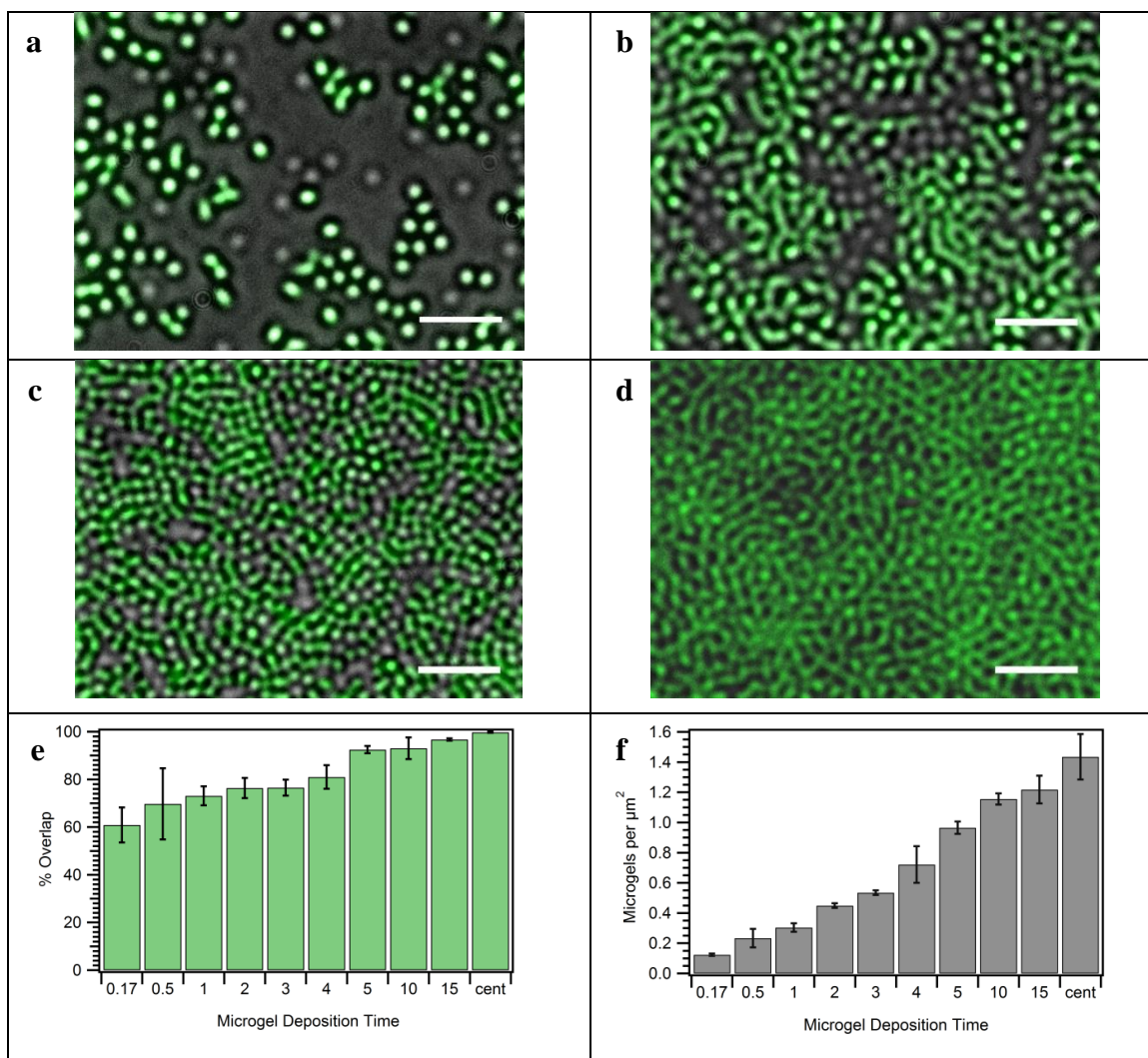


Figure 4.3. Composite images of samples composed from two microgel deposition steps with passive deposition times of 1 hr (a), 5 hr (b), 15 hr (c), and centrifugal deposition (d). The % overlap (e) and particles per μm^2 (f) are shown for varied deposition times (in hrs) and centrifugation. $n = 5$, scale bar = $5 \mu\text{m}$.

The data presented in **Figure 4.3** show the marked differences between films assembled with varied deposition time and technique. The composite (brightfield overlaid with fluorescence) images (**Figure 4.3a-d**) give a good visual representation of the morphological changes of the microgels and suggest a redistribution of polyelectrolyte. The increase in % overlap with increasing microgel deposition time adds

validity to this suggested redistribution, as increasing % overlap is indicative of an increase in PLL redistribution (**Figure 4.3e**).

To understand this % overlap, it is helpful to consider a film in which the polyelectrolyte does not redistribute. If the same deposition condition is used during the first and second microgel deposition stage, approximately the same number of microgels should deposit during these two steps. If there was not any redistribution of polyelectrolyte after the deposition of the second microgel layer, the % overlap would be ~50%, meaning that all of the microgels from the first layer were labeled, but the microgels within the second layer did not incorporate the polyelectrolyte. If there were redistribution, it would be expected that the % overlap will be > 50%, and the greater the degree of redistribution the greater the % overlap.

In these studies, microgels deposited passively for 1hr had the lowest percent overlap (61%) and the highest passive deposition time of 15 hr resulted in a 96 % overlap. Centrifugal deposition exhibited the greatest degree of redistribution, with the % overlap being ~100%. For passive deposition, increasing the microgel deposition time creates greater coverage of the silanized substrate. The presence of a >50% overlap regardless of deposition time indicated that even at short times, there is in fact some amount of redistribution. However, increasing microgel deposition time allowed for greater PLL redistribution. Results also show that even at long passive deposition times, the highest degree of redistribution (100%) or complete redistribution could not be achieved. This adds validity to previously published results,⁷ which cited centrifugal deposition as being not only a quicker method but also a more robust method allowing for a greater packing and more well-formed microgel multilayers.

The results also showed that centrifugal deposition created greater microgel packing, as indicated by the microgels per μm^2 (**Figure 4.3f**), with centrifugal deposition exhibiting the greatest number of microgels per μm^2 (1.43 microgels/ μm^2) and 1 hr passive deposition exhibiting the lowest (0.12 microgels/ μm^2). Again, even at the longest passive deposition of 15 hr, the microgels per μm^2 (1.21 microgels/ μm^2) was still lower than with centrifugal deposition, indicating that the greatest packing could only be achieved by centrifugal force. Considering this packing in conjunction with the % overlap, the results suggest that increased packing allows for maximal redistribution of polyelectrolyte upon additional microgel deposition steps which cannot be reached by passive deposition alone. This builds a better picture of polyelectrolyte behavior within the initial deposition steps of microgel film assembly. Keeping this behavior in mind, the behavior of the microgel can now be explored and analyzed.

From an analysis of the % overlap and microgels per μm^2 of the above samples, an unexpected behavior of the microgel emerged. Surprisingly, during the second microgel deposition step newly deposited microgels appeared to pack with (or next to) previously deposited microgels as opposed to positioning on top of previously deposited microgels. This was true for both the passive and active deposition techniques, which is somewhat surprising due to the fact that the overall surface charge of the sample after PLL* exposure is positive and microgels within the second deposition step are negative. At lower deposition times it could be true that microgels being deposited during the second deposition step do not “see” previously deposited microgels. However, centrifugally deposited microgels are considered optimally packed, so this lack of film growth and instead continued monolayer packing is surprising.

In order to begin developing an understanding of the interactions at play that allow for a redistribution of polyelectrolyte and increased packing over film growth, real-time monitoring of microgel deposition was utilized. For this, MG-20 microgels were first deposited by passive or active deposition. These films were then exposed to PLL* and the deposition of the second MG-20 microgel layer onto the PLL* - microgel surface was monitored in real-time. From this, a variety of interactions were visualized that may aid in developing a more detailed picture of the microgel and polyelectrolyte behavior during early stages of film development. The interactions of microgels from solution with a PLL-microgel surface in which microgels are passively deposited can be seen in **Figure 4.4**. Areas of deposition are labeled with red circles and fluorescence images (**Figure 4.4d, g, l, p**) were taken after tracking to analyze the movement (or lack thereof) of PLL* into the newly deposited microgels.

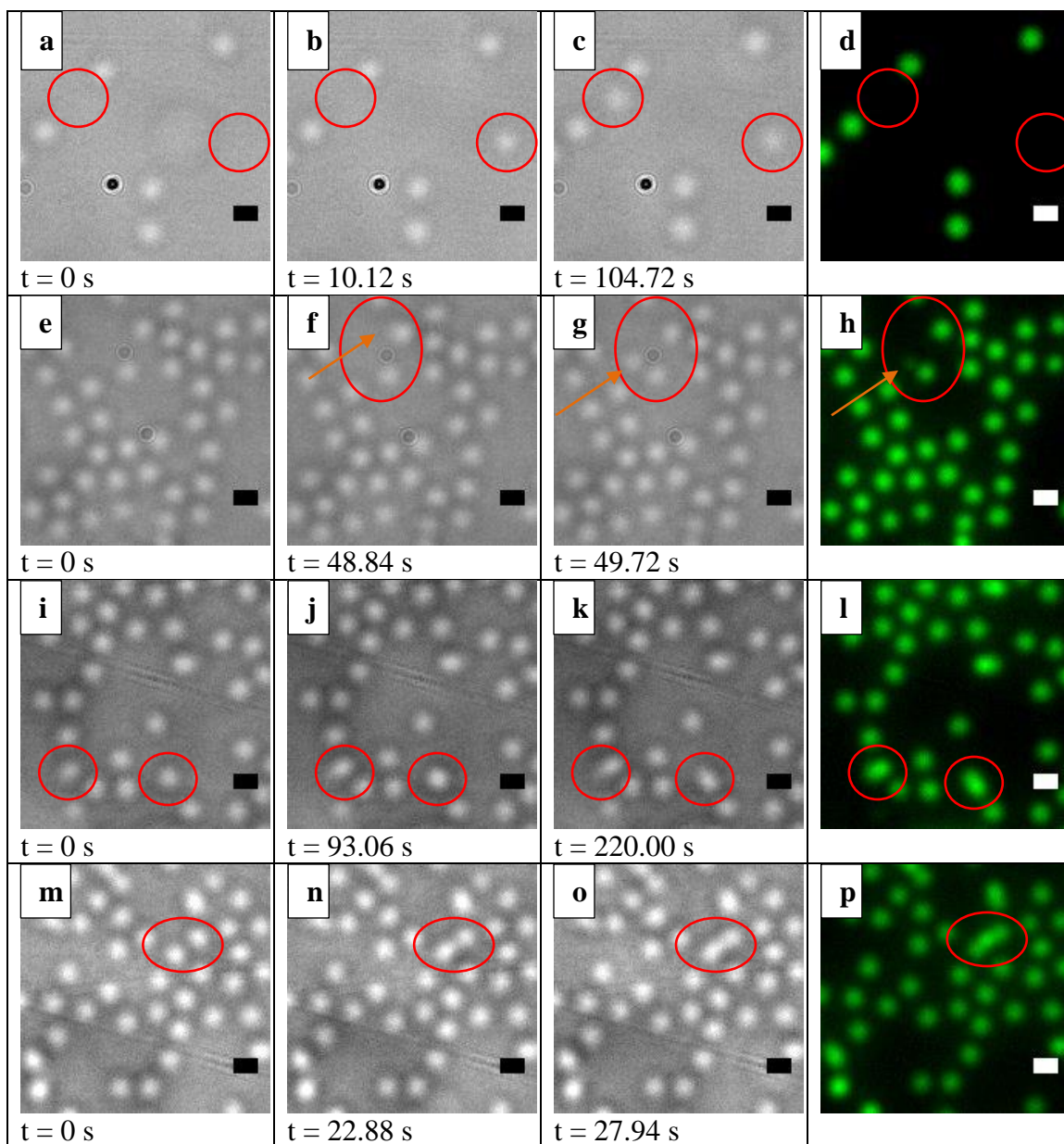


Figure 4.4. Real-time tracking of microgels depositing onto a PLL-microgel surface. Microgels from solution deposited either directly onto the surface (a-d), “sampled” the microgel surface before deposition (e-h), directly landed on microgels and slid to the substrate surface (i-l), or landed and settled between previously deposited microgels (m-p). Red circles indicate areas of deposition. Scale bar = 1 μm .

Several types of interactions were observed by tracking the deposition of microgels from solution onto passively deposited PLL^{*}-microgel surfaces and the predominant interactions will be described here. First, microgels from solution can

diffuse from solution to the sample surface and deposit directly onto the substrate without interacting with the PLL-microgel surface (**Figure 4.4a-c**). The fluorescence image from this deposition (**Figure 4.4d**) shows that the newly deposited microgel does not exhibit any fluorescence and therefore has not incorporated any (measurable amount) of PLL* .

Second, microgels from solution can fall from solution and interact with microgels on the surface (**Figure 4.4e-g**, orange arrow) and then ultimately deposit on the glass substrate (**Figure 4.4h**). In this case, the microgel from solution appears to be sampling the surface before ultimately landing on the silanized substrate. The fluorescence image after the interaction and deposition (**Figure 4.4h**) of the circled microgel (red circle) suggests that the microgel was either interacting in some way with the previously deposited PLL* - microgels, or with the microgel in close proximity to the newly deposited microgel. This is indicated because the newly deposited microgel is slightly fluorescent, indicating PLL* movement. The other two interactions presented (**Figure 4.4i-k** and **Figure 4.4m-o**) show microgels from solution interacting with the microgels on the surface by originally landing on a PLL-labeled microgel, but ultimately sliding off of the microgel and either landing on the substrate surface (**Figure 4.4i-k**) or resting between two previously deposited microgels (**Figure 4.4m-o**). Fluorescence images of these microgels after deposition show that the newly deposited microgels are now fluorescent, suggesting a redistribution of PLL* to the newly deposited microgels.

Microgels from solution showed less diverse interactions with PLL* -microgels in which microgels are centrifugally deposited as can be seen in **Figure 4.5**. Three interactions are shown here that exemplify the events witnessed during tracking of centrifugally deposited microgel surfaces after exposure to PLL and subsequent exposure

to a microgel solution. First, black arrows within **Figure 4.5a** and **Figure 4.5c** indicate newly deposited microgels that have landed directly onto a PLL* - microgel within the centrifugally deposited layer. **Figure 4.5b** and **Figure 4.5d** represent the point at which this newly deposited microgel slides from the PLL-microgel surface to the substrate surface. The amount of time required for this movement to take place is varied, here it took 23.54 s for interaction 1 (**Figure 4.5b**, yellow square) and 17.38 s for interaction 2 (**Figure 4.5d**, red circle). Alternatively, microgels from solution could also diffuse from solution and “sample” the underlying microgel surface and ultimately land directly on the silanized substrate. (**Figure 4.5e**, blue square) Also worth noting is the tendency for these newly deposited microgels to maximize surface coverage with previously deposited microgels, wherein the rearrangement of the newly deposited microgels continued until the microgel was packed into the previously deposited microgels at which point there was no longer microgel movement. For all 3 interaction conditions, the fluorescence image shows a redistribution of polyelectrolyte to the newly added microgels (**Figure 4.5f**). As opposed to passive deposition, when microgels from solution interact with a surface containing centrifugally deposited microgels all interactions result in some amount of PLL* redistribution. Taking into account the interactions shown in **Figure 4.4**, this may indicate that limiting the available underlying substrate results in greater interactions of microgels from solution with PLL-labeled microgels, and therefore greater PLL redistribution.

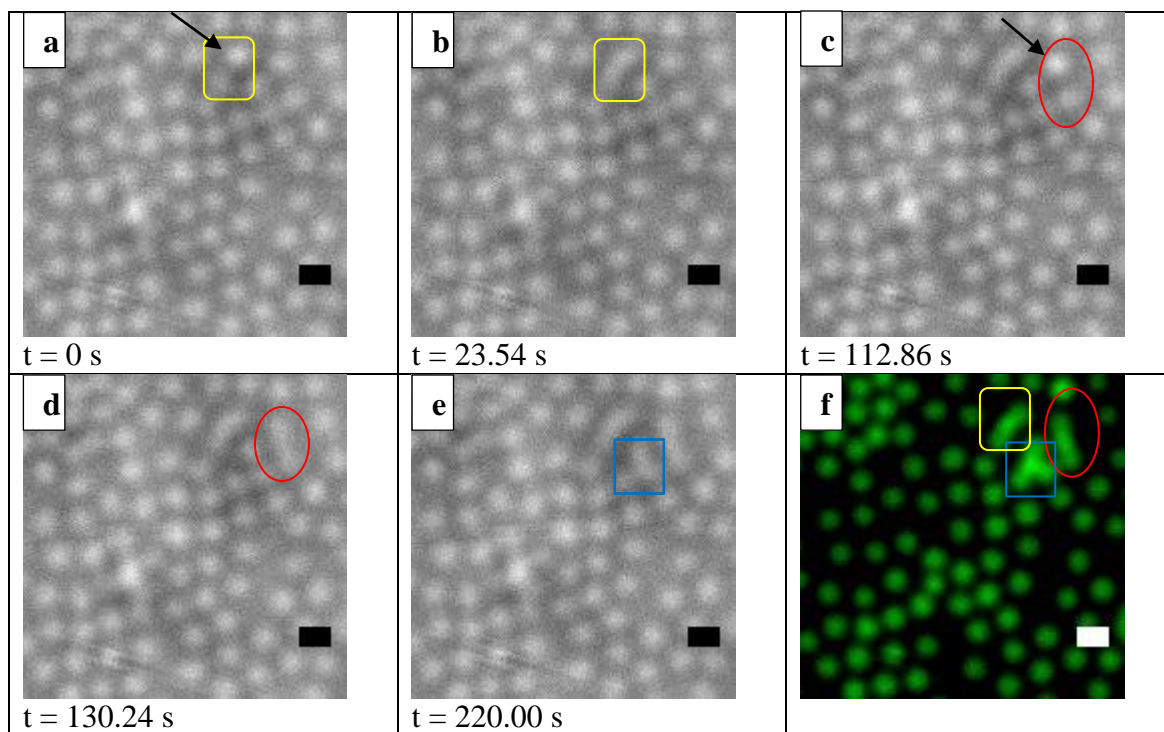


Figure 4.5. Real-time tracking of microgels depositing onto a centrifugally deposited microgel surface after exposure to PLL. The yellow square shows microgel deposition onto an underlying microgel (a) and slide-off onto the substrate (b). The red circle also shows deposition onto the microgel (c) and slide-off onto the substrate (d). The blue square shows deposition of a microgel between 3 PLL-labeled microgels. Fluorescence images show PLL redistribution after microgel deposition (f). Scale bar = 1 μm .

There are several implications worth noting from the tracked interactions of microgels from solution with passively and actively deposited microgel surfaces. First, tracking of surfaces containing actively deposited microgels, which predominately exhibit, uniform redistribution, suggest that greater packing of the surface reduces the probability that microgels will interact directly with the silanized substrate. This may suggest that the greater polyelectrolyte redistribution witnessed for actively deposited surfaces (**Figure 4.3e**) is not only attributed to the tighter microgel packing and smaller microgel footprint, but also the limited availability of the underlying silanized substrate for newly deposited microgels to directly interact.

Alternatively, the tracking of passively deposited microgel surfaces suggest that when microgels from solution interact with a surface containing poorly packed microgels labeled with PLL^{*}, there is a lower degree of polyelectrolyte redistribution. When the microgel from solution interacts directly with the silanized substrate without interacting with the underlying PLL^{*}-microgel surface, redistribution of polyelectrolyte to the newly deposited microgel is limited. This is most obvious in **Figure 4.4d** where microgels deposited during tracking did not exhibit any fluorescence. Second, results suggest microgels from solution “sample” the underlying surface, and during this process can pick up polyelectrolyte before deposition onto the silanized substrate (**Figure 5.4h**). Lastly, microgels from solution could land on PLL-microgels contained on the surface; however these newly deposited microgels did not stay directly on the PLL-labeled microgels and tended to slide from the surface of the microgel to the underlying substrate. This suggests an array of possible interactions of the microgel in solution with underlying PLL^{*}-microgel surface, which can result in varying degrees of polyelectrolyte redistribution. These interactions may be an indication of the varying degree of redistribution observed for increasing passive deposition time (**Figure 4.3e**), wherein increasing deposition time results in decreased substrate availability and therefore increased interaction of microgels from solution with the underlying PLL^{*}-microgel surface. Additional testing is necessary to quantify this, but the interactions observed give a good first insight into a direct visualization of the interactions that may be attributed to the witnessed (or lack) PLL^{*} redistribution (**Figure 4.3e**).

Results also suggest a preference of the microgel to ultimately deposit onto the silanized substrate surface, which may be explained by either a desire to rest on a hard

flat substrate as opposed to the soft contoured surface of the microgel or a preference of the microgel to maximize contact with other microgels, which can be accomplished when the newly deposited microgel “rolls” from the underlying microgel to its final location between PLL^{*}-labeled microgels. An indication of the latter behavior is most obvious for interaction 3 (blue square) from **Figure 4.5e**, wherein the microgel from solution arrived at the underlying microgel surface and shifted position between microgels before interacting permanently between three microgels (**Figure 4.5e**). Again, additional testing is needed to quantify this behavior, but the observed interactions suggest the above.

Although a complete picture of the pathway for deposition of the microgel from solution onto the underlying surface cannot be determined from these results alone, the behaviors observed can give important insight into some of the behavior that may be attributed to polyelectrolyte redistribution and thus the early pathway of microgel film assembly. Whereas it had been thought in previous years that each microgel deposition step led to an increase in microgel film thickness, the data presented within suggest that microgel films will in fact grow laterally before growing in thickness regardless of the packing of the initial microgel deposition step. These data also show an interesting behavior of the polyelectrolyte, which had been previously thought of as a “glue” within microgel multilayer thin films. Here, it can be seen that the polyelectrolyte exhibits rearrangement with microgels depositing from solution. This suggests a behavior or interaction between microgels and polyelectrolyte that has previously not been realized. Additional insight into polyelectrolyte behavior within microgel assemblies will be explored in **Chapter 5**, but the results shown herein serve as a first look and realization of the intricacies involved with polyelectrolyte-microgel behavior and assembly.

4.3.2. Microgel Interactions with PDADMAC-Labeled Microgel Surfaces

To this point, all of the data shown in this chapter have used the polyelectrolyte PLL. PLL is considered a weak polyelectrolyte,^{24,26,27} which has a tendency to exhibit diffusivity.²⁵ To determine whether the redistributive behavior of PLL exhibited above is limited to diffusive polyelectrolytes, a strong polyelectrolyte was explored. PDADMAC is an inherently strong polyelectrolyte²⁰ and was therefore chosen for these studies. By showing that the interaction of microgels with polyelectrolyte is not limited to the inherent charge characteristics of the polyelectrolyte, it can be determined that microgel behavior with polyelectrolyte is due to in large part to microgel complexity. For this, a microgel monolayer composed of MG-20 deposited by centrifugal deposition (**Figure 4.6a**) was exposed to PDADMAC and then MG-10 (10% AAc-containing) microgels were passively exposed to the surface (**Figure 4.6b**). Although centrifugation created an optimally packed monolayer, after exposure to PDADMAC and subsequent addition of MG-10, the newly deposited microgels adhered to the substrate surface. This film was then exposed to PDADMAC and MG-20 was passively deposited (**Figure 4.6c**), and the same result was seen.

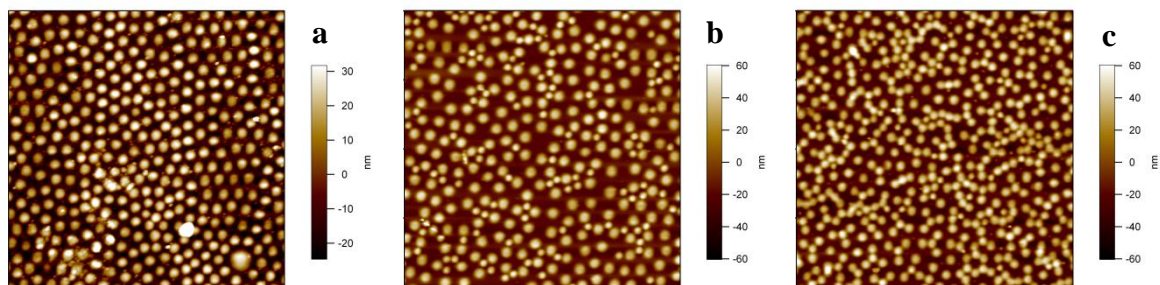


Figure 4.6. AFM height images of microgel films after a single MG-20 exposure (a), after PDADMAC and subsequent MG-10 exposure (b) and upon an additional PDADMAC exposure and subsequent deposition of MG-20 (c). Images are $20 \times 20 \mu\text{m}$.

When centrifugally deposited microgels are exposed to PDADMAC and then exposed to a microgel of different composition, the second microgel type appears to show preference to rest between the centrifugally deposited microgels as opposed to interacting and assembling atop the microgels from the first deposition step. This matches well with the results presented in **Figure 4.5** and **Figure 4.6** for microgels exposed to PLL, wherein a variety of surface interactions were witnessed, however microgels from solution tended to ultimately adhere to the silanized substrate surface as opposed to resting on the surface of PLL-labeled microgels. As a next step, tracking was utilized to determine if the interactions witnessed for PLL-microgel surfaces were also observed when microgels from solution were exposed to a PDADMAC-microgel surface. The results for this are shown in **Figure 4.7** below.

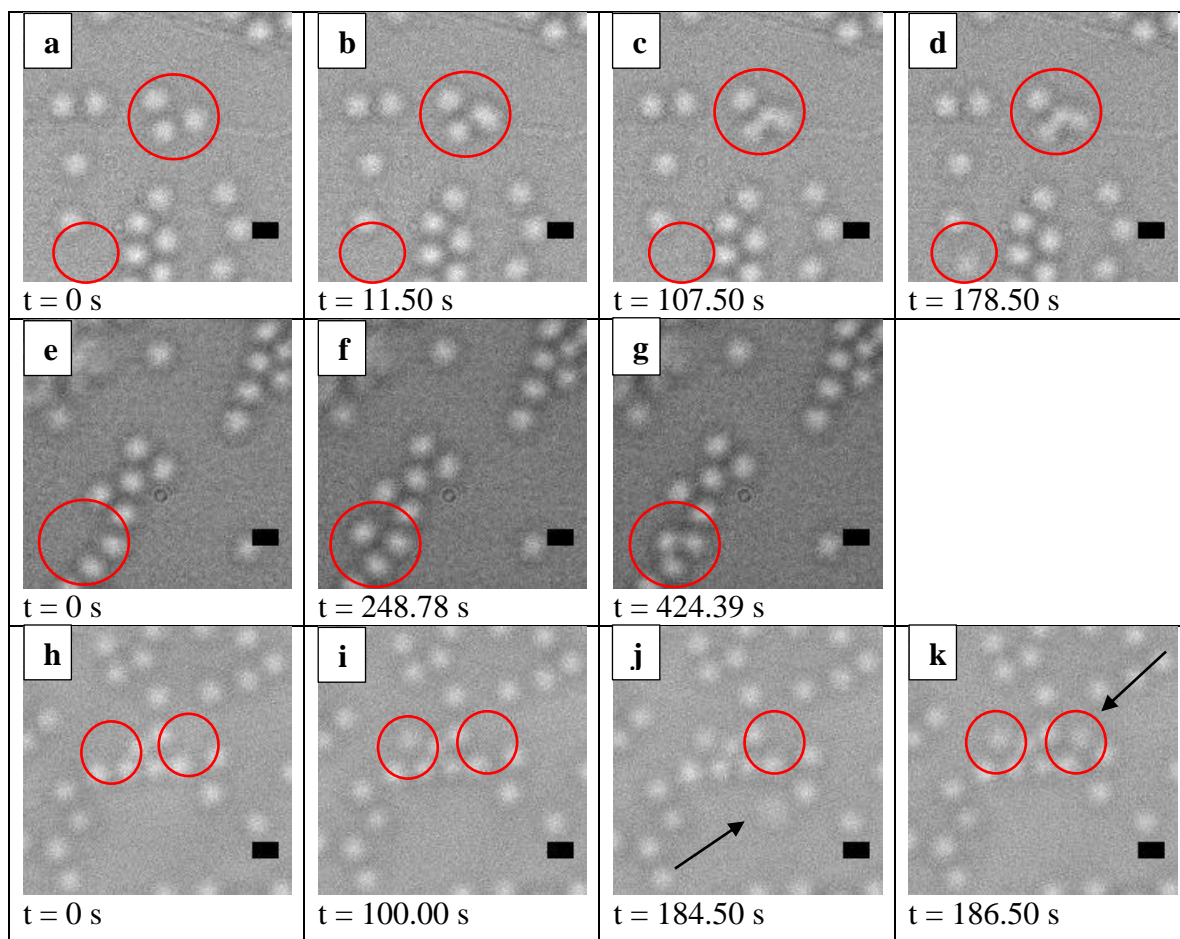


Figure 4.7. Real-time tracking of microgels from solution interacting with a PDADMAC-microgel surface. Microgels from solution deposited directly onto a PDADMAC-microgel (a) and slid off (b-c), deposited directly to the silanized substrate (d), moved into PDADMAC-microgels after depositing onto the silanized substrate (e-g), or sampled the PDADMAC-microgel surface and deposited onto the silanized substrate (h-k). Microgel surface testing is marked with a black arrow (j). Interactions are shown in red circles. Scale bar = 1 μm .

The images obtained by tracking the deposition of microgels from solution onto PDADMAC-microgel surfaces show similar interactions as those exhibited by microgels interacting with a PLL-microgel surface (see **Figure 4.4** and **Figure 4.5**). First, deposition of a microgel from solution to a PDADMAC-labeled microgel resulted in a “slide-off” event, in which the newly deposited microgel does not favor an interaction with the PDADMAC-labeled microgel and instead ultimately rests between two microgels on the substrate (**Figure 4.7a-c**). During the tracking of this first event,

another deposition event was also witnessed in which a microgel from solution directly deposits onto the silanized substrate without interacting with the PDADMAC-microgel surface (**Figure 4.7d**). Similar to what was seen for PLL containing surfaces, microgels from solution tested the PDADMAC-microgel surface before permanently attaching to the substrate surface (**Figure 4.7h-k**). For this interaction, an arrow (**Figure 4.7j**) indicates a microgel that is “sampling” the surface before resting near PDADMAC-microgels on the silanized substrate (**Figure 4.7k**). Also shown in **Figure 4.7** is an interaction in which the microgel attaches to the silanized surface (**Figure 4.7f**) and appears to “move” into PDADMAC-microgels (**Figure 4.7e**). This interaction could be another indication of the preference of microgels to maximize surface contact after deposition, as the movement creates an increase in surface contact between the newly deposited microgel and the PDADMAC-microgel surface. Importantly, the interactions observed for microgels from solution depositing onto a PDADMAC-microgel surface are similar to those observed for PLL-microgel surfaces, validating that this behavior is not polyelectrolyte dependent but an inherent feature of microgel/polyelectrolyte surface interactions. In addition, this array of visualized interactions by real-time tracking may be attributed to the visualized polyelectrolyte redistribution (or lack thereof) as seen in **Figure 4.3e**.

4.4. Conclusions and Outlook

The data presented above mark the first visual representation of the dynamic behavior of polyelectrolytes with microgels during deposition onto a charged substrate. As noted earlier, the assembly process of microgel thin films by LbL with a linear polyelectrolyte has been thought previously as a one-to-one assembly method, wherein a

deposition of each charged species results in irreversible incorporation and each deposition step results in an increase in film thickness. However, the data presented herein shows that during the earliest deposition stages, the microgels from solution exhibit an array of interactions with the surface and preferentially choose the silanized substrate in order to create maximal packing. Even if centrifugal deposition is used to create well-packed microgels during the first deposition step, microgels within the second microgel deposition step choose to ultimately land on the silanized substrate. This means that film growth or increase in film thickness may not take place until after the initial substrate is completely covered. This complexity is another example of the colloidal/polymer duality of the microgel, wherein the microgel does not act solely as a colloidal sphere, but is able to contract and react to the environment to create an optimally organized surface.

Aside from the packing of the microgels within the first two microgel deposition cycles, the behavior of the polyelectrolyte was visualized. After the first microgel deposition step, the microgel surface is exposed to a positively charged linear polyelectrolyte and charge reversal results. After exposure of this polyelectrolyte-microgel surface to another microgel deposition step, the polyelectrolyte exhibits rearrangement (**Figure 4.2**). It was shown that as the packing of microgels after the first microgel deposition step increased, the degree of polyelectrolyte redistribution increases. When considering the various interactions witnessed during tracking, this increase in redistribution can be attributed to a decrease in available types of interaction with the surface. For instance, when the surface is maximally packed with polyelectrolyte-labeled microgels, microgels in solution appear to prefer to interact in some way with the

polyelectrolyte-microgel surface before ultimately resting on the substrate surface. In contrast, when the surface is not maximally packed, microgels from solution are capable of depositing directly onto the surface without contacting the polyelectrolyte-microgels on the surface. For films containing PLL, a fluorescence image was taken after tracking to visualize the fluorescently-labeled polyelectrolyte. These images showed that when the newly deposited microgels interacted and deposited in such a way that it displayed surface contact with PLL^{*}-microgels, they displayed fluorescence (**Figure 4.5**).

Alternatively, if the newly deposited microgel interacted minimally or not at all with the underlying PLL-microgel surface, the newly deposited microgel displayed little to no fluorescence (**Figure 4.4**). These studies show the first example of the polyelectrolyte not acting as “glue,” but as a component which exhibits dynamic behavior with microgels, and this behavior should be considered when building a complete picture of film assembly.

The implications of this behavior on the larger scale cannot be inferred from this data alone and the diffusivity and exchange of polyelectrolyte within larger scale films will be explored in **Chapter 5**. However, this data does present the interactions at play during the beginning stages of film development, and these interactions could have significant implications on the microgel film assembly process. A visualization of microgel films during multilayer assembly can show how these early stages affect film growth. Using AFM, the assembly of a microgel film was visualized after the deposition of each microgel layer by centrifugation. In **Figure 4.8**, the morphology of each microgel layer is visualized by AFM after the addition of each deposition step for a 4 layer microgel film.

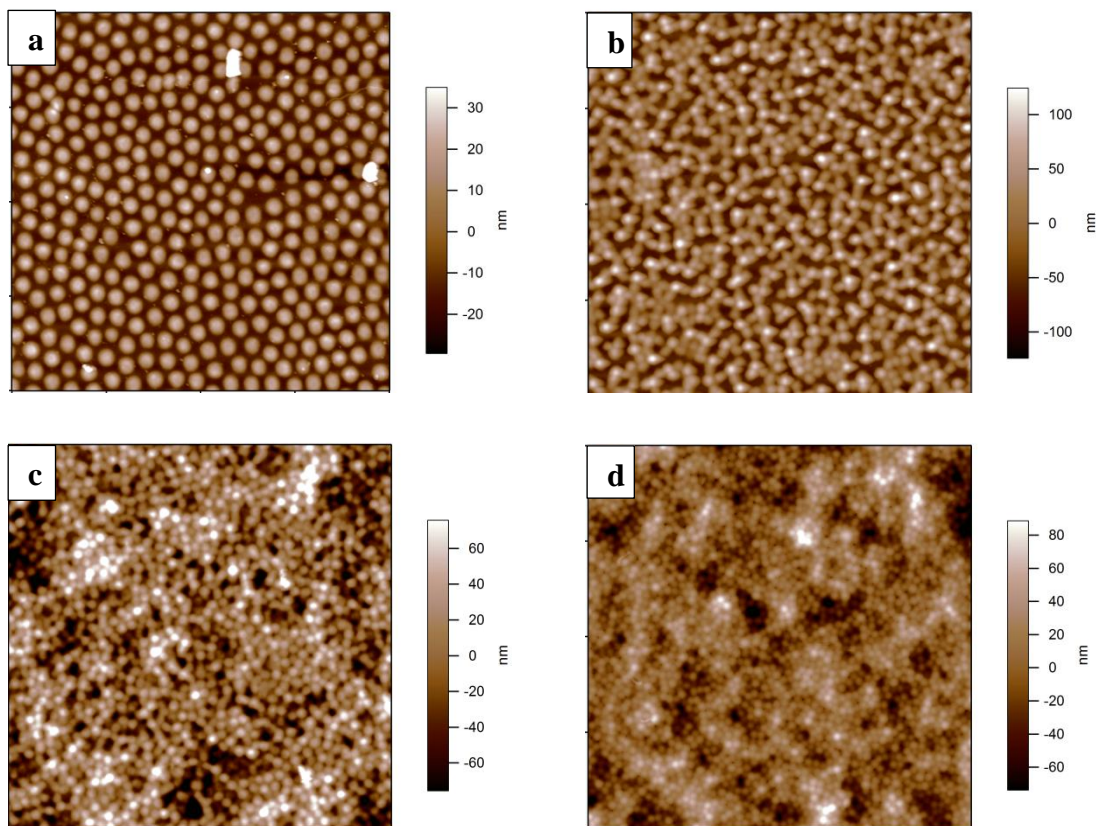


Figure 4.8. AFM images of an MG-20 microgel film assembly after microgel deposition 1 (a), deposition 2 (b), deposition 3 (c), and deposition 4 (d). PDADMAC was deposited between each microgel deposition step. Images are 20x20 μm .

It can be seen in **Figure 4.8** that complete coverage of the substrate is not witnessed until the 3rd or 4th microgel deposition step. These images emphasize the results seen previously, wherein complex interactions and rearrangement result in substrate preference and lateral growth over growth in film thickness. As the substrate becomes less available, the film begins to build in thickness. This shows that the complex interactions at play at these early stages of film assembly are the deciding factor in whether a film will grow in a well-defined uniform manner, or whether it will grow poorly. Again, the results presented herein do not represent a complete picture of film assembly, but these results do show how the complexity of the microgel with a charged

species can dictate the growth behavior within the foundational stages of microgel film assembly. These studies emphasize the previously reported polymer/colloid duality of the microgel, showing how it affects interactions with other charged species and also how this affects its behavior within assemblies. Continued efforts to understand the interaction of these two intricate entities will aid in the development of a true model of microgel multilayer film assembly.

4.5. References

- [1] Lyon, L. A.; Fernandez-Nieves, A., The Polymer/Colloid Duality of Microgel Suspensions. *Annu. Rev. Phys. Chem.* **2012**, *63*, 25-43.
- [2] Holden, D. A.; Hendrickson, G.; Lyon, L. A.; White, H. S., Resistive Pulse Analysis of Microgel Deformation During Nanopore Translocation. *J. Phys. Chem. C* **2011**, *115*, 2999-3004.
- [3] Senff, H.; Richtering, W., Influence of Cross-Link Density on Rheological Properties of Temperature-Sensitive Microgel Suspensions. *Colloid Polym. Sci.* **2000**, *278*, 830-840.
- [4] Smith, M. H.; Lyon, L. A., Multifunctional Nanogels for Sirna Delivery. *Acc. Chem. Res.* **2012**, *45*, 985-993.
- [5] Hendrickson, G. R.; Lyon, L. A., Microgel Translocation through Pores under Confinement. *Angew. Chem., Int. Ed.* **2010**, *49*, 2193-2197.
- [6] Holden, D. A.; Hendrickson, G. R.; Lan, W. J.; Lyon, L. A.; White, H. S., Electrical Signature of the Deformation and Dehydration of Microgels During Translocation through Nanopores. *Soft Matter* **2011**, *7*, 8035-8040.
- [7] South, A. B.; Whitmire, R. E.; Garcia, A. J.; Lyon, L. A., Centrifugal Deposition of Microgels for the Rapid Assembly of Nonfouling Thin Films. *ACS Appl. Mater. Interfaces* **2009**, *1*, 2747-2754.
- [8] Serpe, M. J.; Jones, C. D.; Lyon, L. A., Layer-by-Layer Deposition of Thermoresponsive Microgel Thin Films. *Langmuir* **2003**, *19*, 8759-8764.
- [9] South, A. B.; Lyon, L. A., Autonomic Self-Healing of Hydrogel Thin Films. *Angew. Chem., Int. Ed.* **2010**, *49*, 767-771.

- [10] Clarke, K. C.; Lyon, L. A., Modulation of the Deswelling Temperature of Thermoresponsive Microgel Films. *Langmuir* **2013**, *29*, 12852-12857.
- [11] Debord, S. B.; Lyon, L. A., Influence of Particle Volume Fraction on Packing in Responsive Hydrogel Colloidal Crystals. *The Journal of Physical Chemistry B* **2003**, *107*, 2927-2932.
- [12] St John, A. N.; Lyon, L. A., Local Control over Phase Transitions in Microgel Assemblies. *J. Phys. Chem. B* **2008**, *112*, 11258-11263.
- [13] Iyer, A. S.; Lyon, L. A., Self-Healing Colloidal Crystals. *Angew. Chem., Int. Ed.* **2009**, *48*, 4562-4566.
- [14] Nolan, C. M.; Serpe, M. J.; Lyon, L. A., Thermally Modulated Insulin Release from Microgel Thin Films. *Biomacromolecules* **2004**, *5*, 1940-1946.
- [15] Sorrell, C. D.; Lyon, L. A., Bimodal Swelling Responses in Microgel Thin Films. *J. Phys. Chem. B* **2007**, *111*, 4060-4066.
- [16] Debord, J. D.; Lyon, L. A., Thermoresponsive Photonic Crystals. *J. Phys. Chem. B* **2000**, *104*, 6327-6331.
- [17] Hendrickson, G. R.; Smith, M. H.; South, A. B.; Lyon, L. A., Design of Multiresponsive Hydrogel Particles and Assemblies. *Adv. Funct. Mater.* **2010**, 1697-1712.
- [18] Nayak, S.; Lyon, L. A., Soft Nanotechnology with Soft Nanoparticles. *Angew. Chem., Int. Ed.* **2005**, *44*, 7686-7708.
- [19] Lyon, L. A.; Meng, Z. Y.; Singh, N.; Sorrell, C. D.; John, A. S., Thermoresponsive Microgel-Based Materials. *Chem. Soc. Rev.* **2009**, *38*, 865-874.
- [20] Dubas, S. T.; Schlenoff, J. B., Factors Controlling the Growth of Polyelectrolyte Multilayers. *Macromolecules* **1999**, *32*, 8153-8160.
- [21] Schlenoff, J. B.; Dubas, S. T., Mechanism of Polyelectrolyte Multilayer Growth: Charge Overcompensation and Distribution. *Macromolecules* **2001**, *34*, 592-598.
- [22] Porcel, C.; Lavallo, P.; Ball, V.; Decher, G.; Senger, B.; Voegel, J. C.; Schaaf, P., From Exponential to Linear Growth in Polyelectrolyte Multilayers. *Langmuir* **2006**, *22*, 4376-4383.

- [23] Ostrander, J. W.; Mamedov, A. A.; Kotov, N. A., Two Modes of Linear Layer-by-Layer Growth of Nanoparticle-Polyelectrolyte Multilayers and Different Interactions in the Layer-by-Layer Deposition. *J. Am. Chem. Soc.* **2001**, *123*, 1101-1110.
- [24] Picart, C.; Lavalle, P.; Hubert, P.; Cuisinier, F. J. G.; Decher, G.; Schaaf, P.; Voegel, J. C., Buildup Mechanism for Poly(L-Lysine)/Hyaluronic Acid Films onto a Solid Surface. *Langmuir* **2001**, *17*, 7414-7424.
- [25] Picart, C.; Mutterer, J.; Richert, L.; Luo, Y.; Prestwich, G. D.; Schaaf, P.; Voegel, J. C.; Lavalle, P., Molecular Basis for the Explanation of the Exponential Growth of Polyelectrolyte Multilayers. *Proc. Natl. Acad. Sci. U. S. A.* **2002**, *99*, 12531-12535.
- [26] Lavalle, P.; Gergely, C.; Cuisinier, F. J. G.; Decher, G.; Schaaf, P.; Voegel, J. C.; Picart, C., Comparison of the Structure of Polyelectrolyte Multilayer Films Exhibiting a Linear and an Exponential Growth Regime: An in Situ Atomic Force Microscopy Study. *Macromolecules* **2002**, *35*, 4458-4465.
- [27] Elbert, D. L.; Herbert, C. B.; Hubbell, J. A., Thin Polymer Layers Formed by Polyelectrolyte Multilayer Techniques on Biological Surfaces. *Langmuir* **1999**, *15*, 5355-5362.

CHAPTER 5
EXPLORING POLYELECTROLYTE BEHAVIOR IN MICROGEL
MULTILAYER THIN FILMS

Portions Adapted From:

Spears, M. W.; Herman, E. S.; Gaulding, J. C.; Lyon, L. A., Dynamic Materials from Microgel Multilayers. *Langmuir*. **2014**, *30*, 6314–6323.

Herman, E.S.; Lyon, L.A. Polyelectrolyte Exchange and Diffusion in Microgel Multilayer Thin Film Formation. *Soft Matter*. Submitted.

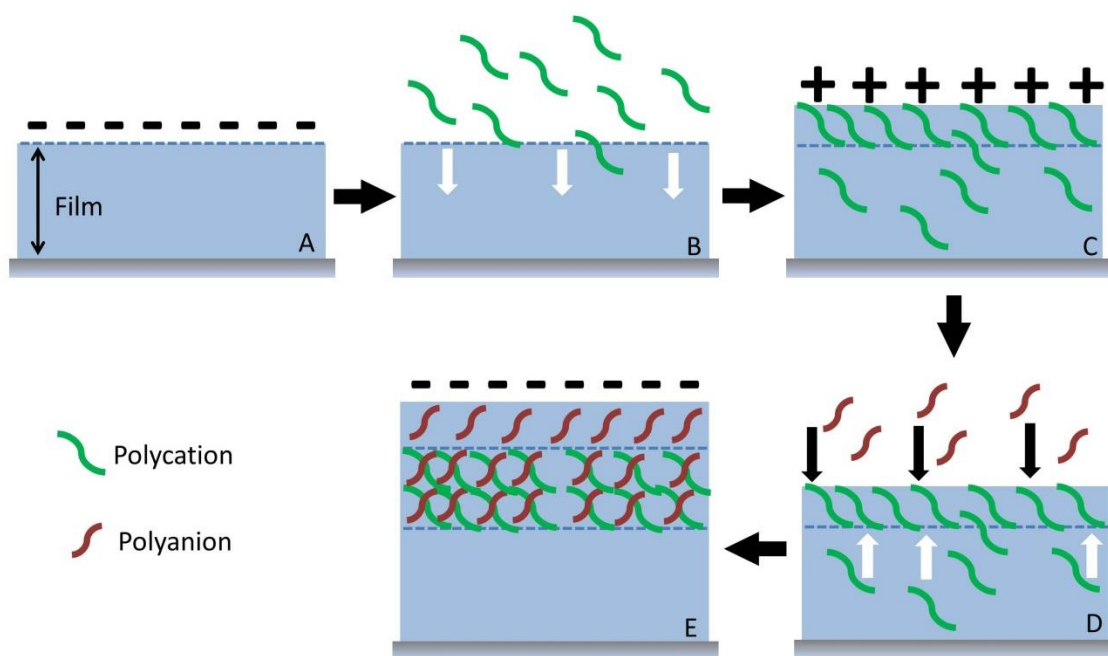
5.1. Introduction

The fabrication and self-assembly of functional polymeric thin films has been an area of interest over the years for a variety of applications. For example, the inherent ease of incorporation of environmental responsivity within polymers has been used to create microgel multilayer thin films for controlled drug release,^{1,2} polymeric brush thin films for sensing applications,^{3,4} or self-healing hydrogel films,^{5,6} just to name a few. An assortment of techniques has been explored in an effort to produce such films, with one technique in particular being noted as revolutionizing the realm of thin film research. Known as Layer-by-Layer (LbL) assembly, this technique allows for a simplicity, reproducibility, efficiency, and versatility^{7,8} previously lacking in other deposition techniques. Several approaches can be employed for the production of films through LbL,⁹⁻¹¹ with the most common being Coulombic LbL. For this, a charged surface is exposed to an oppositely charged species in solution. This charged species will decorate the substrate surface, resulting in charge reversal and charge overcompensation. Subsequent immersion into a solution of species exhibiting the same (new) charge as the

surface will again result in deposition and an associated surface charge reversal. This process can be repeated to a desired film thickness. The technique was first demonstrated by Iler et al in 1964,¹² but was not popularized until 1992 when Decher et al. illustrated the utility of the technique through the alternating deposition of charged polyelectrolytes.¹³ This technique has since grown to incorporate and employ other charged species, such as nanoparticles, proteins, and DNA.¹⁴⁻¹⁶

As is true with many techniques, with a growing interest in Coulombic LbL came an understanding that not all systems were as simplistic as described above. This has become most evident in the extensive research in polyelectrolyte thin films.¹⁷ In the early years, it was believed that films created through the LbL technique grew exclusively in a linear fashion, with the same amount of polymer (or thickness) being added in each step. However, significant complexity in film growth was brought to light when it was found that the poly-L-lysine (PLL)/sodium alginate (Alg) system exhibited supralinear growth.¹⁸ Although some polyelectrolyte pairs such as polystyrene sulfonate (PSS)/polyallylamine hydrochloride (PAH) do interact in a way that produces linear film growth,¹⁹ an increasing number of polyelectrolytes have been shown to interact in a way that leads to exponential growth.^{20,21} Exponential growth has been attributed to the mobility of one or both polyelectrolytes involved in film formation, which allows for the diffusion of polyelectrolytes in and out of the film as each layer is added (**Scheme 5.1**).^{20, 22-24} If the film surface is not permeable to the polyelectrolyte solution to which it is exposed, then the film will build at the film surface (linear growth), whereas if the film is permeable, polyelectrolyte will diffuse in and out of the film upon exposure to the oppositely charged polyelectrolyte or upon washing, which results in exponential growth.

The structure of exponentially grown polyelectrolyte films and the permeability of polyelectrolytes has been studied through a variety of techniques^{22,25,26} and the influence of such behavior in response to external parameters, such as pH and salt concentration, has also been characterized.^{21,27,28} Dynamic growth behavior has also been witnessed in films containing a non-linear polyelectrolyte component, such as proteins²⁹ or nanoparticles,³⁰ however our understanding of growth behavior and assembly in films containing a non-linear polyelectrolyte component (i.e. a microgel) is currently under-developed.



Scheme 5.1. Schematic drawing of the mechanism of exponential polyelectrolyte film growth, starting with a negatively charged film (a). The film is put in contact with a polycation solution (b), which diffuses into the film concentrating at the top of the film and creating charge overcompensation. After rinsing (c), some interpenetrated polycation remains within the film. Exposure to an oppositely charged polyanion (d) creates diffusion of the excess polycation “out” of the film and polyanion will diffuse “in”. Concomitant charge overcompensation and charge reversal results (e).

The formation of polymeric thin films through the incorporation of soft colloidal microgel-sized hydrogels (microgels) has been a useful area of study due to the porosity

and versatility of microgels, which allows for the incorporation of various charged species. These qualities have shown practicality in the formation of films with versatile application, such as microgel films exhibiting self-healing behavior,³¹ resistance to cell adhesion³² and drug delivery capabilities.^{1,2} Microgel thin films are prepared in our lab through a modified LbL technique wherein centrifugal deposition is used to allow for the formation of well-packed negatively charged microgels followed by exposure to a positively charged linear polyelectrolyte.³² This process is repeated until a desired microgel-polyelectrolyte film thickness is achieved. Studies of these multilayer films have revealed their ability to self-heal³¹ and resist cellular adhesion.³² However, an understanding of the interactions at play that allow for such behavior is under-developed and a deeper understanding of these materials is desired. More recent research on these microgel-polyelectrolyte films has gone into better understanding the role of the microgel within dynamic behavior,³³ but as noted therein additional testing is necessary to understand the fundamental parameters of these microgel film components.

To that end, the role of the polyelectrolyte within microgel thin film assembly was analyzed and the results are presented herein. For this, the diffusion of the polyelectrolyte, Poly-L-Lysine (PLL), within microgel-polyelectrolyte films is explored. Through the incorporation of fluorescently-labeled PLL (PLL^{*}) at various stages of film construction, the incorporation of polyelectrolyte can be monitored by UV-VIS spectrophotometry and polyelectrolyte diffusion can be visualized via confocal laser scanning microscopy (CLSM). Mechanical stress is then used to visualize the behavior of PLL during damage events and after healing to give insight into long-range polyelectrolyte redistribution and exchange. This study seeks to gain a better

understanding of polyelectrolyte diffusion and exchange within microgel thin films in order to create a more complete picture of the interaction of microgel thin film components. From a more detailed understanding, insight into the source of dynamic behavior within microgel thin films may be realized.

5.2. Experimental

5.2.1. Materials

All chemicals were purchased and used as described in **Chapter 2- Chapter 4**. In addition, fluorescent red carboxylate-modified polystyrene latex beads were purchased and used as received. Water used in all reactions, particle purifications, and buffer preparations was purified to a resistance of 18 M Ω (Barnstead E-Pure System), and filtered through a 0.2 μ m filter to remove particulate matter.

5.2.2. Microgel Synthesis and Characterization

Microgels (78% NIPAm, 10% AAc, 2% BIS) were synthesized as described in **Chapter 3**. Microgels were purified through centrifugation and resuspension in distilled deionized water and were lyophilized to increase storage stability. Microgels were characterized by DLS as described in **Chapter 3**, with an $r_h = 495$ nm.

5.2.3. Polyelectrolyte Preparation

Conjugated PLL (PLL^{*}) was prepared as described in **Section 4.2.3**. The conjugated PLL was purified by dialysis with distilled deionized water using dialysis tubing with a molecular weight cutoff of 12-14,000 Da (VWR Scientific).

5.2.4. Microgel Thin Film Assembly

Microgel-PLL thin films were prepared by a modified LbL technique as previously described.³² After functionalization with (3-aminopropyl)-trimethoxysilane (APTMS), glass coverslips were placed in 24-well plates and submerged in pH 7.4 HIS PBS. The HIS PBS was then removed and a 0.1 mg/mL microgel solution was placed on the glass coverslips and the microgels were deposited through centrifugation at $2250 \times g$ for 10 min using an Eppendorf 5804R centrifuge equipped with a microwell plate rotor. Films were then removed and rinsed with distilled deionized water and placed in either labeled or non-labeled PLL at a concentration of 1 mg/mL. PLL was deposited while shaking for 2 h. This process was repeated until a total of 11 microgel layers and 10 PLL layers were achieved. Three types of films were prepared with fluorescently labeled PLL introduced at layer 1, 5, or 10 (PLL^{*}₁, PLL^{*}₅ or PLL^{*}₁₀, respectively) while all other PLL layers were non-labeled. A film containing fluorescently-labeled PLL throughout the film was also constructed for comparison. Additionally, films visualized via CLSM contained red fluorescent carboxylated polystyrene beads at microgel layer 1, 5 and 11 for determination of film depth/thickness.

5.2.5. Polyelectrolyte Diffusion and Exchange Characterization

Polyelectrolyte behavior within the aforementioned films was monitored by CLSM microscopy using a Zeiss LSM 700 confocal microscope with a plan apochromat 63X oil objective with a numerical aperture (NA) of 1.4 (Carl Zeiss, Inc., Thornwood, NY). An excitation wavelength of 488 nm was used to image the z-stacks AlexaFluor 488 labeled PLL and 555 nm was used image the carboxylated red fluorescent beads. To prepare samples, a rubber gasket was first affixed to a glass slide. A drop of water was

placed in the center of the gasket and glass coverslips containing deposited films were affixed to the rubber gaskets allowing for in-liquid CLSM imaging. Orthogonal views of AlexaFluor 488 PLL/microgel films were analyzed using ImageJ software.

Polyelectrolyte diffusion into and out of the films was also studied using a Tecan M200 Pro series plate reader. Films were created using the technique described above (see **Section 5.2.4.2**) on a glass substrate. After the addition of each polyelectrolyte and microgel layer, the film was analyzed by placing the one sample per well in a 24-well plate and recording the absorbance at 495 nm. Films were created by introducing fluorescently labeled PLL at varying layer number, with all films containing a total of 11 microgel layers and 10 polyelectrolyte layers.

5.2.6. Microgel Thin Film Thickness Measurements

The thickness of the swollen microgel films was analyzed by in-liquid AFM using an Asylum Research MFP-3D AFM (Santa Barbara, CA). For in-liquid imaging, Asylum Research iDrive cantilevers were used (Force Constant = 0.09 N/m). Films were constructed on glass coverslips as described above and a scratch was made with a straight edge razor to expose the glass surface. Films were fixated to a glass slide using silver paint and samples were allowed to equilibrate in HIS PBS for approximately 30 min. Films were then imaged perpendicularly to the scratch region with a scan size of 50 μm to allow for analysis of film height on either side of the scratch. The MFP-3D software written in the IgorPro (WaveMetrics Inc., Lake Oswego, OR) environment was used to analyze the height of films by drawing line traces across 4 height maps of scratched regions.

5.2.7. Mechanical Deformation and Polyelectrolyte Exchange in Microgel Thin Films

To analyze PLL long-range redistribution, films composed on the elastic substrate PDMS using the technique described above (modified LbL) were mechanically deformed and healed by exposure to a solvent. Microgel films were stretched by 10%, and healed upon exposure to water and subsequent drying. Films before and after damage as well as after healing were analyzed by Atomic Force Microscopy (AFM) using a Nanosurf (Boston, MA) Easyscan 2. Cantilevers used were aluminum coated silicon ACLA cantilevers (Force Constant = 45 N/m) purchased from AppNano (Santa Clara, CA).

Confocal laser scanning microscopy (CLSM) was employed to visualize polyelectrolyte behavior within microgel films before, during and after damage. Films composed with varying fluorescent PLL introduction ((PLL^{*}₁, PLL^{*}₅, and PLL^{*}₁₀) and films containing all fluorescent PLL were analyzed. A Zeiss LSM 700 confocal microscope was used with a long working distance 40x objective with a numerical aperture (NA) of 0.6 (Carl Zeiss, Inc., Thornwood, NY). An excitation wavelength of 488 nm was used to image z-stacks of the aforementioned films. The films were prepared for imaging by affixing the non-microgel film containing PDMS side to a glass slide.

5.3. Results and Discussion

To determine the behavior of the polyelectrolyte within microgel films, the polyelectrolyte, PLL, was chosen for incorporation within such films. This particular linear polycation was chosen for two reasons. First, PLL can easily incorporate a fluorophore due to its primary amine group, which can be functionalized by coupling to

an acid-containing fluorophore, and second this polyelectrolyte is well studied and its diffusivity is well characterized within the realm of linear polyelectrolyte-based films.^{19,20,22,34} It has been shown through extensive study of this particular polyelectrolyte that its behavior within linear polyelectrolyte-based is diffusive, which has been attributed to PLL being an inherently weak polyelectrolyte.^{19,24,35} Part of the foundational work that led to the current model of film growth involved the first visualization of the diffusivity of a polyelectrolyte, specifically PLL, through CLSM wherein it was shown that PLL was capable of diffusing through an entire film thickness.²² These results were used to build a model for non-linear growth behavior of polyelectrolyte-based films, which was attributed to an “in” and “out” diffusion of polyelectrolyte. Based on this literature precedent, this particular polyelectrolyte was chosen for creating a foundational understanding of the polyelectrolyte behavior within microgel-polyelectrolyte films

5.3.1. Polyelectrolyte Diffusion and Exchange

The first step in developing an understanding of the behavior of the polyelectrolyte within microgel thin films was to investigate the diffusive properties of the polyelectrolyte within such films using optical techniques. As described above, the incorporation and diffusion of purely linear polyelectrolyte films is well studied, and early approaches utilized microscopy techniques to show the ability of the diffusive polyelectrolyte, PLL, to incorporate across an entire film depth regardless of point of incorporation during film formation, creating a direct visualization of the “in” and “out” diffusion process as had previously been described.^{23,25} For this reason, CLSM was exploited for PLL-microgel films. PLL* was incorporated into films at polyelectrolyte

layer 1, 5, and 10 (designated PLL^{*}₁, PLL^{*}₅ and PLL^{*}₁₀, respectively) within a film containing 11 microgel layers and 10 PLL layers. The distribution of the PLL was visualized in the z-dimension as shown in Fig. 2. Rhodamine-labeled anionic beads were incorporated during microgel deposition layers 1, 5, and 11 as “markers” for the bottom, middle, and top of the film.

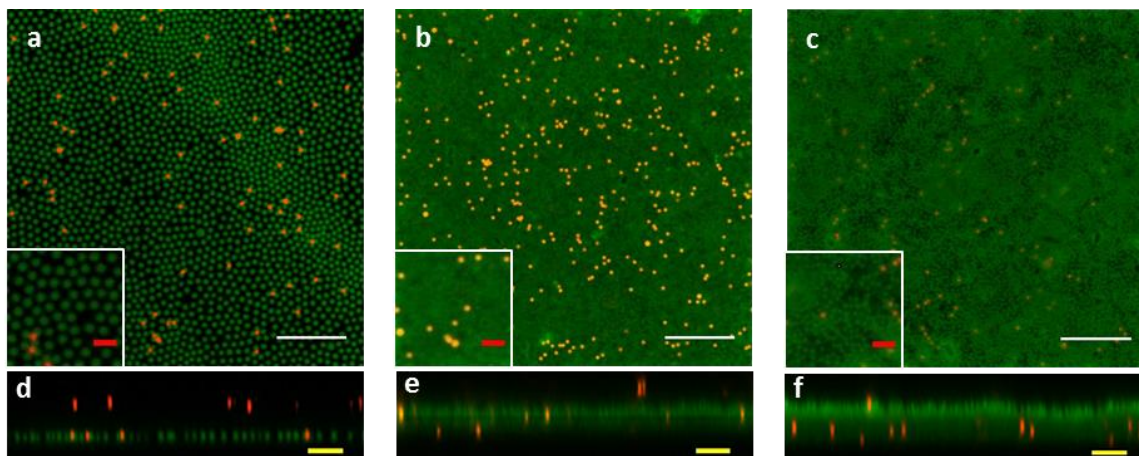


Figure 5.1. CLSM images of PLL-microgel films containing 11 microgel layers and 10 PLL layers. Each panel shows the addition of a labeled polyelectrolyte layer, PLL^{*}₁ (a,d) PLL^{*}₅ (b,e) and PLL^{*}₁₀ (c,f). Scale bar (a,b,c) = 10 μm and inset (red) = 2 μm. Scale bar (d,e,f) = 5 μm. Rhodamine-labeled polyanion beads are shown in microgel layers 1 and 11 (d) and in layer 5 (e,f) for film depth information.

From **Figure 5.1**, it can be seen that the incorporation of the fluorescently-labeled PLL is highly concentrated at the layer of incorporation. It is important to note that these observations are characteristically different from those reported for purely linear PLL-containing films, wherein incorporation of a fluorescent tag resulted in uniform distribution of PLL throughout the film thickness. It is not possible to conclusively determine the degree to which the PLL^{*} diffuses into and exchanges with PLL from neighboring layers, however it seems clear from these data that any such exchange is likely limited to approximately +/- 1 layer adjacent to the layer of PLL^{*} addition.

One could potentially say that the differences witnessed between the three films portrayed in **Figure 5.1** were due to differences in film assembly, uniformity, or thickness. To address this claim, the morphology of the films was explored using in-liquid AFM and the thickness was determined by measuring the height between the substrate and the top of the film (**Figure 5.2**). Based on the observations made via AFM, all 3 films have similar morphology and the distinctive heights of the films are not characteristically different enough to create the drastic differences seen by CLSM of the three film types.

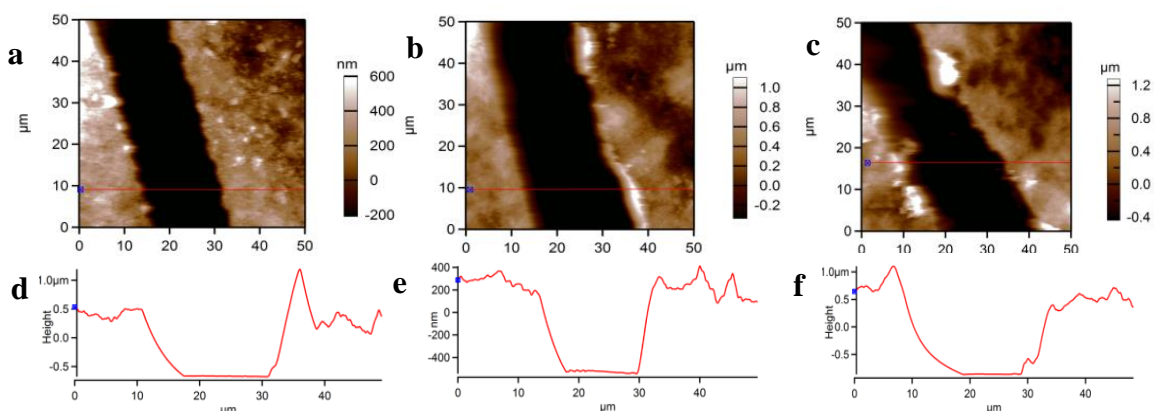


Figure 5.2. In-liquid AFM images of PLL₁₀-microgel₁₁ films with PLL*₁ (a) PLL*₅ (b) and PLL*₁₀ (c). The heights of the films were calculated from height maps, and representative height maps for a, b, and c are shown in d ($1.1 \pm 0.2 \mu\text{m}$), e ($0.9 \pm 0.2 \mu\text{m}$) and f ($1.3 \pm 0.2 \mu\text{m}$), respectively.

To further probe PLL incorporation, diffusion, and exchange, the optical extinction of the PLL-microgel films were recorded after the addition of each layer. Recording the extinction after the addition of each layer should reveal the amount of PLL* incorporated within each PLL addition, and from this the diffusion and exchange behavior of the polyelectrolyte within microgel-polyelectrolyte films can be distinguished. In **Figure 5.3**, the absorbance (at 495 nm) after every layer addition (microgel and PLL) for the films described above is shown.

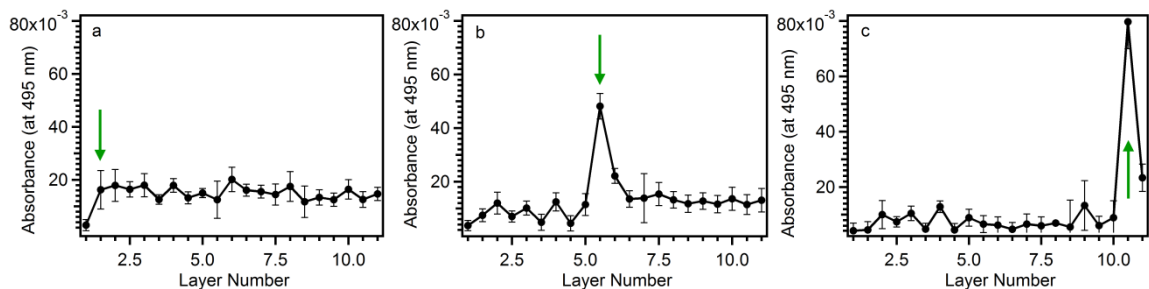


Figure 5.3. Normalized absorbance at 495 nm of PLL₁₀-microgel₁₁₁ films with PLL₁^{*} (a) PLL₅^{*} (b) and PLL₁₀^{*} (c). Green arrows indicate the point of incorporation of PLL_n^{*}. n=44.

The microgel film containing PLL₁^{*} (**Figure 5.3a**) shows an increase in absorbance after PLL₁^{*} incorporation (green arrow) indicating an influx of the fluorescent polyelectrolyte followed by negligible (if any) loss of absorbance upon accumulation of additional microgel and polyelectrolyte layers. Conversely, films with PLL₅^{*} (**Figure 5.3b**) and PLL₁₀^{*} (**Figure 5.3c**) show a large spike upon incorporation of the fluorescently-labeled polyelectrolyte and a decrease in absorbance upon addition of more film layers. Keeping in mind the previously described film model for thin film assembly (see **Scheme 5.1**), this trend can be explained as follows. When the negatively charged microgel surface is exposed to the positively charged PLL, the PLL diffuses into the bulk of the film. Upon washing and exposure to an additional microgel treatment, excess PLL is removed from the film and the absorbance decreases to a lower, but stable value. In the case of the film containing PLL₁^{*} (**Figure 5.3a**), this plateau is reached immediately since there is only one layer of microgels into which the PLL can diffuse. Further evidence of this behavior was seen by collecting the washing solution after addition of PLL₅^{*} and PLL₁₀^{*} and collecting the microgel solution after the addition of a subsequent microgel layer. The absorbance of these solutions were recorded at 495 nm and normalized against HIS PBS or a 0.1 mg/mL microgel solution to determine the amount

of excess PLL* being released into the solution (**Figure 5.4**). These data show that after 3 washes with HIS PBS, the majority of the excess fluorescent polyelectrolyte has been removed. Upon addition of another microgel layer and therefore exposure of the positively charged surface to an oppositely charged species, further excess polyelectrolyte is released. This suggests further that the characteristic diffusive properties of the polyelectrolyte hold true in microgel containing films.

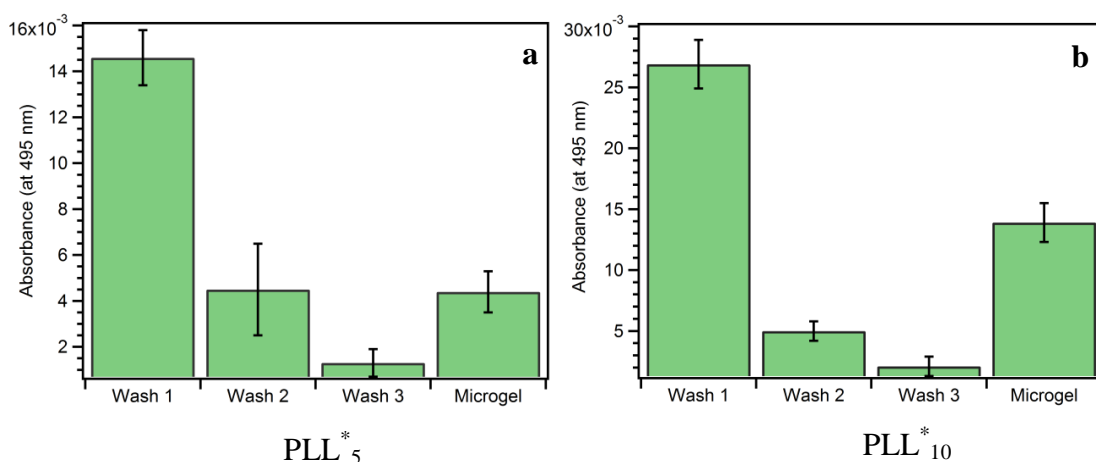


Figure 5.4. Normalized absorbance (at 495 nm) of wash and microgel solutions. After the addition of PLL*₅ (a) and PLL*₁₀ (b), films were washed 3 times and an additional microgel layer was added. These solutions were collected and the absorbance was recorded at 495 nm. n=44.

The results in **Figure 5.4** strongly suggest that there is diffusivity of PLL* into and out of the microgel-PLL films and that this diffusivity matches nicely with the previously described model for diffusive polyelectrolytes. However, previous studies have also addressed the issue of polyelectrolyte exchange that accompanies diffusivity. Indeed, polyelectrolyte exchange, wherein polyelectrolyte from solution exchanges with polyelectrolyte within the film, is recognized as being a prominent feature within purely polyelectrolyte films.²³ Although the absorbance data showed evidence for diffusion, the CLSM data in **Figure 5.1** suggested a lack of polyelectrolyte exchange due to fact that

the fluorescence is concentrated at the layer of introduction of the fluorescently-labeled polyelectrolyte. If there had been a significant amount of exchange throughout the film, fluorescence would be more evenly distributed throughout the film thickness regardless of the layer of introduction of the fluorescently-labeled polyelectrolyte, as has been seen in previous studies.²³ To determine the degree of exchange, films were constructed with PLL* introduced at various polycation deposition stages and the absorbance was analyzed. In this case, six different films were assembled with a single PLL* layer being added at PLL deposition step 1-5, and 10. The absorbance after each layer (microgel or PLL) was recorded at 495 nm and a plateau in the absorbance was observed for each sample. This plateau was attributed to permanently incorporated PLL*, or the point at which exchange and diffusion is limited or non-existent. The value for the plateaued PLL* absorbance was calculated from the point at which fluctuations in absorbance were no longer present. The results for this can be seen in **Figure 5.5** below.

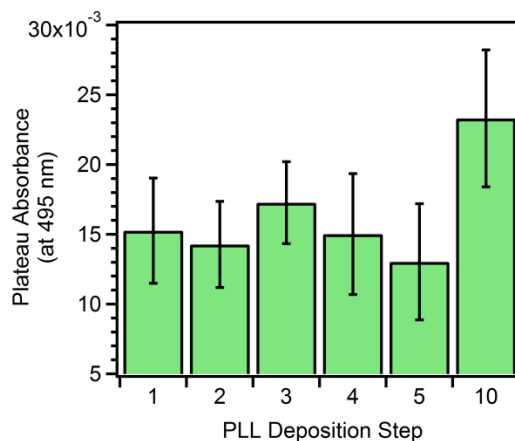


Figure 5.5. The plateau absorbance (at 495 nm) of films composed through the incorporation of PLL* at varied PLL deposition step. PLL Deposition Step corresponds to the PLL deposition step at which the PLL* was incorporated. n=44.

From these data we can see that the plateau absorbance is approximately the same for the PLL deposition step 1-5 films regardless of the point of incorporation of PLL* . This suggests that the amount of polyelectrolyte incorporated is not significantly influenced by the thickness of the film to which it is exposed, which may be indicative of a lack of polyelectrolyte exchange. If a significant amount of exchange were occurring, the plateau absorbance would fluctuate with the increasing deposition step at which PLL* is deposited. This is due to the fact that higher deposition steps also correspond to an overall increased film depth and therefore more PLL availability for exchange. If exchange were a large factor, this increased PLL availability would create fluctuations in the absorbance depending on the deposition step in which PLL* is incorporated. The lack of variation in the plateau absorbance across all films suggests lack of exchange, and this matches well with the CLSM images, which show a concentration of the polyelectrolyte at the point of PLL* incorporation. The significant difference between PLL*₁₀ and the other films, is due to the last deposition step being a microgel layer for this sample. Note that while for all other films a decrease in absorbance was noticed after the addition of microgels, the plateau in absorbance was not reached until the subsequent polyelectrolyte deposition step. Since the PLL*₁₀ film was not exposed to an additional polyelectrolyte deposition step, it apparently still contains excess PLL* that has not yet been displaced by the next PLL treatment.

5.3.2. Mechanical Film Deformation

The above data show that the polyelectrolyte is diffusive and suggest that the microgel film does not exhibit extensive exchange or redistribution of polyelectrolyte during film formation. To further investigate polyelectrolyte exchange (or lack thereof),

we measured the degree of polyelectrolyte redistribution following mechanical film disruption. It has been shown previously that dry microgel films can be easily damaged upon stretching, poking, or scratching, and this damage can be healed upon immersion in water or even exposure to a humid environment.^{31,33} By stretching and scratching the film and causing mechanical perturbation of the entire microgel film, the degree to which this perturbation influences PLL* redistribution can be determined. Self-healing properties have been shown for films composed with the polyelectrolyte PDADMAC³¹ as stated previously and this phenomenon was also observed for microgel films composed with the polyelectrolyte, PLL (**Figure 5.6**). In the AFM images presented in **Figure 5.6**, areas outside of optimal imaging resolution are designated in red (high areas) and blue (low areas), and can be attributed to film defects and do not designate areas of deformation.

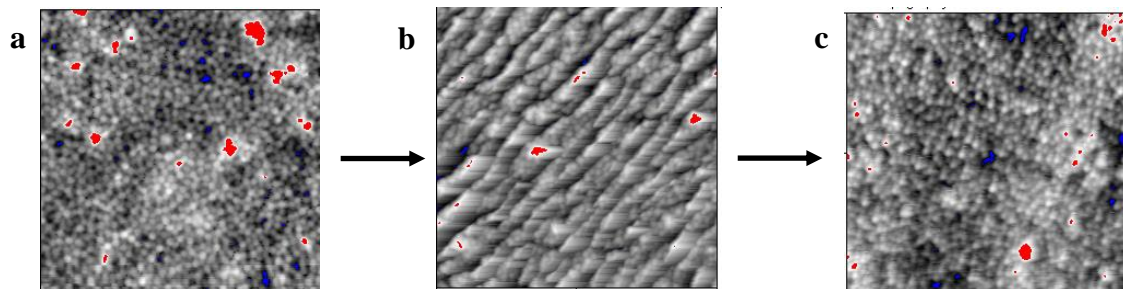


Figure 5.6. AFM images of PLL-microgel films before (a), after damage (b), and after healing (c). Images are $20 \times 20 \mu\text{m}$.

From **Figure 5.6**, we can conclude that films composed with PLL instead of the polyelectrolyte PDADMAC exhibit the self-healing behavior that has been seen previously with microgel containing films. This damage and healing can now be used to mechanically deform the microgel film, and polyelectrolyte redistribution and exchange can be explored across the entire microgel film depth.

5.3.3. Mechanical Perturbation of PLL-Microgel Films

The data above has shown the complex interaction of the polyelectrolyte, PLL, during microgel film assembly and how this behavior agrees or differs from the standard model for purely linear polyelectrolyte film growth. However, a deeper understanding of the behavior of the polyelectrolyte could be explored by perturbing the film as an entire entity and looking at the long range rearrangement and redistribution of the polyelectrolyte. It was hypothesized that the microgel-polyelectrolyte system lacked significant exchange during film assembly, and a possible explanation for this could be a strong interaction between the microgel and the polyelectrolyte, which does not allow for significant exchange. By disrupting the system via mechanical damage, which causes noticeable structural defects across the film, and then healing, additional insight into this interaction might be obtained.

Figure 5.7 illustrates the characteristic damage and healing of a film constructed with fluorescently-labeled PLL throughout (PLL^{*}_{all}) on an elastic substrate (PDMS) and imaged using CLSM.

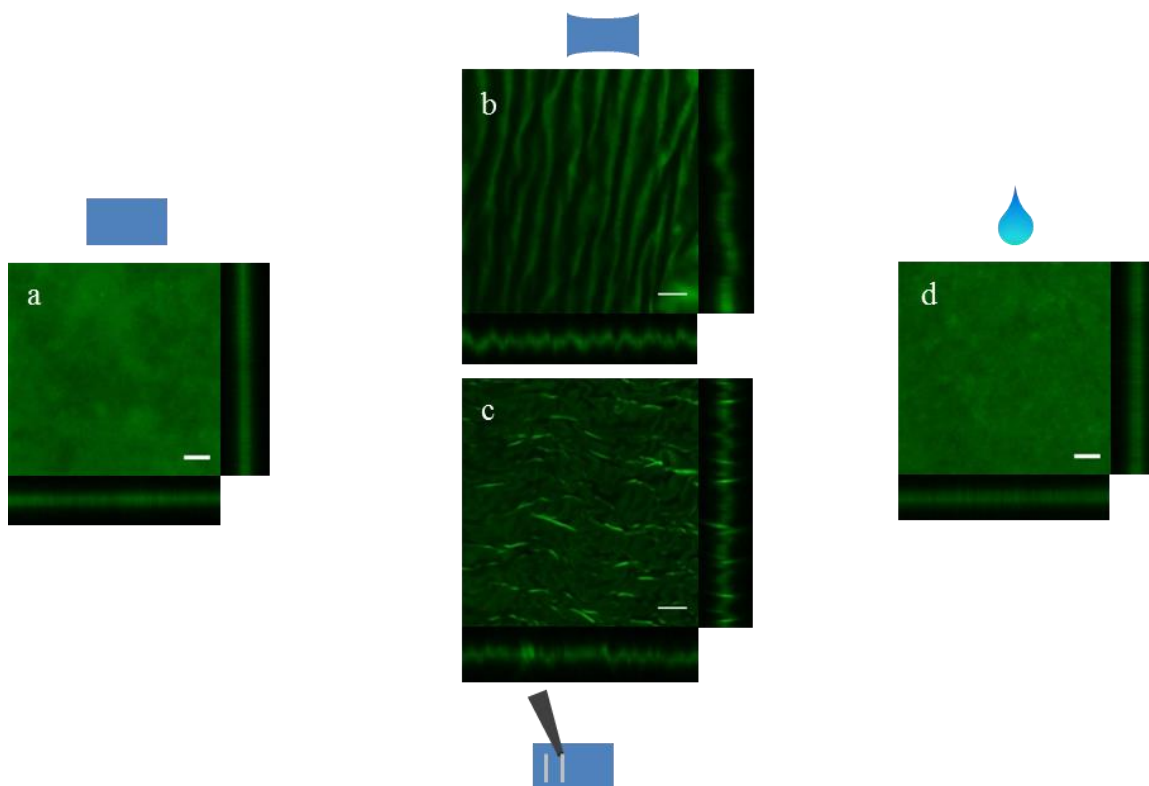


Figure 5.7. CLSM images of the PLL^{*}_{all} film before (a), after stretching (b), after scratching (c) and after healing (d) with representative orthogonal views (z-dimension). Scale bar = 10 μ m.

As seen in **Figure 5.7**, the PLL^{*}_{all} film showed the characteristic buckling of the microgel film upon stretching,³³ which is marked by ridges of higher and lower film density. After the introduction of deionized water and drying, the damage was no longer visible. Scratching the surface also produced damage as seen previously³¹, wherein the film is wrinkled in the direction of the damage. This damage also appears to create areas of overlap of the microgel film, which are marked by areas of brighter fluorescence as seen in **Figure 5.7c**. This suggests that scratching the film causes the film to fold upon itself causing areas of increased film thickness. Prior to damage, the fluorescence is evenly distributed throughout, and after healing this same even distribution is seen,

suggesting that the healing phenomenon is operative both with respect to film topography/morphology and polyelectrolyte distribution.

To further probe exchange, the films described previously (PLL^{*}₁, PLL^{*}₅ and PLL^{*}₁₀) were assembled and visualized as described above for PLL^{*}_{all}. Representative images of such films before and after damage and healing are shown in **Figure 5.8**.

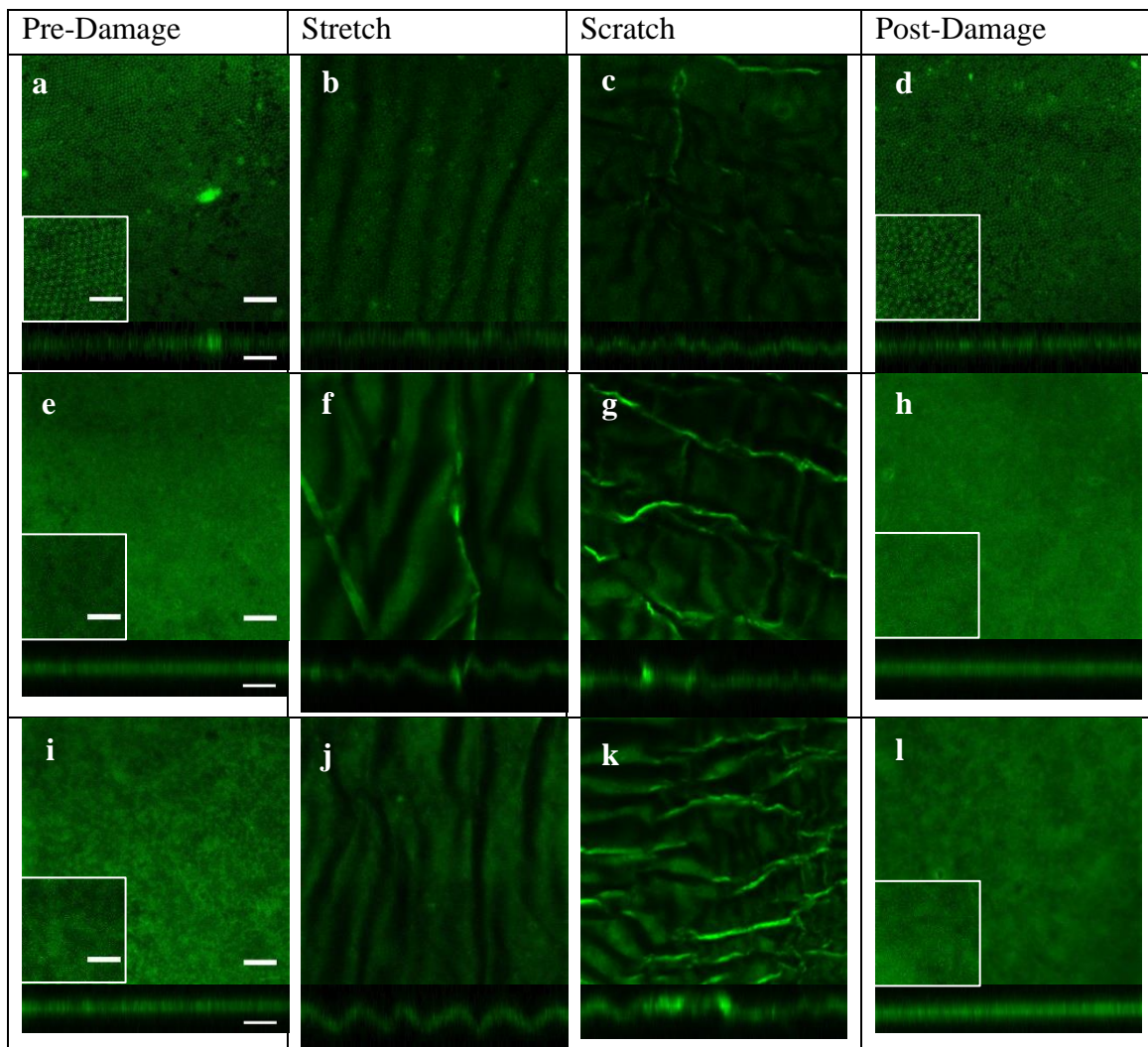


Figure 5.8. CLSM images of films with fluorescently labeled PLL at PLL^{*}₁ (a-d), PLL^{*}₅ (e-h) and PLL^{*}₁₀ (i-l) before damage, during stretching and scratching, and after damage. Scale bar for main images = 10 μ m, and inset image scale bar = 5 μ m.

The damage and healing behavior of all 3 film types were strikingly similar, regardless of the point of introduction of the fluorescently-labeled polyelectrolyte. Prior

to damage, each of the films showed characteristic film morphology and features as shown in Fig. 1. Interestingly, damage and healing does not seem to impact the fluorescence profile as is shown in the inset images (Fig. 7a,d,e,h,i,l), which implies that the localization of fluorescence is not influenced by mechanical deformation of the film. These data suggest that the microgel/PLL interactions are not fully reversible under mechanical deformation. This may add validity to the hypothesis presented above, which stated that the polyelectrolyte lacks long-range exchange or redistribution within the film and it also suggests that perhaps the microgel and polyelectrolyte are strongly interrelated.

5.4. Conclusions and Outlook

Herein, we have shown the ability of PLL* to diffuse into microgel films during deposition and out of microgel films during washing and subsequent microgel deposition. This diffusion “in” and “out” of the film matches nicely with the standard model of diffusive polyelectrolyte assembly. However, results obtained via CLSM and absorbance measurements of films composed with varied PLL* introduction reveal little evidence of polyelectrolyte exchange. To further probe this, mechanical disruption of microgel films with varied PLL* introduction (PLL*₁, PLL*₅, PLL*₁₀, and PLL*_{all}) was utilized and results reveal a lack of exchange and redistribution of PLL and suggest a strong PLL/microgel association that cannot be perturbed by mechanical deformation.

These results present similar diffusive properties but markedly different exchange properties within microgel-polyelectrolyte films as compared to well-studied well-defined linear polyelectrolyte films. A strong interaction of the polyelectrolyte with the microgel is also revealed which stands to redefine the polyelectrolyte as a type of “glue”

within microgel thin films. Rather, the microgel and polycation could be considered as a complex species as opposed to individual components. Clearly, microgel multi-layer films are quite complex and continued efforts to visualize the components of such films during formation will aid in developing a more robust picture of microgel film formation, dynamic behavior, and subsequently future applications.

5.5. References

- [1] Nolan, C. M.; Serpe, M. J.; Lyon, L. A., Thermally Modulated Insulin Release from Microgel Thin Films. *Biomacromolecules* **2004**, *5*, 1940-1946.
- [2] Serpe, M. J.; Yarmey, K. A.; Nolan, C. M.; Lyon, L. A., Doxorubicin Uptake and Release from Microgel Thin Films. *Biomacromolecules* **2004**, *6*, 408-413.
- [3] Stuart, M. A. C.; Huck, W. T. S.; Genzer, J.; Muller, M.; Ober, C.; Stamm, M.; Sukhorukov, G. B.; Szleifer, I.; Tsukruk, V. V.; Urban, M.; Winnik, F.; Zauscher, S.; Luzinov, I.; Minko, S., Emerging Applications of Stimuli-Responsive Polymer Materials. *Nat. Mater.* **2010**, *9*, 101-113.
- [4] Tokarev, I.; Minko, S., Stimuli-Responsive Hydrogel Thin Films. *Soft Matter* **2009**, *5*, 511-524.
- [5] White, S. R.; Sottos, N. R.; Geubelle, P. H.; Moore, J. S.; Kessler, M. R.; Sriram, S. R.; Brown, E. N.; Viswanathan, S., Autonomic Healing of Polymer Composites. *Nature* **2001**, *409*, 794-797.
- [6] Cho, S. H.; White, S. R.; Braun, P. V., Self-Healing Polymer Coatings. *Adv. Mater.* **2009**, *21*, 645-649.
- [7] Hammond, P. T., Form and Function in Multilayer Assembly: New Applications at the Nanoscale. *Adv. Mater.* **2004**, *16*, 1271-1293.
- [8] Decher, G., Fuzzy Nanoassemblies: Toward Layered Polymeric Multicomposites. *Science* **1997**, *277*, 1232-1237.
- [9] Shimazaki, Y.; Mitsuishi, M.; Ito, S.; Yamamoto, M., Preparation of the Layer-by-Layer Deposited Ultrathin Film Based on the Charge-Transfer Interaction. *Langmuir* **1997**, *13*, 1385-1387.

- [10] Stockton, W. B.; Rubner, M. F., Molecular-Level Processing of Conjugated Polymers. 4. Layer-by-Layer Manipulation of Polyaniline Via Hydrogen-Bonding Interactions. *Macromolecules* **1997**, *30*, 2717-2725.
- [11] Crespo-Biel, O.; Dordi, B.; Reinhoudt, D. N.; Huskens, J., Supramolecular Layer-by-Layer Assembly: Alternating Adsorptions of Guest- and Host-Functionalized Molecules and Particles Using Multivalent Supramolecular Interactions. *J. Am. Chem. Soc.* **2005**, *127*, 7594-7600.
- [12] Iler, R. K., Multilayers of Colloidal Particles. *J. Colloid Interface Sci.* **1966**, *21*, 569-594.
- [13] Decher, G.; Hong, J. D.; Schmitt, J., Buildup of Ultrathin Multilayer Films by Self-Assembly Process .3. Consecutively Alternating Adsorption of Anionic and Cationic Polyelectrolytes on Charged Surfaces. *Thin Solid Films* **1992**, *210*, 831-835.
- [14] Kotov, N. A.; Dekany, I.; Fendler, J. H., Layer-by-Layer Self-Assembly of Polyelectrolyte-Semiconductor Nanoparticle Composite Films. *J. Phys. Chem.* **1995**, *99*, 13065-13069.
- [15] Lvov, Y.; Decher, G.; Sukhorukov, G., Assembly of Thin-Films by Means of Successive Deposition of Alternate Layers of DNA and Poly(Allylamine). *Macromolecules* **1993**, *26*, 5396-5399.
- [16] Saurer, E. M.; Flessner, R. M.; Sullivan, S. P.; Prausnitz, M. R.; Lynn, D. M., Layer-by-Layer Assembly of DNA- and Protein-Containing Films on Microneedles for Drug Delivery to the Skin. *Biomacromolecules* **2010**, *11*, 3136-3143.
- [17] Schonhoff, M., Self-Assembled Polyelectrolyte Multilayers. *Curr. Opin. Colloid Interface Sci.* **2003**, *8*, 86-95.
- [18] Lavalle, P.; Voegel, J. C.; Vautier, D.; Senger, B.; Schaaf, P.; Ball, V., Dynamic Aspects of Films Prepared by a Sequential Deposition of Species: Perspectives for Smart and Responsive Materials. *Adv. Mater.* **2011**, *23*, 1191-1221.
- [19] Picart, C.; Lavalle, P.; Hubert, P.; Cuisinier, F. J. G.; Decher, G.; Schaaf, P.; Voegel, J. C., Buildup Mechanism for Poly(L-Lysine)/Hyaluronic Acid Films onto a Solid Surface. *Langmuir* **2001**, *17*, 7414-7424.
- [20] Porcel, C.; Lavalle, P.; Ball, V.; Decher, G.; Senger, B.; Voegel, J. C.; Schaaf, P., From Exponential to Linear Growth in Polyelectrolyte Multilayers. *Langmuir* **2006**, *22*, 4376-4383.

- [21] Picart, C., Polyelectrolyte Multilayer Films: From Physico-Chemical Properties to the Control of Cellular Processes. *Curr. Med. Chem.* **2008**, *15*, 685-697.
- [22] Picart, C.; Mutterer, J.; Richert, L.; Luo, Y.; Prestwich, G. D.; Schaaf, P.; Voegel, J. C.; Lavalle, P., Molecular Basis for the Explanation of the Exponential Growth of Polyelectrolyte Multilayers. *Proc. Natl. Acad. Sci. U. S. A.* **2002**, *99*, 12531-12535.
- [23] Lavalle, P.; Picart, C.; Mutterer, J.; Gergely, C.; Reiss, H.; Voegel, J. C.; Senger, B.; Schaaf, P., Modeling the Buildup of Polyelectrolyte Multilayer Films Having Exponential Growth. *J. Phys. Chem. B* **2004**, *108*, 635-648.
- [24] Lavalle, P.; Gergely, C.; Cuisinier, F. J. G.; Decher, G.; Schaaf, P.; Voegel, J. C.; Picart, C., Comparison of the Structure of Polyelectrolyte Multilayer Films Exhibiting a Linear and an Exponential Growth Regime: An in Situ Atomic Force Microscopy Study. *Macromolecules* **2002**, *35*, 4458-4465.
- [25] Lavalle, P.; Vivet, V.; Jessel, N.; Decher, G.; Voegel, J. C.; Mesini, P. J.; Schaaf, P., Direct Evidence for Vertical Diffusion and Exchange Processes of Polyanions and Polycations in Polyelectrolyte Multilayer Films. *Macromolecules* **2004**, *37*, 1159-1162.
- [26] Hubsch, E.; Ball, V.; Senger, B.; Decher, G.; Voegel, J. C.; Schaaf, P., Controlling the Growth Regime of Polyelectrolyte Multilayer Films: Changing from Exponential to Linear Growth by Adjusting the Composition of Polyelectrolyte Mixtures. *Langmuir* **2004**, *20*, 1980-1985.
- [27] Shiratori, S. S.; Rubner, M. F., Ph-Dependent Thickness Behavior of Sequentially Adsorbed Layers of Weak Polyelectrolytes. *Macromolecules* **2000**, *33*, 4213-4219.
- [28] Dubas, S. T.; Schlenoff, J. B., Factors Controlling the Growth of Polyelectrolyte Multilayers. *Macromolecules* **1999**, *32*, 8153-8160.
- [29] Buijs, J.; Lichtenbelt, J. W. T.; Norde, W.; Lyklema, J., Adsorption of Monoclonal Iggs and Their F(Ab')(2) Fragments onto Polymeric Surfaces. *Colloids and Surfaces B-Biointerfaces* **1995**, *5*, 11-23.
- [30] Ostrander, J. W.; Mamedov, A. A.; Kotov, N. A., Two Modes of Linear Layer-by-Layer Growth of Nanoparticle-Polyelectrolyte Multilayers and Different Interactions in the Layer-by-Layer Deposition. *J. Am. Chem. Soc.* **2001**, *123*, 1101-1110.
- [31] South, A. B.; Lyon, L. A., Autonomic Self-Healing of Hydrogel Thin Films. *Angew. Chem., Int. Ed.* **2010**, *49*, 767-771.

- [32] South, A. B.; Whitmire, R. E.; Garcia, A. J.; Lyon, L. A., Centrifugal Deposition of Microgels for the Rapid Assembly of Nonfouling Thin Films. *ACS Appl. Mater. Interfaces* **2009**, *1*, 2747-2754.
- [33] Gaulding, J. C.; Spears, M. W.; Lyon, L. A., Plastic Deformation, Wrinkling, and Recovery in Microgel Multilayers. *Polymer Chemistry* **2013**, *4*, 4890-4896.
- [34] Porcel, C.; Lavalle, P.; Decher, G.; Senger, B.; Voegel, J. C.; Schaaf, P., Influence of the Polyelectrolyte Molecular Weight on Exponentially Growing Multilayer Films in the Linear Regime. *Langmuir* **2007**, *23*, 1898-1904.
- [35] Elbert, D. L.; Herbert, C. B.; Hubbell, J. A., Thin Polymer Layers Formed by Polyelectrolyte Multilayer Techniques on Biological Surfaces. *Langmuir* **1999**, *15*, 5355-5362.

CHAPTER 6

CONCLUSIONS AND FUTURE DIRECTIONS

6.1. Hollow Microgels

In **Chapter 2** it was shown that “hollow” microgels could be created by first synthesizing core microgel particles with an incorporated degradable component and adding a non-degradable microgel shell. It was also shown in that chapter the variation in incorporation of the degradable component during synthesis depending on the choice of monomer. This emphasized the complex degradation pathways present for core microgels composed with DHEA as shown in previous studies¹ and consequently hollow microgels contained varying degrees of “hollowness.” Previously, synthesis and cross-linker concentrations have been shown to create varied polymer distribution² and the studies described in **Chapter 2** highlight this complexity in the formation of microgel particles. Two types of hollow constructs were analyzed via DLS and AFM, and the results suggested a higher swellability of hollow microgels formed from core/shell microgels wherein the degradable core exhibited greater density and even incorporation of the degradable cross-linker.¹ Future studies could focus on understanding the payload capacity of the two hollow microgels studied herein to assess the viability of one over the other as a hollow microgel container with potential application in drug delivery. For instance, a fluorescent component could be incorporated into the core, along with the degradable component. The extinction coefficient can be measured for the degradation of the core to calculate the amount of core lost upon degradation and the 2 core/shell types could be compared. Similarly, the “hollow” constructs could be loaded with a fluorescent component after degradation and the absorbance can be measured to

determine the loading capacity of the core/shell microgel. From studies such as these, the loading capacity of these two “hollow” microgel types can be determined and their application can be further understood.

6.2. Surface Charge of Microgels and Microgel Assemblies

In **Chapter 3**, KPFM was explored as a method for measuring the surface potential of individual anionic microgels. KPFM has been utilized previously as a method for monitoring changes of the surface potential of charged species in different environmental conditions.^{3,4} Similarly, this method was employed for the characterization of individual anionic microgels in differing deposition conditions and upon exposure to a cationic polyelectrolyte. From this study it was determined that lowering the ionic strength of the solution in which the microgels are deposited results in less charge shielding of the anionic microgels and therefore a greater surface potential. It was also shown that the surface potential of the anionic microgel decreases upon exposure to a positively charged polyelectrolyte, and surprisingly this decrease in overall potential is also present after a subsequent second microgel solution deposition. The results of **Chapter 3** implied a complexity between microgels and another charged species, a linear polyelectrolyte. These initial studies showed the prospective application of KPFM for analyzing individual microgels and continued efforts with this technique could be dedicated to developing a method for obtaining more quantitative information regarding changes in potential. These studies could begin by exploring the effect of flooding the chamber with N₂ to eliminate reactive oxygen species, or altering the humidity of the AFM chamber to determine the effect of environmental conditions on the recorded surface potential. Also worth exploring would be measuring the surface

potential of a range of charged hard spheres with known surface charges to create a group of standards. These standards could then be compared to the measured surface potential of the microgel and the surface potential of the microgel could be quantitatively determined.

Once a method for gaining quantitative information is developed, the application of KPFM could be expanded. For example, initial studies encompassing the analysis of surface charge on damage and healing of microgel multilayer thin films were shown in the preliminary results of **Chapter 3**. A developed quantitative method for analyzing individual microgels could be translated to a microgel assembly. However, it may be difficult to measure the surface potential accurately on a non-conductive substrate, in which case alternate materials would need to be explored. One method to be explored would be the formation of a microgel multilayer thin film on an elastic substrate containing a conductive component. This could be done by either incorporating a conductive component into a substrate such as PDMS, or alternatively plastic coverslips, which are capable of plastic deformation, could be functionalized with a conductive material similar to the method used for functionalization of the glass coverslips used in **Chapter 3**. This may create a robust method for probing the charge distribution within microgel assemblies.

6.3. Polyelectrolyte Behavior in Microgel Multilayer Films

The remainder of the dissertation focuses on the multifaceted interaction of microgels with other charged species. In **Chapter 4**, the newly realized intricate interaction of an anionic microgel with a linear cationic polyelectrolyte was explored to build an understanding of the ability of the polyelectrolyte to diffuse between microgels

localized in close proximity to one another. **Chapter 3** suggested the diffusive behavior of the polyelectrolyte and **Chapter 4** used optical methods to confirm this behavior and disclose the close relationship between the localization of the microgel and the diffusion of the polyelectrolyte. The complexity of the microgel due to its polymer/colloid duality⁵ was also shown to play an essential role in this diffusive behavior as microgel packing affected the degree of polyelectrolyte diffusion and rearrangement within newly deposited microgels.

Unveiling the dynamic behavior of anionic microgels with linear cationic polyelectrolyte opened questions of their behavior within multilayer assemblies, which have been an area of study in the group for a number of years.^{6,7,8,9} The behavior of the polyelectrolyte had previously been thought of as a “glue” that held together layers of microgels, but the studies of **Chapter 4** suggested this was not necessarily true. **Chapter 5** uses CLSM and UV-vis spectroscopy to visualize the underlying behavior of the polyelectrolyte with the microgel during the creation of microgel-polyelectrolyte multilayer films. An in-depth analysis of the behavior of the polyelectrolyte revealed that the polyelectrolyte was in fact diffusive throughout the entire film depth, but the polyelectrolyte was only permanently integrated at the site of incorporation and the diffusivity witnessed in **Chapter 4** was a localized phenomenon. The behavior witnessed in **Chapter 5** also suggested that although the polyelectrolyte is diffusive, the amount of polyelectrolyte added upon each polyelectrolyte deposition step is approximately the same, regardless of the point of incorporation. This suggests that the microgel and polyelectrolyte are strongly interrelated and act as a single unit, as opposed to separate

entities which may give insight into the dynamic behavior witnessed for microgel multilayer films.^{6,7,9}

6.3.1. Future Directions

Keeping in mind the close relationship between the polyelectrolyte and the microgel, several research directions could be explored. Knowing that the polyelectrolyte exhibits complex behavior with the microgel opens an avenue of experiments that had not previously been considered. To expand upon the work shown in this thesis, several avenues could be explored to more completely define the behavior of the polyelectrolyte with the microgel. For example, the incorporation of a fluorescently labeled microgel in conjunction with the fluorescently-labeled polyelectrolyte would allow for an analysis of the movement (or lack thereof) of the microgel, and the colocalization of the microgel and polyelectrolyte could be explored by CLSM. This would also allow for an analysis of the two components simultaneously.

Another avenue to explore would be to change the environmental conditions (such as pH or temperature) and monitor how this affects the interaction of the two charged species. This could be done on the scale utilized in **Chapter 4**, or could also be used during film assembly. For instance, the effect of deswelling the particles during film assembly on the deposition of the polyelectrolyte could be determined. This may also give insight into the localization of the polyelectrolyte since the ability of the polyelectrolyte to localize within the microgel is limited in the deswollen state.

Within the realm of understanding interactions within microgel assemblies, a fluorescently-labeled charged species could also be delivered after film assembly, and the localization of this charged species could give insight into the overall charge distribution

of the film, or which species dominates the microgel multilayer film. Preliminary results within the Lyon lab by Dr. Ling Zhang (unpublished) suggested that microgel multilayer films absorb negatively charged protein more easily unless deposition conditions are altered. By incorporating a fluorescently-labeled charged species, perhaps in conjunction with a fluorescently-labeled microgel thin film component, the interaction of loading and the charged species located within could be better understood. For instance, this analysis may reveal additional movement of charged species after loading, which may indicate a less permanent association of charged species within microgel multilayer thin films.

6.3.2. Preliminary Results

Also worth noting are experiments aimed to understand the utility of microgel multilayer films from the polyelectrolyte perspective. Primarily, research has focused on the microgel because of its inherent complexity, but perhaps by analyzing the behavior of the polyelectrolyte within such films, new and interesting information regarding film formation and assembly can be revealed.

6.3.2.1. Revealing Microgel Multilayer Film Growth Behavior

In **Chapter 5**, the behavior of the polyelectrolyte was analyzed by incorporating a fluorescently-labeled linear polyelectrolyte at various stages during microgel multilayer film formation. This varied incorporation revealed that the amount of polyelectrolyte irreversibly incorporated after each polyelectrolyte deposition step was approximately equal regardless of the layer of incorporation, suggesting a lack of long range exchange and a strong interaction between the microgel and the polyelectrolyte. This understanding of the degree of incorporation of polyelectrolyte during film formation may be used in analyzing the assembly of multilayer microgel films. For this, microgel/

polyelectrolyte multilayer films wherein the polyelectrolyte is fluorescently-labeled could be analyzed after every deposition step to reveal multilayer growth behavior. Preliminary results of this are shown in **Figure 6.1**. For this, the fluorescently-labeled polyelectrolyte, PLL^{*}, is used as described in **Chapter 4**.

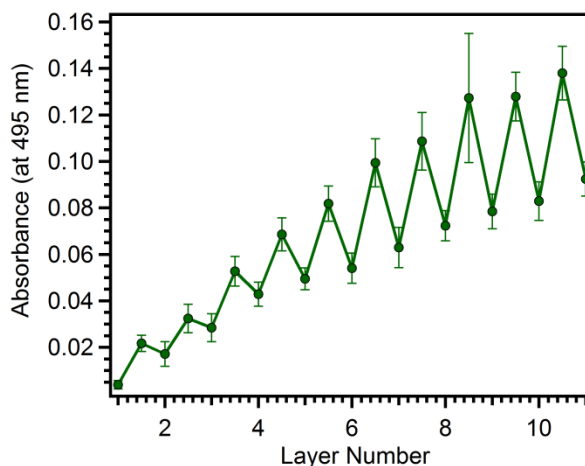


Figure 6.1. Absorbance (at 495 nm) of microgel-PLL^{*} films after each deposition step as recorded by UV-VIS spectrometry. PLL^{*} was added at each polyelectrolyte deposition step.

The absorbance data above show a stair step-like pattern that can be attributed to an influx of polyelectrolyte during polyelectrolyte deposition and efflux of polyelectrolyte upon washing and subsequent addition of microgels. After each microgel deposition step the absorbance reading represents a point at which the majority of unincorporated polyelectrolyte has been removed. A plot of the absorbance (at 495 nm) of each microgel deposition step is shown in **Figure 6.2**.

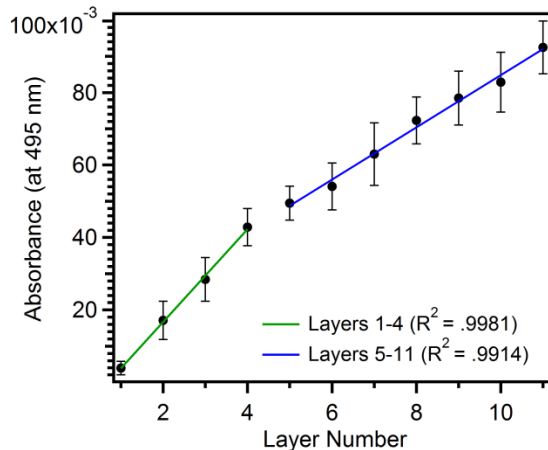


Figure 6.2. Absorbance (at 495 nm) as a function of microgel deposition step, or layer number.

The absorbance behavior in **Figure 6.2** shows two patterns, with the absorbance within the first four deposition steps increasing at a faster rate than the subsequent deposition steps. Linear fits of the two regimes shows good correlation between the data points. Taken in conjunction with previous results from **Chapter 5** suggesting even incorporation of polyelectrolyte at every deposition step, the absorbance data may correspond to the growth behavior of the microgel multilayer film. These results are preliminary and future experiments could aim to understand this correlation and the resultant growth behavior, perhaps in conjunction with AFM which has been used previously to measure film thickness. In this way, the thickness of the film can be determined by AFM (either in-liquid or dry) for each microgel deposition step and in conjunction the amount of polyelectrolyte associated with each layer can be monitored by UV-vis spectrometry. This may give insight into the pattern of microgel thin film assembly (linear versus non-linear). This would also give insight into whether the foundational layers, or the stage of film assembly in which the substrate is still exposed, creates alterations in the growth of microgel multilayer thin films. This was suggested by

the work in **Chapter 4**, but AFM in conjunction with UV-vis may give additional insight into the effect of exposed substrate on film assembly behavior.

6.3.2.2. Altering the Incorporation of Polyelectrolyte

The results presented within **Chapter 4** and **Chapter 5** represent a fundamental study and subsequent understanding of the behavior of polyelectrolyte within microgel-polyelectrolyte films. Building upon this fundamental understanding, possible applications could be visualized. For example, knowing the permanent incorporation of the polyelectrolyte is localized at the layer of deposition, the incorporation of polyelectrolyte could be controlled to create microgel multilayer films with multiple types of positively charged polyelectrolytes or positively charged species. A first pass method for determining the validity of this application would be to incorporate two types of polyelectrolytes at different stages of film formation. The studies presented herein use the fluorescently-tagged polyelectrolyte, PLL. Since the behavior of PLL has been studied extensively previously and its interaction with microgels has been documented in this dissertation, this polyelectrolyte could be used in conjunction with another fluorescently-tagged polyelectrolyte such as Rhodamine-labeled PDADMAC (Rh-PDADMAC). Rh-PDADMAC has been provided by Andre Laschewsky¹⁰ of the University of Potsdam and initial results suggest a difficulty of the lyophilized polyelectrolyte to re-suspend. Future experiments should focus on optimizing the conditions for re-suspension and deposition of Rh-PDADMAC followed by the deposition of Rh-PDADMAC and PLL* at varied stages of microgel film assembly to determine if microgel multilayer films with multiple regions of positively charged species or functionalities could be created.

6.4 Concluding Remarks

This dissertation aims to develop a greater fundamental understanding of microgels as they exist as a single entity and as they exist in complex assemblies. This includes developing a fundamental understanding of the other component of microgel assemblies, the polyelectrolyte. A more robust understanding of the interactions of microgel thin film building blocks has resulted in a more developed picture of microgel thin film assembly, and as outlined above many experiments still exist to create a more developed, robust understanding of these materials. An even deeper fundamental understanding would give insight into dynamic behavior exhibited for microgel multilayer films and possibly increase the potential applications of these materials. The results presented within represent the first stages of understanding the interactions of the building blocks of microgel multilayer thin films and future efforts should aim to expand upon these fundamental findings shown in this dissertation to continue the development of these materials.

6.5. References

- [1] Smith, M. H.; Herman, E. S.; Lyon, L. A., Network Deconstruction Reveals Network Structure in Responsive Microgels. *The Journal of Physical Chemistry B* **2011**, *115*, 3761-3764.
- [2] Stieger, M.; Richtering, W.; Pedersen, J. S.; Lindner, P., Small-Angle Neutron Scattering Study of Structural Changes in Temperature Sensitive Microgel Colloids. *The Journal of Chemical Physics* **2004**, *120*, 6197-6206.
- [3] Park, J.; Yang, J.; Lee, G.; Lee, C. Y.; Na, S.; Lee, S. W.; Haam, S.; Huh, Y.-M.; Yoon, D. S.; Eom, K.; Kwon, T., Single-Molecule Recognition of Biomolecular Interaction Via Kelvin Probe Force Microscopy. *ACS Nano* **2011**, *5*, 6981-6990.
- [4] Thompson, M.; Cheran, L. E.; Zhang, M. Q.; Chacko, M.; Huo, H.; Sadeghi, S., Label-Free Detection of Nucleic Acid and Protein Microarrays by Scanning Kelvin Nanoprobe. *Biosens. Bioelectron.* **2005**, *20*, 1471-1481.

- [5] Lyon, L. A.; Fernandez-Nieves, A., The Polymer/Colloid Duality of Microgel Suspensions. *Annu. Rev. Phys. Chem.* **2012**, *63*, 25-43.
- [6] South, A. B.; Whitmire, R. E.; Garcia, A. J.; Lyon, L. A., Centrifugal Deposition of Microgels for the Rapid Assembly of Nonfouling Thin Films. *ACS Appl. Mater. Interfaces* **2009**, *1*, 2747-2754.
- [7] South, A. B.; Lyon, L. A., Autonomic Self-Healing of Hydrogel Thin Films. *Angew. Chem., Int. Ed.* **2010**, *49*, 767-771.
- [8] Nolan, C. M.; Serpe, M. J.; Lyon, L. A., Thermally Modulated Insulin Release from Microgel Thin Films. *Biomacromolecules* **2004**, *5*, 1940-1946.
- [9] Serpe, M. J.; Yarmey, K. A.; Nolan, C. M.; Lyon, L. A., Doxorubicin Uptake and Release from Microgel Thin Films. *Biomacromolecules* **2004**, *6*, 408-413.
- [10] Wong, J. E.; Muller, C. B.; Laschewsky, A.; Richtering, W., Direct Evidence of Layer-by-Layer Assembly of Polyelectrolyte Multilayers on Soft and Porous Temperature-Sensitive PnIPam Microgel Using Fluorescence Correlation Spectroscopy. *J. Phys. Chem. B* **2007**, *111*, 8527-8531.

APPENDIX A

THE FORMATION OF GLASS NANOPORES FOR USE IN RESISTIVE PULSE ANALYSIS (RPA)

A.1. Introduction

A versatile method for analyzing materials within the nano- to micrometer size range, such as small molecules,¹ nucleic acids, and colloidal particles,² is a technique known as resistive pulse analysis (RPA). The principle of RPA centers on the use of a pore of a defined size through which current flows. An object can be driven through this pore by various methods, such as by electrophoresis or pressure, at which point this current is interrupted. The duration and amplitude of the interruption in electrical signal can be analyzed in such a way that information regarding structure or dynamic properties, such as softness can be recognized.^{1,3} Aside from gaining structural information of nanomaterials, resistive pulse analysis with nanopores can be used to give insight into the interaction of materials with a biological environment, which would be useful in applications such as drug delivery wherein an understanding of the cellular uptake or filtration of the drug delivery vehicle from the body is desired.^{2,4}

The composition of the nanopores used within this method ranges from biological, such as α -hemolysin,⁵ to solid-state, such as glass⁴ or silicon nitride membranes.⁶ Glass nanopores in particular have been applied for the analysis of microgel translocation. Because microgels are “soft”, they are capable of deforming and translocating through pores that are ~10 times smaller than the diameter of the microgel.² This has allowed for the analysis of single translocation events that gave insight into the structural properties of the microgel, such as softness and flexibility, and how these

properties affect the ability of these materials to transverse across membranes.^{7,8} This appendix is dedicated to the construction of glass nanopore membranes for use in RPA analysis of microgels during translocation events. Although the application of glass nanopores was not achieved, the construction of such pores was accomplished and this will be discussed herein.

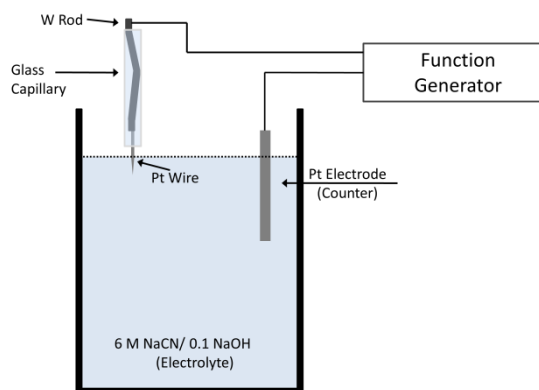
A.2. Experimental

A.2.1. Materials

For the beginning stages of pore fabrication wherein a disk electrode is built (described below), Pt wire (D = 25 μm , Alfa Aesar), tungsten rods (D = 0.010, FHC, Inc), glass capillaries (O.D. = 1.65 mm, I.D. = 0.75, Dagan Corporation), Loctite[®] 0151[™] Hysol[®] two-part epoxy, and Ag paint (FHC, Inc.) were purchased and used as received. For intermediate fabrication processes, sodium cyanide (NaCN), potassium hydroxide (KOH), and calcium chloride (CaCl_2) were purchased from Sigma Aldrich and used as received. Microcut silicon carbide grinding paper in 3 grit sizes (P800, P2400, P4000), Microcloth (D = 77 mm), and Micropolish Alumina powder (D = 0.05 μm) were purchased from Buehler and used as received. For the characterization of disk electrodes and glass capillaries, ferrocene was purchased from Alfa Aesar, and tetra-n-butylammonium hexafluorophosphate (TBAPF_6), acetonitrile, KCl, bleach and Ag wire (D = 1 mm) were purchased and used as received from Sigma Aldrich. All solutions were made using distilled deionized water purified to a resistance of 18 M Ω (Barnstead E-pure System).

A.2.2. Disk Electrode Formation

Glass nanopores were fabricated by a method developed by the White group at the University of Utah.⁹ To begin, a Pt wire (around 1-2 cm in length) is first attached to a tungsten rod using conductive Ag paint. The Pt wire attached to the tungsten (W) rod is placed in a glass capillary and the rod is bent slightly to secure the rod inside of the capillary. The W rod is moved to expose the Pt wire at the surface of the glass capillary, and the Pt wire is gently maneuvered until the wire is exactly centered in the middle of the glass capillary and parallel to the glass capillary walls. The Pt wire is then electrochemically etched using a 6 M NaCN/ 0.1 NaOH solution. This is achieved by first attaching the W wire to a micromanipulator, which allows for precision when placing the Pt wire in the etching solution. A counter electrode composed of platinum is also placed into the solution and both the W wire and the counter electrode are hooked to a function generator (see **Scheme A.1**). Once the Pt wire is placed only slightly into the etching solution an AC voltage (sine wave with 3.6 V amplitude and 100 Hz frequency) is applied and bubbling signifies the etching of the Pt wire. When etching has completed, the bubbling subsides and the wire is removed from solution. The Pt tip is then rinsed with distilled deionized water.



Scheme A.1. Scheme showing the experimental setup for the chemical etching of Pt Wires to produce sharp Pt tips.

After etching of the Pt wire, the Pt wire pulled back and sealed into the glass capillary by softening the glass in a H_2-O_2 flame. The melting was monitored frequently using an optical microscope to ensure even melting, lack of bubbles, and to monitor the degree of melting. Over-melting must be avoided at this stage in order to minimize the time required for Pt etching when creating the glass nanopore (described below) and also to minimize the size of the pore, which can be achieved at the apex of the sharpened Pt tip. Under-melting can also cause problems because this can lead to a loose association of the glass capillary with the Pt wire. This loose association will lead to removal of the Pt wire before sanding of the glass capillary (described below), which will eliminate the ability to create Pt electrodes and thus glass nanopores. Once the glass capillary has been melted sufficiently, the open end of the capillary is sealed using epoxy. Next, the glass capillary is sanded to expose the Pt surface (thus creating a Pt electrode). For this, sand papers of different grit were used to sand the capillary down and create a smooth capillary surface. During the sanding process the capillary was checked frequently via optical microscopy to monitor the depth of sanding, the smoothness, and the contact angle. As the sanding approached the Pt wire, a reflection of the Pt wire

could be seen if the capillary was held at the right angle. This reflection was used to monitor how close the Pt wire was to being exposed. The closer the reflection to the actual Pt wire, the closer the Pt wire was to being exposed. Once the Pt wire and its reflection were adequately close to one another (almost touching), sanding was continued using a polishing pad wetted with a conductive 1M KCl solution and a small amount of micropolish. A conductivity sensor is also used during this step to monitor the exposure of the Pt wire. For this, a wire is placed under the polishing pad, which is conductive due to the KCl solution, and a second wire is connected to the W rod that is still attached to the Pt wire. These are then connected to a home-built conductivity meter that can monitor the resistance across the polishing pad and the W rod. The original design for this came from the White group⁹ and the unit used in these studies was built by Richard Bedell of the Georgia Tech electronics shop. The unit designed by Richard Bedell improved upon the previously designed model,⁹ wherein the authors described a conductivity circuit that suffered from leakage current and inefficiency in the signal obtained upon exposure of the platinum wire. The conductivity circuit designed by Richard contained a reference voltage, which was added to eliminate changes in signal due to battery strength, and several components to increase sensitivity and eliminate noise or excessive currents. Careful testing by Richard verified the improvements of the newly built conductivity meter, wherein the results obtained were reproducible over a range of resistances. **Figure A.1** shows the general principal behind the use of the conductivity meter. This image shows the resistance of a glass-sealed Pt disk electrode during polishing computed from simulations conducted in the White group. Before the Pt tip is exposed to the surface, the resistance of the glass layer dominates. Upon exposure

of the Pt, the resistance spreads at the electrolyte/wire surface. The conductivity meter is designed to give an audible signal when a certain resistance (R) is obtained, which corresponds to a certain Pt disk radius based on **Equation A.1**:

$$R = (4\kappa\alpha)^{-1} \quad \text{Equation A.1.}$$

where κ is the conductivity of the KCl solution and α is the radius of the Pt wire, or electrode as it now exist at the glass surface. This was used as the model for the creation of the conductivity meter used by the White group and is a good method for determining the point of exposure of the Pt surface and the in-home built conductivity meter produced by Richard Bedell was modeled after the conductivity meter produced by the White group.⁹

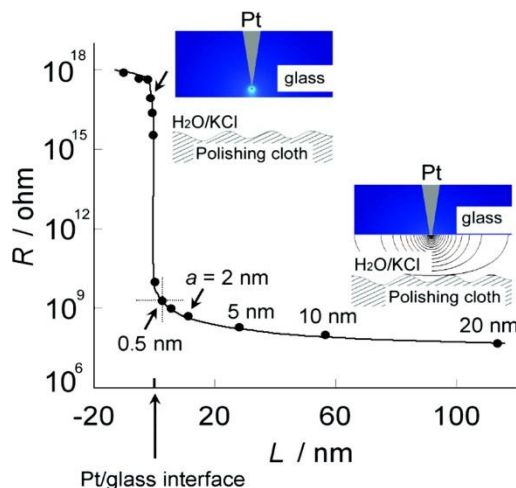


Figure A.1. Resistance versus disk radii. These results were obtained from simulations of the resistance of a glass-sealed Pt disk electrode during polishing.⁹

Although the conductivity meter worked as a first method for determining the exposure of the Pt surface, a more quantitative method for determining electrode size was desired and a previously published method for this determination was used.⁹ Here, the disk electrode is placed in a 5 mM ferrocene solution with 0.1 mM TBAPF₆ in acetonitrile. A wire is connected to the W rod and an Ag/AgCl counter electrode is also

placed in the solution. A cyclic voltamogram (CV) is collected by sweeping across 0.2 to 0.7 V at 10 mV/s. If the Pt wire is exposed, the CV will show an oxidation and reduction of the ferrocene from which the size of the Pt disk can be calculated and the magnitude of the change is dependent on the electrode size. **Figure A.2** shows a representative CV of ferrocene, and **Equation A.2** represents the method for determining the Pt disk size.

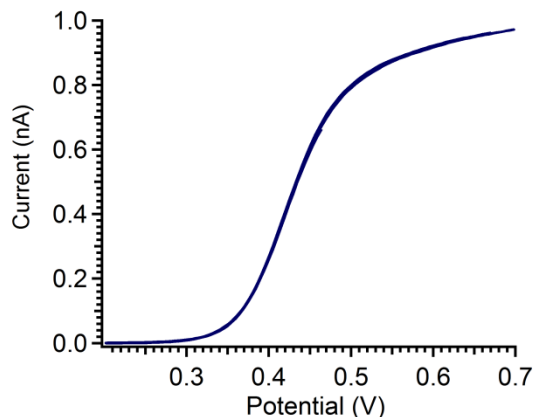


Figure A.2. CV representing the voltammetric response of a Pt microelectrode in a ferrocene solution.

$$r = \frac{\Delta i}{4nFC D} \quad \text{Equation A.2.}$$

Above, **Equation A.2** represents the method for determining the radius (r) where Δi is the difference between the plateau and the baseline current, n is the number of electrons ($n=1$), F is Faraday's constant (96,485 Amp·s/mol), C is the ferrocene concentration (0.004623 mol/L) and D is the ferrocene diffusion constant (0.000025 cm²/s). From this equation, a pore size of 25 nm was calculated for the disk electrode shown in **Figure A.2**. Pt disks measuring $\leq 1 \mu\text{m}$ were used to create glass nanopores as described in the next section.

A.2.3. Glass Nanopore Formation

Once the Pt electrode size was defined and its viability as a glass nanopore was determined, the Pt disk was etched from the glass membrane. Here, a function generator is used in conjunction with a ramp function from +3.0 to -2.9 V at 1 kHz. One lead is attached to the W rod, which is still attached to the Pt wire, and another lead is attached to a Pt electrode and both are placed in a 20% CaCl_2 etching solution. After a couple of weeks, the Pt should be etched from the surface. To finish creating the nanopores, the remaining Pt wire must be removed by scoring the glass capillary and gently twisting and pulling the glass capillary end that is epoxied to the W rod with the remaining Pt wire from the glass surface (see **Scheme A.2**). Once this is done, the glass nanopore is rinsed with and stored in distilled deionized water until use.



Scheme A.2. Pt wire etching with CaCl_2 and subsequent removal to create a hollow glass nanopore.

Once constructed, glass nanopore can then be sized by monitoring current flow through the open pore. First, Ag/AgCl electrodes are created by exposing Ag wire to bleach. These newly made electrodes are then placed inside the pore and in the surrounding solution. A 1M KCl solution, which is sufficiently high enough to reduce rectification, is placed inside and outside of the glass nanopore. The voltage was then swept from -0.1 V to +0.1 V and the current was recorded. A representative graph of this

voltage sweep across a glass nanopore can be seen in **Figure A.3** and the analysis of these results to determine the pore radius was achieved by using **Equation A.3**.

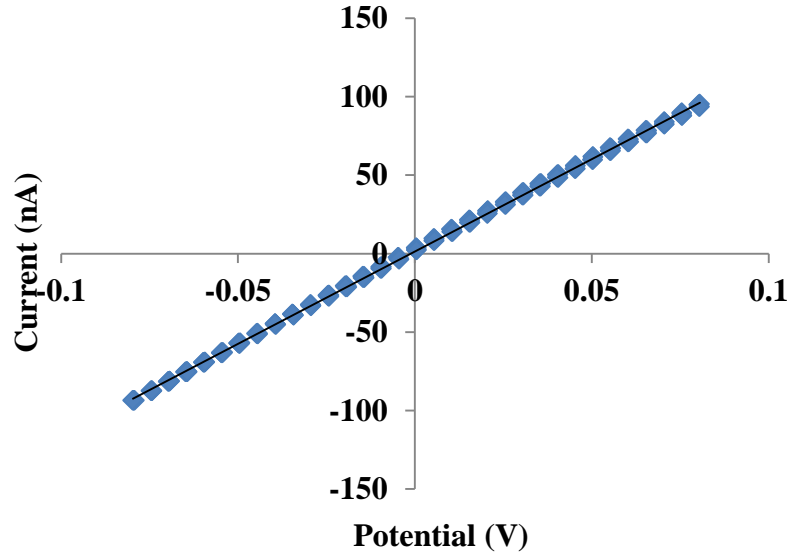


Figure A.3. A representative graph of the current as a function of applied potential for a glass nanopore.

$$r_p = \frac{1}{\kappa R_p} \left(\frac{1}{\pi \tan \theta} \right) + \frac{1}{4} \quad \text{Equation A.3.}$$

The radius of the glass nanopore (r_p) can be determined from Equation A.3 above, wherein κ is the solution conductivity, R_p is the pore resistance, and θ is the half-cone angle. The pore resistance is determined from the slope of the current as a function of applied potential and the half-cone angle can be determined from the half-cone angle from the Pt wire used in the creating of the glass pore. For the graph shown in **Figure A.3**, the pore size was determined to be 223 nm using **Equation A.3**.

A.3. Conclusions and Future Outlook

In this Appendix, the production of glass nanopore membranes was described. Ultimately, the utility of these glass nanopores would be RPA, wherein microgels are passed across the membrane and fluctuations in the current are recorded and analyzed to learn information about microgel softness and deformation across small pores. However, throughout these studies the pores proved to be unable to provide microgel passage and a change in current was not witnessed. Future experiments should focus on understanding the current shortcomings or errors present within the fabrication technique in order to bring this technique to fruition. Alternative methods for fabricating pores for RPA could include pipette pulling to create micropipettes of approximately 300 nm to 6 μm in size,¹⁰ or ion-beam sculpting to create Si_3N_4 membranes with diameters around 100 nm.¹¹ The benefit of glass nanopores membranes by the technique described herein is of course cost effectiveness as the other two methods described here would require expensive equipment. However, if efforts towards the production of glass nanopore membranes continue to be ineffective, other methods may need to be explored to understand microgel softness and deformability on the single particle scale. Currently, the use of Izon's qNano has shown promise as an alternative nanopore-based detection system, which uses Tunable Resistive Pulse Sensing (TRPS) to monitor single particle events across a synthetic adjustable nanopore. As the first commercially available nanopore system, this may be a good alternative is glass nanopore production continues to be limited.

A.4. References

- [1] Deamer, D. W.; Branton, D., Characterization of Nucleic Acids by Nanopore Analysis. *Acc. Chem. Res.* **2002**, *35*, 817-825.
- [2] Hendrickson, G. R.; Lyon, L. A., Microgel Translocation through Pores under Confinement. *Angew. Chem., Int. Ed.* **2010**, *49*, 2193-2197.

- [3] Gu, L.-Q.; Ritzo, B.; Wang, Y., Biosensing: When Less Is More in a Nanopore. *Nat Nano* **2012**, *7*, 212-213.
- [4] Holden, D. A.; Watkins, J. J.; White, H. S., Resistive-Pulse Detection of Multilamellar Liposomes. *Langmuir* **2012**, *28*, 7572-7577.
- [5] Meller, A.; Nivon, L.; Brandin, E.; Golovchenko, J.; Branton, D., Rapid Nanopore Discrimination between Single Polynucleotide Molecules. *Proc. Natl. Acad. Sci. U. S. A.* **2000**, *97*, 1079-1084.
- [6] Dekker, C., Solid-State Nanopores. *Nat. Nanotechnol.* **2007**, *2*, 209-215.
- [7] Holden, D. A.; Hendrickson, G.; Lyon, L. A.; White, H. S., Resistive Pulse Analysis of Microgel Deformation During Nanopore Translocation. *J. Phys. Chem. C* **2011**, *115*, 2999-3004.
- [8] Holden, D. A.; Hendrickson, G. R.; Lan, W. J.; Lyon, L. A.; White, H. S., Electrical Signature of the Deformation and Dehydration of Microgels During Translocation through Nanopores. *Soft Matter* **2011**, *7*, 8035-8040.
- [9] Zhang, B.; Galusha, J.; Shiozawa, P. G.; Wang, G. L.; Bergren, A. J.; Jones, R. M.; White, R. J.; Ervin, E. N.; Cauley, C. C.; White, H. S., Bench-Top Method for Fabricating Glass-Sealed Nanodisk Electrodes, Glass Nanopore Electrodes, and Glass Nanopore Membranes of Controlled Size. *Anal. Chem.* **2007**, *79*, 4778-4787.
- [10] Steinbock, L. J.; Stober, G.; Keyser, U. F., Sensing DNA-Coatings of Microparticles Using Micropipettes. *Biosens. Bioelectron.* **2009**, *24*, 2423-2427.
- [11] Li, J.; Stein, D.; McMullan, C.; Branton, D.; Aziz, M. J.; Golovchenko, J. A., Ion-Beam Sculpting at Nanometre Length Scales. *Nature* **2001**, *412*, 166-169.

APPENDIX B

DESIGN PARAMETERS FOR THE SYNTHESIS OF LARGE SCALE AND DEUTERATED MICROGELS

Portions adapted from:

Liu, W.; Scotti, A.; Hyatt, J. S.; Herman, E. S.; Lyon, L. A.; Gasser, U.; Fernandez-Nieves, A., The CONTIN Algorithm and Its Application to Determine the Size Distribution of Microgel Suspensions. In Preparation.

Gasser, U.; Hyatt, J. S.; Lietor-Santos, J. J.; Herman, E. S.; Lyon, L. A.; Fernandez-Nieves, A., Form Factor of pNIPAm Microgels in Overpacked States. *J. Chem. Phys.* **2014**, *141*, 034901(1)-034901(9).

B.1. Introduction

As described in **Chapter 1**, microgels are cross-linked polymer networks in the nano- to micrometer size range that are capable of responding to changes in environmental factors, such as temperature,¹ pH,² or external osmotic pressure.³ Because of their inherent softness, versatility and responsivity, microgels have found utility in a variety of applications.⁴ Because of this, fundamental studies have been employed to monitor the viability of these materials across a diverse array of disciplines. For example, the phase transitions and crystallization of microgel suspensions have been an area of fundamental study within the physics community due to the volume fraction dependence on size and swelling transition^{5,6} as well as the inherently different behavior of microgels in packed colloidal phases as compared to hard spheres.⁷

The characteristically distinct behavior of microgels in suspension as compared to other colloidal systems stems from their interparticle interactions, which can result in microgel compression, de-swelling, or interpenetration of polymer chains.⁸ In one particularly interesting example, packed colloidal microgels showed an ability to affect de-swelling of microgels through the incorporation of larger microgels within a packed colloidal phase wherein the larger microgels were able to compress and deswell to form a defect-free colloidal crystal.⁹ These interactions are not present in hard sphere colloidal systems, wherein the interparticle interactions are solely dictated by (invariant) excluded volume.¹⁰ Because of this distinguishing behavior of microgels within close packed systems, the intricacies involved within have been of interest in order to develop an understanding of the structural properties of densely packed microgel systems.

In this Appendix, the formation of various microgel compositions is presented and their use in characterizing packed colloidal systems is discussed. First, microgel solutions with varied hydrodynamic radius were created by varying the surfactant concentration during polymerization. In an effort to understand the size and size distribution within packed systems, small angle neutron scattering (SANS) was explored by Andrea Scotti at the Paul Scherrer Institute (PSI). First, SANS was used to unveil the validity of the CONTIN method for obtaining the size distribution of microgel colloidal suspensions¹¹ and continued efforts within this realm are being conducted to understand the polydispersity effect on glass transition. Deuterated microgels and hydrogenated microgels with similar composition and size were also synthesized for SANS experiments aimed at understanding internal structure and single-particle size.¹² These SANS experiments were done by Urs Gasser (PSI) and John Hyatt (Georgia Tech). From

this work, a deeper understanding of the behavior and characterization of microgels within packed colloidal phases was obtained, and in conjunction a detailed understanding of the synthetic conditions required to obtain hydrogenated and deuterated microgels of a required size was determined.

B.2. Experimental

B.2.1. Materials

All reagents were purchased from Sigma-Aldrich (St Louis, MO) and used as received, unless otherwise noted. The monomer N-isopropylacrylamide (NIPAm) was recrystallized from hexane (VWR international, West Chester, PA) and dried under vacuum prior to use. The monomer, deuterated N-isopropylacrylamide (D-NIPAm) was purchased from Polymer Source, Inc. (Montreal, Quebec) and used as received. The surfactant sodium dodecyl sulfate (SDS), initiator ammonium persulfate (APS) and cross-linker BIS (N,N'-methylenebisacrylamide) were used as received. Water used in all reactions and particle purifications was purified to a resistance of 18 M Ω (Barnstead E-Pure system).

B.2.2. Synthesis of Microgels with Varied r_h

Microgels with varied hydrodynamic radius (r_h) were prepared by precipitation polymerization with a total monomer concentration of 100 mM. The NIPAM monomer (98 wt%), the crosslinker, N,N'-methylenebisacrylamide (BIS, 2 wt%) and surfactant sodium dodecyl sulphate (SDS), at a concentration that varies between 0.50 mM and 1.25 mM depending on the aimed particle size, are all dissolved in 1995 mL of distilled, deionized water, which is then subsequently filtered through a 0.2 μm Supor membrane

filter into a 2L 3-neck round bottom flask. The solution is then heated to 70°C by immersion into a water bath and subjected to a nitrogen atmosphere while stirring. After 1 hour, the reaction is initiated by addition of 5 mL of ammonium persulfate (APS, 1.0 mM) and the reaction proceeds for 22 hours. The resultant suspension is then cooled down to room temperature, filtered through a 0.8 µm Supor membrane filter to remove undesired aggregates, and cleaned using dialysis. Samples were then freeze-dried for prolonged viability.

Microgels were also prepared by altering the total monomer concentration for a total monomer concentration between 100 mM and 190 mM to determine the feasibility of altering the monomer concentration as a means to control microgel size. For this, the surfactant, SDS, was kept constant at 1.0 mM and all other conditions were maintained as described above.

B.2.3. Synthesis of Deuterated Microgels

Deuterated microgels (D1-NIPAm) were synthesized using precipitation polymerization and similar synthetic conditions as were previously published¹³ with a total monomer concentration of 120 mM. D-NIPAm (98%), BIS (2 %) and SDS (2.0 mM) were dissolved in 99 mL of distilled, deionized water. Solution was filtered through a 0.2 µm Supor membrane filter into a 200 mL 3-neck roundbottom flask. Solution was heated to 70 °C in an oil bath under nitrogen while stirring (400 rpm). After 1 hour, reaction was initiated through the addition of 1 mL APS (4.0 mM). The reaction took place for 22 hours and was terminated by cooling to room temperature. Solution was filtered through Watman paper (pore size-42.5 mm) to remove aggregates. The particle solution was purified through centrifugation at $468,442 \times g$ for 1 hour at 20 °C. The

supernatant was then removed, and particles were re-suspended in distilled deionized water. This process was repeated twice to ensure the removal of unreacted monomer, cross-linker, surfactant and initiator. Synthesis and purification were repeated twice for a total volume of ~300 mL.

Hydrogenated microgels (H-NIPAm) of similar size to D1-NIPAm were desired, and for this a total monomer concentration of 80 mM was used. The H-NIPAm (98%), BIS (2 %) and SDS (1 mM) were dissolved in 245 mL of distilled, deionized water. The monomer solution was filtered through a 0.2 μm Supor membrane filter into a 500 mL 3-neck roundbottom flask and heated to 70 °C in an oil bath under nitrogen while stirring (450 rpm). After 2 hours, the reaction was initiated through the addition of 5 mL of APS (1 mM). The reaction took place for 14 hours and was terminated by cooling to room temperature. The solution was filtered through Watman paper (pore size-42.5 mm) to remove aggregates and purified through centrifugation at 70,000 rpm for 20 minutes. The supernatant was then removed and particles were resuspended in distilled, deionized water. Centrifugation was repeated twice ensure the removal of unreacted monomer, cross-linker, surfactant and initiator. The total volume after synthesis and purification was ~250 mL.

In addition to hydrogenated and deuterated microgels of the same size, it was also desired to achieve deuterated microgels of larger size. To polymerize larger D-NIPAm microgels, the SDS concentration was altered. For this, an SDS concentration of 1.5 mM (D2-NIPAm) and .95 mM (D3-NIPAm) were used and all other synthesis conditions were kept consistent as listed above for D1-NIPAm, with a total monomer concentration

of 120 mM. for D2 and D3-NIPAm, microgels were cleaned by dialysis and freeze-dried for extended lifetime of the samples.

B.2.4. Characterization Techniques

Dynamic Light Scattering (DLS; Protein Solutions DynaPro DLS equipped with a temperature-controlled microsampler) was used to determine the hydrodynamic radius (r_h) and polydispersity of microgel samples. All DLS measurements were taken at 20 °C. Light scattering data was recorded in intervals of 10 seconds with an average of 20 measurements with a photodiode detector fixed at 90° relative to the incident laser light (783.9 nm). The Dynamics Software package was used to calculate the diffusion coefficient for the microgel particles from the autocorrelation decay of the fluctuations in scattered light intensity. The average r_h was calculated from the measured diffusion coefficients by using the Stokes-Einstein equation. The dispersion medium used for the measurements was distilled deionized water.

Microgels were also characterized by Andrea Scotti and John Hyatt by DLS using an LS Instruments 3D DLS Spectrometer in the lab of Alberto Fernandez-Nieves, which is equipped with a vertically polarized He-Ne laser with wavelength 632.8nm as the light source, a motor driven goniometer, two APD photon detectors, and a two channel multiple tau digital correlator connected to a PC. All measurements were made in water (refractive index, $n=1.331$ at $\lambda=632.8\text{nm}$) and at 21°C, where the viscosity is $\eta= 9.78 \times 10^{-4}$ cP.

Microgels were also characterized by small-angle x-ray scattering (SAXS) and small-angle neutron scattering (SANS) at the Swiss Light Source at Paul Scherrer Institut (PSI) in Villigen Switzerland Andrea Scotti and Urs Gasser.

B.3 Results

B.3.1. Neutral Microgels with Varied r_h

As stated above, the characteristically distinct behavior of microgels creates unique behavior in suspension. This in turn causes differences in the phase behavior of microgel suspensions compared to systems with hard colloidal particles, wherein the fraction of space occupied is the main concern. Because of this, it would be beneficial to find additional methods for characterizing microgel suspensions in an effort to be able to unveil the interactions and complexities involved in the phase behavior of said suspensions. For this, microgel solutions with varied size and polydispersity were desired. From this, regularization methods for defining the particle size and polydispersity can be developed and compared to previous methods for determining these values. By developing better regularization methods, better, more robust values can be obtained for size and polydispersity that better define the colloidal suspension.

To this end, a method for synthesizing microgels, which allowed for control over microgel size, polydispersity, and reproducibility was desired. Several parameters can be adjusted in order to adjust the size of microgels, such as temperature, monomer, initiator or surfactant concentration. For example, surfactant free emulsion polymerization in conjunction with temperature ramping has been used to create large microgels with diameters on the order of 2.5-5 μm ¹⁴ Alternatively, controlling the surfactant and initiator concentration have been used to create nanogels.¹⁵ Each parameter presents a different method for controlling the size of the microgel, but a detailed description of the modification of each parameter is not recorded or intuitive. To begin, the monomer concentration was altered to see the effects of altering the total monomer available during

synthesis, while maintaining the same initiator and surfactant concentration. From a hypothetical standpoint, it would seem that maintaining the initiator while increasing the monomer concentration would create microgels with a greater over size. This is due to the fact that the initiator, ammonium persulfate (APS), is a free-radical initiator, and upon heating it breaks to form radicals and therefore a source of oligoradical growth. By maintaining the initiator while increasing the monomer concentration, the available sites for oligoradical growth are maintained while the available monomer available for chain growth is increased. Select results for this are shown in **Table B.1**.

Table B.1. DLS r_h data of microgel solutions with varied total monomer concentration during synthesis. *Value obtained by Akriti Singh.

Sample	Monomer	Cross-linker	SDS, mM	APS, mM	[Total Monomer], mM	r_h , nm	PolyD
1	NIPAm, 98%	BIS, 2%	1.0	1.0	190	131	10 %
2	NIPAm, 98%	BIS, 2%	1.0	1.0	170	138	11 %
3	NIPAm, 98%	BIS, 2%	1.0	1.0	150	131	12 %
4*	NIPAm, 98%	BIS, 2%	1.0	1.0	100	130	21%

Surprisingly, changing the monomer concentration did not have a significant effect on the r_h of microgels. Knowing this, a different technique for controlling the size of microgels was desired. Next, the concentration of the surfactant, sodium dodecyl sulfate (SDS) was used to try to control the size of neutral microgels. Surfactant acts as a stabilizer for the growing microgel. By increasing the surfactant concentration, the stability of the microgel at early stages of microgel growth is increased causing a decreased probability of aggregation with other microgels in early stages of growth and therefore an increase in particle number and decrease in particle size.¹⁵ By varying the

SDS concentration between 0.5 mM and 3 mM while maintain the monomer composition (98% NIPAm and 2% BIS), monomer and initiator concentration, the size of microgels could be controlled. **Table B.2** shows representative examples of this control.

Table B.2. DLS Cumulants data and SAXS data of microgel samples prepared with varied SDS concentration (sample number and measurements provided by Andrea Scotti).

Sample	SDS, mM	APS, mM	[Total Monomer], mM	Cumulant r_h , nm	Error	r_h , nm SAXS	PolyD
S31	3.00	1.0	100	77	0.6	//	//
S27	2.00	1.0	100	97	0.9	//	//
S112	1.50	1.0	100	113	1.0	//	//
S122	1.25	1.0	100	125	1.0	//	//
S17	1.00	1.0	100	132	0.8	131	10 %
S131	0.95	1.0	100	149	1.0	//	//
S71	0.75	1.0	100	164	1.0	170	11%
S61	0.50	1.0	100	182	2.0	186	12%

From the DLS data shown above, control over the microgel size can be acquired by changing the SDS concentration while maintaining the other synthesis parameters. From this, microgels ranging in size from ~77 nm to ~180 nm can be acquired in a reproducible fashion. Although it has been shown previously that SDS and APS could be altered simultaneously to acquire negatively charged microgels,¹⁵ these results present the first example of maintain the APS concentration while altering the SDS concentration to attain microgels reproducibly of a particle size with an acceptable polydispersity (~10%). By preparing samples using SDS concentrations ranging from 0.5 to 3 mM, monodisperse samples of a specific size could be used for analyzing the validity of a regularization method, known as CONTIN. Monodisperse samples as well as mixed microgel samples with varied polydispersity were analyzed by this method in conjunction with the Cumulants method and SANS. Results showed that the CONTIN method was a powerful method for the determination of colloid size and distribution, adding to methods

for analyzing colloidal suspensions.¹¹ In addition to unveiling the CONTIN method as a regularization method, the reproducibility of synthesizing monodisperse microgel samples of a particular size allows for the analysis of samples of a particular polydispersity by mixing such samples and this polydispersity effect on the formation of packed colloidal phases and/or glassy states. These parameters are currently under investigation by Andrea Scotti at PSI.

B.3.2. Deuterated NIPAm Synthesis

Another method for understanding the behavior of microgels within packed colloidal phases has also been explored through the incorporation of deuterated microgels (D-pNIPAm) within microgel suspensions. These mixed deuterated/hydrogenated microgel suspensions are analyzed by SANS using two methods. The first method is known as a “tracer” method, in which small amounts of hydrogenated microgels (H-pNIPAm) are placed into a dense solution of deuterated microgels which is contrast matched with a mixture of H₂O/D₂O. By contrast matching the solvent to D-pNIPAm, the information obtained from SANS will directly correlate to H-pNIPAm. Secondly, the zero average contrast (ZAC) method¹⁶ is used to obtain information from a 50/50 mixture of H-pNIPAm and D-pNIPAm. A detailed description of these analyses will not be given here, but the synthesis conditions that allow for an analysis of such systems will be described. For a detailed description of the analysis of these systems, the reader is referred to reference 12.

In order to analyze the systems described above, it was necessary to develop a method for synthesizing monodisperse samples of D-pNIPAm microgels of a specific size. In this case, it was desired that the size of the D-pNIPAm be smaller than 200 nm,

and these microgels must size match microgels composed of H-NIPAm. Early synthesis results for D-pNIPAm microgels suggested that the synthesis conditions required for deuterated NIPAm were markedly different than those required for hydrogenated NIPAm. An example of this can be seen in **Table B.3.**, wherein H-pNIPAm and D-pNIPAm microgels of similar size were synthesized, but the synthesis conditions required were dissimilar.

Table B.3. DLS data are shown for D-pNIPAm and H-pNIPAm microgels of similar size. *Values presented were taken from Reference 12 and were obtained by John Hyatt. Differences in r_h and polydispersity can be attributed to variation in solvent.

Monomer	Cross-linker	SDS, mM	APS, mM	[Total Monomer] mM	r_h , nm	* r_h , nm	* r_h , nm SANS
D-NIPAm, 98%	BIS, 2%	2.0	4.0	120	140±20%	136±5%	132±2%
H-NIPAm, 98%	BIS, 2%	1.0	1.0	80	141±14%	149±5%	146±2%

Differences in the synthesis conditions required for the production of D-pNIPAm microgels can possibly be due to the limitation of the availability of self-crosslinking sites on the deuterated NIPAm. In **Chapter 2**, the sites of self-cross-linking on NIPAm were presented and the possible implications of varied reaction rates between monomer and cross-linker were presented. For D-NIPAm and H-NIPAm, the reaction rates may not differ greatly, but one site of self-crosslinking is unavailable. The tertiary hydrogen located on the isopropyl group is unavailable for self-cross-linking in D-NIPAm as it is deuterated and will not be as easily removed for initiation at this site. The degree of self-cross-linking in H-NIPAm containing microgels has been shown to have great effect on the heterogeneity of the microgel,¹⁷ and cause changes in the microgel growth behavior. This lack of a self-cross-linking site in D-NIPAm could be the source of differences in the required synthesis conditions. Although this cannot be proven from this work alone,

this may be a good starting point for understanding differences in the synthetic conditions required.

Once synthesis conditions were optimized to form monodisperse D-pNIPAm microgels of a desired size, conditions for varying the D-pNIPAm microgel size were explored. For this, once again the SDS concentration was altered in order to generate varied microgel size. As shown above, altering the SDS concentration created H-pNIPAm microgels of various sizes in a controlled manner. This same technique was utilized for D-pNIPAm microgels in an effort to find a way to also control deuterated microgel size. **Table B.4.** shows the results of this.

Table B.4. DLS data for D-pNIPAm microgels produced through varying the SDS concentration.

Monomer	Cross-linker	SDS, mM	APS, mM	[Total Monomer] mM	r_h , nm
D-NIPAm, 98%	BIS, 2%	1.50	4.0	120	148±50%
D-NIPAm, 98%	BIS, 2%	0.95	1.0	120	304±21%

As shown in the **Table B.4**, the SDS concentration could be used to alter the size of the D-pNIPAm microgels, but the microgels suffered from polydispersity. Part of this polydispersity could be due to solvent conditions, as the deuterated microgel solutions were diluted in distilled deionized water, but due to the deuteration of the particle size measurements may be better suited in deuterated solvent. Additional work within this realm is needed in order to determine if these results are consistent or if D-pNIPAm microgels can be synthesized across a specific size range in any controlled manner. Future efforts could be aimed towards changing other synthesis conditions, such as initiator concentration or synthesis temperature, to obtain a more reproducible, monodisperse sample of deuterated microgels.

B.4. Conclusions

This appendix has presented synthesis conditions for the production of H-pNIPAm microgels in a controlled manner, in which the SDS concentration was varied in order to control the hydrodynamic radius of microgels as well as synthesis conditions for the production of D-pNIPAm in a controlled manner. The control over the size of H-pNIPAm using SDS concentration as a tool for controlling size is extremely useful obtaining microgel suspensions with a controlled polydispersity, as well as in the efforts ongoing in which the effect of polydispersity on the formation of the glassy state of microgels is explored. The formation of D-pNIPAm microgels is currently limited as only a single deuterated microgel size can be synthesized in a controlled manner. Continued efforts within this area should focus on understanding the parameters necessary for creating deuterated microgels of controlled size and polydispersity as work continues within the realm of understanding microgel systems within colloidal suspensions.

B.5. Acknowledgements

Many thanks to Andrea Scotti, Urs Gasser and Akriti Singh for the analysis of some of the microgel types described herein.

B.6. References

- [1] Pelton, R., Temperature-Sensitive Aqueous Microgels. *Adv. Colloid Interface Sci.* **2000**, *85*, 1-33.
- [2] Hoare, T.; Pelton, R., Highly Ph and Temperature Responsive Microgels Functionalized with Vinylacetic Acid. *Macromolecules* **2004**, *37*, 2544-2550.

- [3] Fernandez-Nieves, A.; Fernandez-Barbero, A.; Vincent, B.; de las Nieves, F. J., Osmotic De-Swelling of Ionic Microgel Particles. *J. Chem. Phys.* **2003**, *119*, 10383-10388.
- [4] Lyon, L. A.; Meng, Z. Y.; Singh, N.; Sorrell, C. D.; John, A. S., Thermoresponsive Microgel-Based Materials. *Chem. Soc. Rev.* **2009**, *38*, 865-874.
- [5] Mattsson, J.; Wyss, H. M.; Fernandez-Nieves, A.; Miyazaki, K.; Hu, Z. B.; Reichman, D. R.; Weitz, D. A., Soft Colloids Make Strong Glasses. *Nature* **2009**, *462*, 83-86.
- [6] St John, A. N.; Lyon, L. A., Local Control over Phase Transitions in Microgel Assemblies. *J. Phys. Chem. B* **2008**, *112*, 11258-11263.
- [7] St. John, A. N.; Breedveld, V.; Lyon, L. A., Phase Behavior in Highly Concentrated Assemblies of Microgels with Soft Repulsive Interaction Potentials. *The Journal of Physical Chemistry B* **2007**, *111*, 7796-7801.
- [8] Lyon, L. A.; Fernandez-Nieves, A., The Polymer/Colloid Duality of Microgel Suspensions. *Annu. Rev. Phys. Chem.* **2012**, *63*, 25-43.
- [9] Iyer, A. S.; Lyon, L. A., Self-Healing Colloidal Crystals. *Angew. Chem., Int. Ed.* **2009**, *48*, 4562-4566.
- [10] Pusey, P. N.; Vanmegen, W., Phase-Behavior of Concentrated Suspensions of Nearly Hard Colloidal Spheres. *Nature* **1986**, *320*, 340-342.
- [11] Liu, W.; Scotti, A.; Hyatt, J. S.; Herman, E. S.; Lyon, L. A.; Gasser, U.; Fernandez-Nieves, A., The Contin Algorithm and Its Application to Determine the Size Distribution of Microgel Suspensions. In Preparation.
- [12] Gasser, U.; Hyatt, J. S.; Lietor-Santos, J. J.; Herman, E. S.; Lyon, L. A.; Fernandez-Nieves, A., Form Factor of Pnipam Microgels in Overpacked States. *J. Chem. Phys.* **2014**, *141*, 034901(1)-034901(9)..
- [13] Ahmed, Z.; Gooding, E. A.; Pimenov, K. V.; Wang, L.; Asher, S. A., Uv Resonance Raman Determination of Molecular Mechanism of Poly(N-Isopropylacrylamide) Volume Phase Transition. *The Journal of Physical Chemistry B* **2009**, *113*, 4248-4256.
- [14] Meng, Z.; Smith, M.; Lyon, L. A., Temperature-Programmed Synthesis of Micron-Sized Multi-Responsive Microgels. *Colloid Polym. Sci.* **2009**, *287*, 277-285.

- [15] Blackburn, W. H.; Lyon, L. A., Size-Controlled Synthesis of Monodisperse Core/Shell Nanogels. *Colloid Polym. Sci.* **2008**, *286*, 563-569.
- [16] Willner, L.; Jucknischke, O.; Richter, D.; Roovers, J.; Zhou, L. L.; Toporowski, P. M.; Fetters, L. J.; Huang, J. S.; Lin, M. Y.; Hadjichristidis, N., Structural Investigation of Star Polymers in Solution by Small-Angle Neutron-Scattering. *Macromolecules* **1994**, *27*, 3821-3829.
- [17] Smith, M. H.; Herman, E. S.; Lyon, L. A., Network Deconstruction Reveals Network Structure in Responsive Microgels. *The Journal of Physical Chemistry B* **2011**, *115*, 3761-3764.

VITA

Emily Sue Herman was born in the great state of Indiana in the town of South Bend. She attended Penn High School in Mishawaka, Indiana, where she fell in love with chemistry for the first time during Chemistry 1 and 2 with Diane Bowersox. Emily went on to attend Saint Mary's College in Notre Dame, IN, and received her B.S. in Chemistry with a minor in Mathematics in 2008. Emily then moved to Atlanta to pursue her doctoral degree in Chemistry under the direction of Dr. L. Andrew Lyon. In her free time, Emily enjoys watching college football (Go Irish), going to new places and trying new foods, playing kickball, and spending time with friends, family and her main man, Dan.